CHERENKOV STUDIES
OF
EXTENSIVE AIR SHOWER DEVELOPMENT

By

D.F. LIEBING, B.Sc. (HONS).

A Thesis
presented for the degree of
DOCTOR OF PHILOSOPHY
at the
UNIVERSITY OF ADELAIDE
(Department of Physics)

May 1983

- TO MY PARENTS -

CONTENTS

SUMMARY

The all-particle spectrum of primary cosmic rays exhibits a pronounced steepening at an energy of approximately 3.10^6 Gev/nucleus. The origin of this feature is not well-understood, models being hampered by lack of knowledge of the nature of the primary cosmic rays and the interactions mechanisms at energies $\gtrsim 10^5$ Gev/nucleus.

This thesis discusses the use of the full-width at half-maximum of the Cherenkov radiation pulse produced by extensive air showers initiated by these particles as a measure of the development of individual air showers. An experiment is described which provides two simultaneous measurements of the Cherenkov pulse associated with extensive air showers with vertical sea-level sizes in the range $\sim 10^5$-10^7 particles.

The data from this experiment are analysed with the assistance of simulated pulse shapes, incorporating the instrumental response, deduced from contemporary air shower simulations. A discussion of the interpretation of this analysis and its consequences for current theories of primary cosmic ray composition and nuclear interactions at $\sim 10^7$ Gev/nucleus concludes the work.

This thesis contains neither material which has been accepted for the award of any other degree or diploma, nor, to the best of the author's knowledge and belief, any material previously published or written by any other person, except where due reference is made.

Signed

D.F. Liebing

Adelaide

May 1983

ACKNOWLEDGEMENTS

I thank Professor J.R. Prescott for provision of the facilities of the Physics Department of the University of Adelaide and his interest in the work. I would like to thank my supervisor, Dr. Alan Gregory, for the assistance, concern and guidance afforded me throughout the course of my candidature. I am also indebted to the interest and, at times almost overwhelming, enthusiasm displayed by Dr. Roger Clay for all aspects of the project. The final stages of the project would have been considerably more demanding without their freely given advice and encouragement.

I am grateful to Dr. John Patterson and Dr. Michael Hillas for the provision of the simulations incorporated in the analysis and to Peter Gerhardy for ensuring the smooth operation of the particle array during the experiment. Useful discussions on several subjects were also had with Dr. Raymond Protheroe. The patience and understanding of Dr. R.C. Lamb is also gratefully acknowledged.

Several members of the Physics Department: Neville Wild, Lindsay Hettner, Bruce Candy, Alex Didenko and Tony Barrett, provided considerable assistance with the design, construction and maintenance of the equipment necessary for the successful completion of the project. To them, I express my sincere thanks. The staff of 'Electronic Services' - John Smith, Brian Fuller and Mike Shorthose provided advice and assistance on various matters, as did Peter Schebella, Keith Powell and David Fearnside of the Physics Department workshop.

The members of the CRGGC Int., particularly Philip Crouch, Peter Gerhardy, Greg Thornton and

Bruce Dawson and my other fellow students provided me with a congenial atmosphere in which to work and were not found wanting in times of crisis.

For the actual production of the thesis, I am indebted to Jack Szeszycki who skillfully and uncomplainingly transformed my scratchings into diagrams and to Pattie Owen who patiently and thoroughly typed the final manuscript.

Finally, I wish to thank my family for their continued support, encouragement and assistance throughout my candidature.

CHAPTER ONE

THE COSMIC RADIATION

1.1 INTRODUCTION

Some seventy years after their discovery, primary cosmic rays are still providing a seemingly inexhaustible subject for fundamental investigations: Which nuclei are they? Where do they originate? How do they acquire their energy? Our attempts to answer these questions are constrained by two sets of incomplete data:

(1) The structure of the galactic interstellar medium (ISM) and magnetic field;

(2) The energy spectrum, composition and isotropy of the primary particles at all known energies ($\sim 10^{0}$-10^{11} Gev).

In this chapter we first survey the current status of each set of data, with particular emphasis on determinations of the primary composition and spectral features in the energy range $\sim 10^{5}$- 10^{7} Gev, then discuss presently accepted models of origin and acceleration deduced from the data. The scope of the author's work and its contribution to the completeness of the above data sets is then briefly outlined.

1.2 GALACTIC STRUCTURE

1.2.1 INTERSTELLAR MEDIUM (ISM)

Relatively recent observations of the galactic soft x-ray background and interstellar ultraviolet absorption

lines (e.g. Tanaka and Bleeker 1977, Jenkins 1978), coupled with theoretical studies (Cox and Smith 1974, McKee and Ostriker 1977) have revealed the importance of the role played by supernovae and their associated shock waves in the determination of the structure and evolution of the ISM. Comprehensive accounts of the subject may be found in the reviews of McCray and Snow (1979) and McKee (1981), the relevant features of which are summarised below.

Current models of stellar evolution suggest that, on average, a supernova occurs in our galaxy approximately once every twenty-five to thirty years. The energy released by a typical supernova, $\sim 10^{41}$ joules, is sufficient to drive a violent shock wave out through the interstellar medium to distances well in excess of one hundred parsecs (pc), sweeping away any low density material in its path and replacing it with the hot, low density 'coronal' gas ($T \sim 10^{5 \cdot 7} K$, $n \sim 10^{-2 \cdot 5} cm^{-3}$) typical of supernova remnant interiors. The volume which would be affected by such frequent supernovae is such that ~70-80% of the galactic volume is believed to be occupied by coronal gas and any point on the galactic plane is crossed by a supernova shock wave approximately once every two thousand years. At the boundary of the shock the swept up mass accumulates into small 'clouds', ~100 solar masses, which may then coalesce to form clouds of increasing mass, limited by gravitational collapse, of up to $\sim 2.10^5$ solar masses. Ionization by ultraviolet starlight and heating by absorption of soft

x-rays results in the formation of a layer of 'warm' ionized gas ($T \sim 10^{3 \cdot 9} K$, $n \sim 10^{-1} cm^{-3}$) on the surface of these clouds with a layer of 'warm', neutral gas ($T \sim 10^{3 \cdot 9} K$, $n \sim 10^{-0 \cdot 4} cm^{-3}$) beneath it. Together, these are thought to occupy a further ∿15-30% of the galactic volume. Beneath the warm, neutral layer lies a core of cold, densely packed molecules, mainly hydrogen, ($T \sim 80K$, $n \sim 10^{1 \cdot 6} cm^{-3}$) containing almost the entire mass of the ISM but occupying only ∿2-5% of the galactic volume.

Sections of a sufficiently massive molecular cloud may become gravitationally unstable and collapse under their own gravitational influence to form stars. In turn these drive shock fronts, resulting either from the stellar winds of evolving stars or the supernova of an evolved star, into the cloud, triggering further stellar collapses. The end result is the formation of a chain of progressively younger stellar associations within a molecular cloud; the Orion complex is believed to be an example of such a region. Bruhweiler et al (1980) have suggested that the rapidly evolving stellar associations produced in such circumstances may, through the combined effects of their stellar winds and relatively rapid sequence of supernovae, produce a large, expanding shell of matter, radius ≲1kpc, the interior of which would be filled with hot, low density coronal gas. Indeed Kafatos et al (1981) suggest that current evidence implies that the solar system itself is enclosed by just such a 'superbubble'.

1.2.2 GALACTIC MAGNETIC FIELD

Again we summarise only the relevant features of the topic. Detailed discussions of observational techniques and their interpretation may be found in the reviews of Hieles (1976), Király and Kóta (1979) and Verschuur (1980).

Reliable determinations of the structure of the galactic magnetic field are limited to the approximately cylindrical region of the galactic plane within $\sim$2kpc of the sun, the extent and magnitude of the field outside this region is still far from certain.

Within this local region there exists a large-scale longitudinal field, strength $\sim$2-3μG, directed towards the galactic longitude $\ell\sim90°$ (Morris and Berge 1964, Gardner et al 1969). Király and Kóta (1979) present evidence indicating that this direction may alter with distance from the sun; changing from $\ell\sim30°$ at $\sim$200pc to $\ell\sim90°$ at $\sim$2kpc. Superimposed on this regular field are both a large-scale ($\sim$100's pc) fluctuating component of approximately equal magnitude and a smaller scale component of more or less random orientation. Locally the field appears smooth on scales of the order of a few parsec (Király and Kóta 1979). The large-scale fluctuating component appears, in part at least, to be associated with 'magnetic bubbles' formed by the trapping of fieldlines in matter swept up by expanding shock waves or superbubbles. The North Polar Spur and Cetus Arc radio loops, and possibly the Gum Nebula, appear to be associated with such objects

(Vallée and Kronberg 1975, Simard-Nordheim and Kronberg 1979, Vallée 1982).

Above the galactic disc the situation is extremely ambiguous. Hillas (1982a) notes that theoretical considerations of field lines trapped in matter expanding away from the galactic plane suggest a strength the order of a few tenths of a microgauss, in apparent conflict with electron synchroton observations which imply a strength little different to that found in the galactic plane.

1.3 OBSERVED FEATURES OF PRIMARY COSMIC RAYS

1.3.1 ENERGY SPECTRUM AND COMPOSITION

DIRECT MEASUREMENTS

The steeply falling nature of the all-particle integral energy spectrum (figure 1.1) has restricted direct determinations of the primary composition and its energy spectrum to energies $\lesssim$ few hundred Gev/nucleon (e.g. Simon et al 1980, Koch-Miramond 1981, Israel et al 1981, Dwyer and Meyer 1981, Webber 1982). However, limited direct information is available on the energy spectra of some of the more populous (H,He) and important (Fe) species up to $\sim 10^4$-10^5 Gev/nucleon (Burnett et al 1982, Sood 1983, Abulova 1981), whilst the pioneering experiment of Grigorov (1971) remains one of the most reliable direct measurements of the all-particle flux for total energies $\lesssim 10^4$ Gev. Unfortunately, the results for individual nuclei in this experiment were probably subject to systematic error

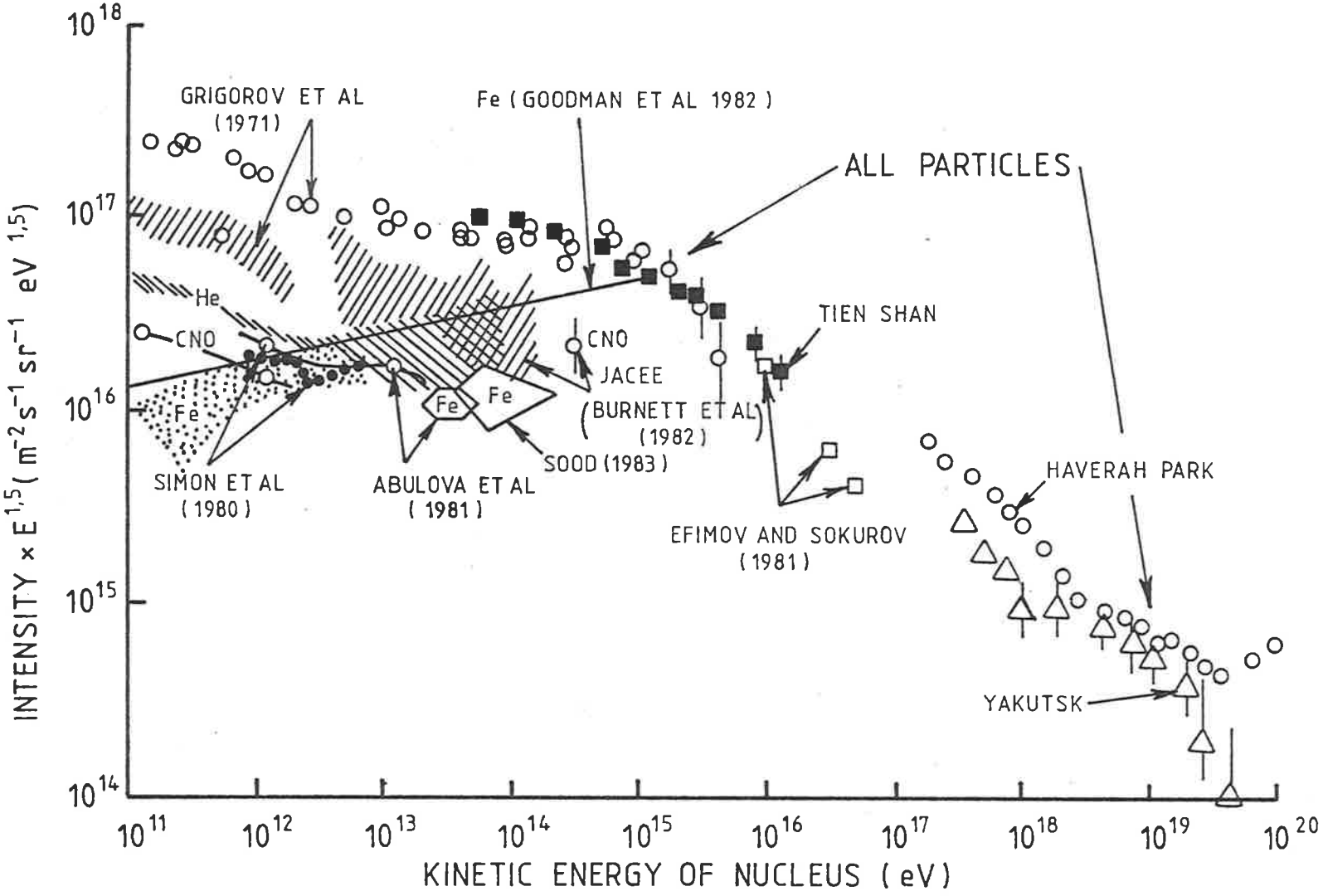

Figure 1.1: The energy spectrum of primary cosmic rays (essentially after Hillas 1981b)

(Ellsworth 1977). One salient feature of these direct determinations is the significant difference in the spectral indices of the light and heavy nuclei, for protons the integral spectrum has a slope $\sim$1.75±.02 whilst that for iron is only $\sim$1.20±.02 (Ryan et al 1972, Balasubrahmanyan and Ormes 1973, Juliusson 1974, Simon et al 1980). Figures 1.2 and 1.3 (after Müller (1982) and Mewaldt (1981) respectively) illustrate the observed elemental abundances, relative to the solar system abundance, for the 'low Z' ($Z<30$) and the 'high Z' ($Z\geq30$) elements respectively. Characteristics of these two charge groups and recent determinations of isotopic abundance ratios are now discussed.

The excess of the three light nuclides Li, Be, B and that of Sc, V, Mn is believed to be due to the spallation of the original primary cosmic rays, e.g. C, N, O, Fe in the interstellar medium. Sufficient statistics on the ratio of these 'secondary' cosmic rays to their primary counterparts have now been accumulated to demonstrate that the mean path length ($g\,cm^{-2}$) traversed by primary cosmic rays in this energy region is rigidity (energy) dependent, decreasing approximately as $E^{-0.4}$ for energies in excess of $\sim$1Gev/nucleon. Figure 1.4, reproduced from Müller (1982), illustrates this phenomenom. The recent analysis of HEAO-3 data by Protheroe and Ormes (1983) indicates that the energy dependence of the mean free path may be even stronger than that suggested by previous experiments, their analysis indicates that at energies in

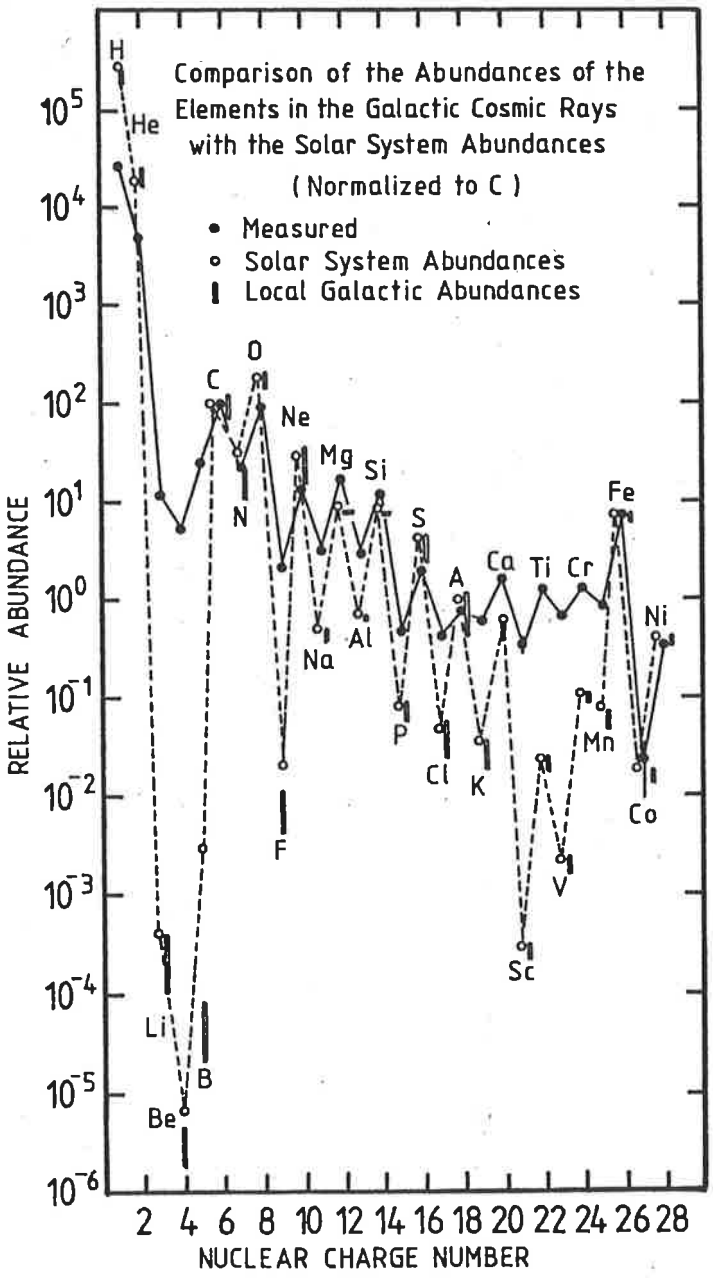

Figure 1.2: The relative abundance of low energy cosmic rays ($Z \leq 30$)
(after Müller 1982)

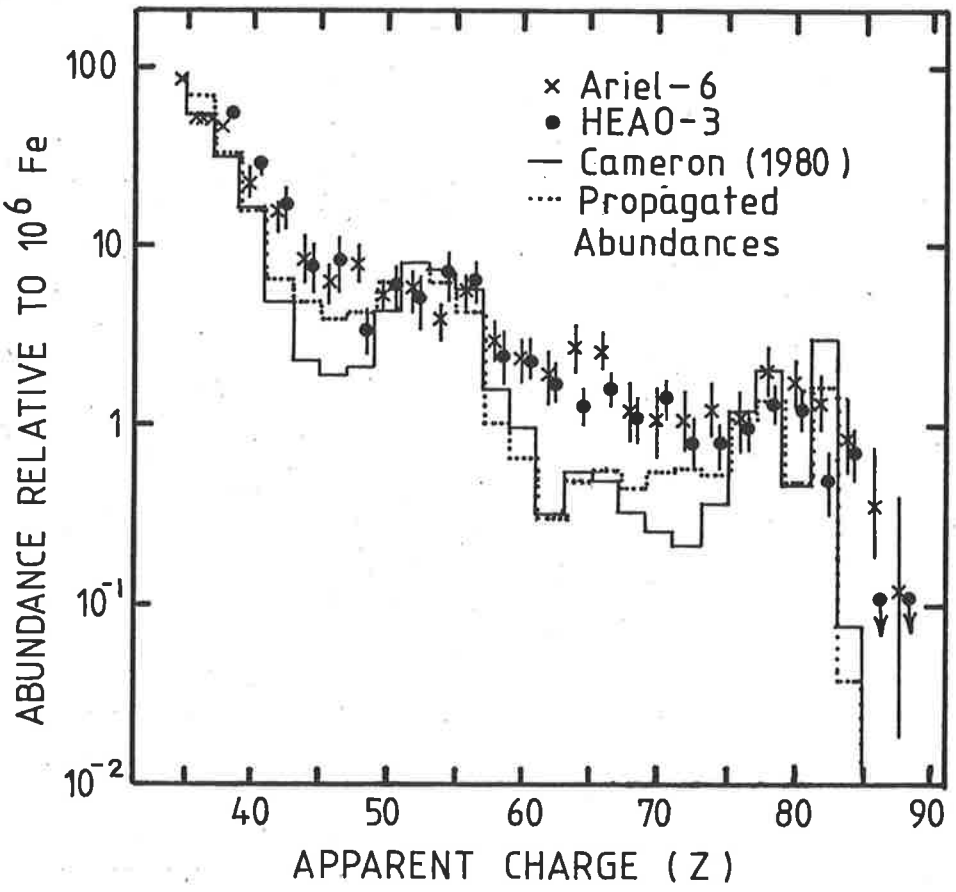

Figure 1.3: A comparison of the observed abundance pattern of low energy, ultra-heavy primary cosmic rays with that predicted by propagating the observed solar system abundances through a 5.5g cm^{-2} exponential pathlength distribution. (after Mewaldt 1981)

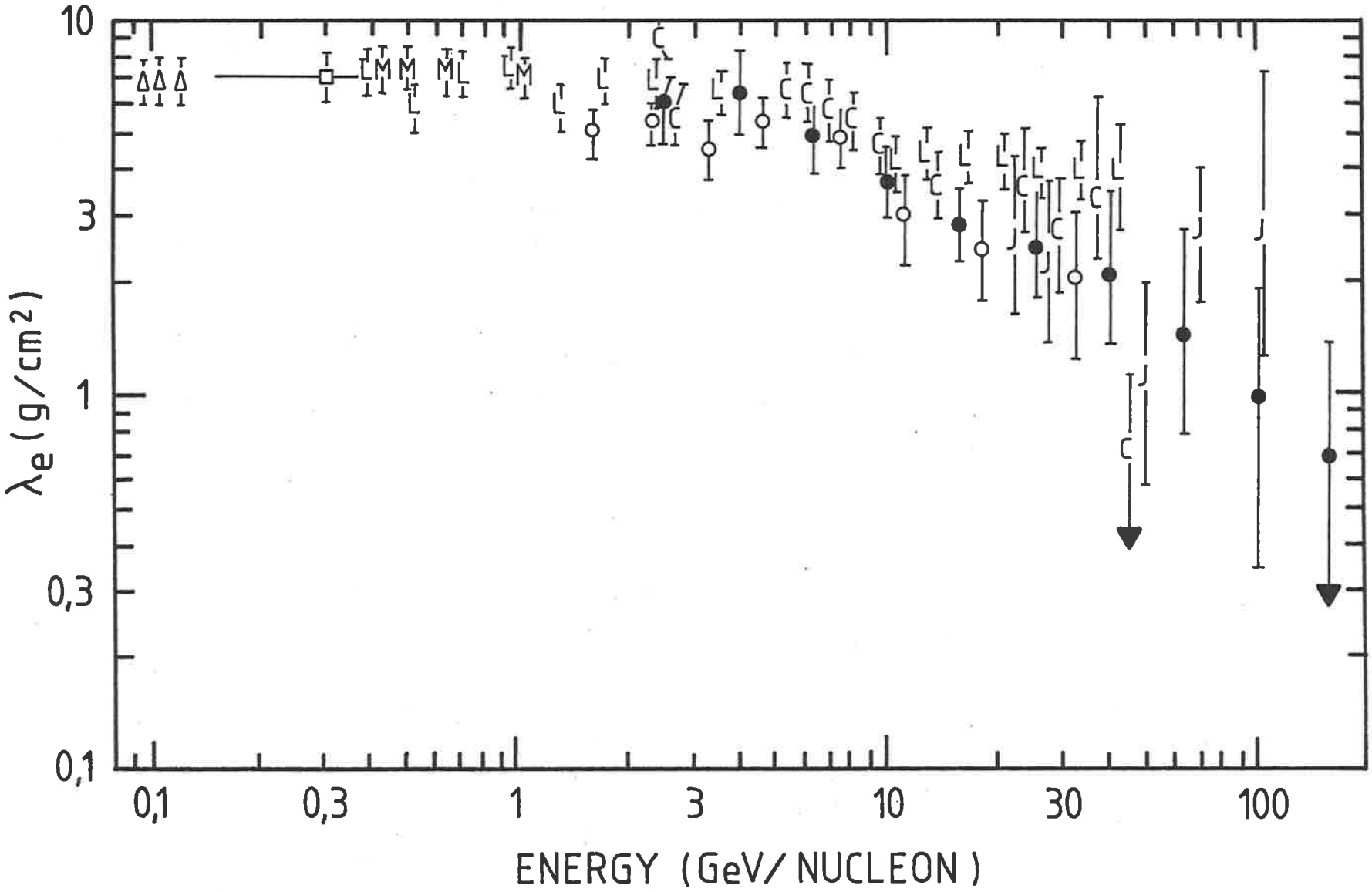

Figure 1.4: Energy dependence of the mean pathlength (g cm^{-2}) of low energy primary cosmic rays. The symbols designate individual experiments referenced in the source; Müller (1982).

excess of ∿2-3 Gev/nucleon the mean path length (λ_e) is given by

$$\lambda_e = (35\pm5)\ R^{-(0.7\pm0.1)}\ g\ cm^{-2}$$

(R is the rigidity GV/c).

Recently it has become apparent that below ∿1-2 Gev/nucleon the mean path length ceases to increase (Perron et al 1981, Protheroe et al 1981) and begins to decrease again (Garcia-Munoz et al 1981). Knowledge of the mean path length traversed by primary cosmic rays and their actual lifetime leads to the conclusion that the mean density of material traversed is ∿0.2 atoms cm^{-3} (Garcia-Munoz 1977), significantly less than the average density of the ISM.

The assumption of a suitable distribution of path lengths (usually exponential) about the measured mean path length enables the observed abundance pattern to be extrapolated back to its source. It would seem (e.g. Cassé and Goret 1978) that atomic parameters, e.g. first ionization potential, not nuclear, are important in the determination of the resulting source abundance patterns. Meyer (1981) notes a similar bias in the abundance pattern of the coronal particles of solar-like stars, suggesting similar injection/acceleration biases for the two sets of particles.

At these energies the flux of particles with charge, z, $\gtrsim$30 is approximately a factor of 10^4 less than that of

the iron nuclei, in spite of the fact that such nuclei constitute ∿2/3 of the known elements. These nuclei are synthesised mainly either by the rapid (r) or slow (s) process of neutron capture, each of which leads to a characteristic elemental abundance pattern and are hence of particular interest. The ratio of the actinides ($30 \leqq Z \leqq 100$) to the platinum-lead group ($84 \leqq Z \leqq 87$) as a measure of the abundance of r-processes elements has attracted considerable attention (Fowler et al 1977, Shirk and Price 1978, Binns et al 1982). Original suggestions of a significant abundance of freshly synthesised r-process material, consistent with a supernova or supernova remnant source (Fowler 1967, Shirk and Price 1978) seem to have given way, with improved techniques and statistics, to models in which r-process elements are not significantly enhanced above normal solar system abundances (Binns et al 1982). The apparent excess of secondary nuclei in the ranges $40 \leqq Z \leqq 48$, $60 \leqq Z \leqq 74$ (figure 1.3), is probably explicable in terms of first ionization potential biases and a slightly greater fragmentation of heavy primary cosmic rays than suggested by current studies (Mewaldt 1981), although Fowler et al (1981) prefer an explanation of the $Z \sim 65$ overabundance in terms of the fission of super-heavy nuclei.

The relative abundance of isotopes of a particular element should reflect the nucleosynthetic history of that element and, to a good approximation, be conserved by any

injection and acceleration processes. Hence, isotopic abundance studies, although relatively new, should be capable of providing considerable information on source abundance patterns. To date the studies indicate a significant overabundance of neutron-rich isotopes, relative to the solar system composition (Mewaldt 1981). In particular:

Ne^{22}/Ne^{20} $\sim$4x solar system ratio

$^{29,30}Si/Si^{28}$ $\sim$1.6x solar system ratio

$^{25,26}Mg/Mg^{24}$ $\sim$1.5-2x solar system ratio.

Although such 'isotopic' anomalies are not unknown in studies of solar system and meteoritic material, the excesses are usually $\lesssim$1%.

At energies in excess of $\sim 10^3$ Gev/nucleus data on individual elements is confined mainly to the more populous H, He nuclei with the results of the JACEE collaboration (Burnett et al 1982) indicating a continuation of the Ryan et al (1972) proton and Helium spectra to $\sim 10^5$ Gev/nucleus. The unique determination of the flux of the important iron nucleus by Sood (1983) must still be regarded as a preliminary result, perhaps providing only a lower limit to the flux at this energy (Clay 1982). With the advent of the Space Shuttle, several groups (e.g. Müller 1982, Ormes 1982) are planning long exposure experiments outside the atmosphere with the aim of making direct measurements of the spectra of individual elements up to $\sim 10^6$ Gev/nucleus.

INDIRECT MEASUREMENTS

Such is the significance attached to the composition in the region $\sim 10^6$ Gev/nucleus where direct measurements are so tantalizingly scarce and the all-particle spectrum exhibits a pronounced steepening (the 'knee') that a great variety of experiments have been performed in an attempt to determine, indirectly, the relative abundance of the two most significant nuclei (H,Fe) in this region. Currently investigations are aimed at determining whether the iron spectrum continues on with the same slope as directly determined at low energy and hence dominates the primary flux at $\sim 10^6$ Gev/nucleus, or whether the composition is essentially similar to that at $\sim 10^2$ Gev/nucleus. In the following section we discuss several experiments designed to answer this question, ignoring, for the moment, those involving atmospheric Cherenkov radiation which are examined in detail in later chapters.

The Tien Shan group have examined the (between shower) fluctuations of the ratio of muon density at a fixed core distance to electron size for extensive air showers (EAS) in this energy region. Heavy primary nuclei are expected to produce a greater average value for this ratio than lighter ones (Hillas 1981b). They find (Nikolsky et al 1981) that their observations are best fitted by a model incorporating the CKP model of nuclear interactions (e.g. de Beer et al 1966) and a primary composition similar to that observed directly at lower energies. Simulations

involving a more standard model of nuclear interactions (radial scaling and increasing nuclear cross-sections [see Chapter 2]) do not produce agreement with observations.

The lateral distribution and other properties of energetic muons ($\sim$220 Gev) observed deep underground have been studied by the Tata Institute. Early analysis of results (Acharya et al 1981) demonstrated poor agreement with models in which the primary composition was either assumed to be unaltered from that observed at low energies or assumed to be enriched in iron at $\sim 10^6$ Gev. Reasonable accord between experiment and theory was however achieved if the composition was assumed similar to that observed at lower energies over most of the range 10^6-10^7 Gev, with a possible decrease in the mean primary mass at $\sim 10^7$ Gev. More recent analysis of the data with the aid of an improved set of simulations to deal with muon interactions in the overlying rock (Yodh et al 1982) demonstrates that good agreement may be achieved with the assumption of a model incorporating standard nuclear physics (radial scaling and increasing nuclear cross-sections) and an enhancement of iron nuclei, to $\sim$40% of the primary cosmic ray flux at $\sim 10^6$ Gev.

A similar situation arose in the study of EAS associated muons by the Moscow group. Early reports of a flux of muons significantly in excess of that predicted by scaling models (Vernov et al 1977) were later discounted with the aid of model calculations incorporating the same

basic assumptions, but paying attention to previously ignored minor effects. Reasonable agreement between the calculated and measured fluxes was observed for scaling models incorporating a mixed composition of ∿40-50% iron in the region 10^6-10^7 Gev (Ouldridge and Hillas 1978, Hillas 1979b). Yodh et al (1982) also report further confirmation of a model of this type from studies of high energy multiple muons observed deep underground at the Homestake goldmine in South Dakota. Such muons originate high in the atmosphere as the decay products of energetic pions and kaons and their flux is extremely sensitive to the mass number of the primary particle ($\sim A^2$, Elbert 1978).

Similar observations of energetic multiple muons have also been conducted by the Utah group (Lowe et al 1975, Elbert et al 1975), although the interpretation of their data would seem more open, e.g. Elbert et al (1981), Elbert (1982). However, in the final analysis the data appear to be consistent with composition enriched in heavy nuclei at $\sim 10^5$ Gev (Elbert 1982). Studies of the relative dispersion of the number of low-energy muons ($\sigma/\bar{N}_\mu$) in showers of a fixed sea-level size conducted by the same group are also consistent with a mixed composition enriched in heavy nuclei at these energies (Elbert et al 1976).

The flux of energetic delayed hadrons at both mountain altitudes and sea-level has been examined by the Maryland group (Goodman et al 1979, 1982). Although both light and heavy primary particles are expected to produce such hadrons, calculations indicate that under certain triggering conditions of the ionization calorimeter, used to detect the hadrons and the associated EAS array, the system provides a particularly sensitive measure of the

fraction of showers initiated by heavy primary particles. Comparisons have been made between the observed rate of delayed hadrons and the rate predicted by various models of primary composition, all of which incorporate radial scaling to simulate the relevant nuclear reactions. Two basic composition models have been examined:

Model I: The light-medium nuclei are assumed to have a common spectral index, γ_P, whilst the iron group nuclei are assumed to have a flatter spectrum, index γ_H, as suggested by direct observations at lower energies.

Model II: Below 10^5 Gev all nuclei are assumed to have a common spectral index, γ, which increases by 0.5 at some magnetic rigidity, Rc.

To date the best values determined for these parameters are:

Model I: $\gamma_P = 2.26 \pm .06$ $\gamma_H = -2.39 \pm .06$

Model II: $\gamma = -2.55 \pm .06$ Rc = 10^6 GV/c.

Differentiation between these models is not currently possible, although comparison between the mountain-level and sea-level results is expected to eventually enable this. We note that both models predict a primary composition of $\sim$40% iron at $\sim 10^6$ Gev, although Model I requires an additional, as yet undiscussed, mechanism to steepen the iron spectrum beyond $\sim 3.10^6$ Gev, in accord with the observed total spectrum (figure 1.1).

The rather simple experiment of measuring the density spectrum of EAS has been shown to be capable of

revealing model independent information on the mean free path of the initiating nucleus (Hillas 1981a). A comparison of the rate of 'dense' air shower cores observed at mountain altitudes with that observed at sea-level leads Hillas to conclude that primary particles in the energy region just before and around the 'knee' have a mean free path of $\lesssim 26 g\ cm^{-2}$ implying a composition containing $\leq 2\%$ protons, if there is no significant alteration in the character of the nuclear interactions.

With the exception of the Tien Shan data it seems that our current observations of EAS in the energy range 10^5-10^7 Gev can be understood in terms of relatively convential nuclear physics, a continuing rise of nuclear cross-sections (Amaldi 1977) and an increasing proportion of heavy primary cosmic rays (see also the review of Gaisser et al 1978). However, in a recent survey of experiments sensitive to the high energy hadrons ($\gtrsim$100 Gev) associated with air showers of energy $\sim 10^6$ Gev, Tonwar (1982) concludes that current observations defy consistent interpretation in terms of the above model and composition.

At energies in excess of $\sim 3.10^6$ Gev measurements of the shape of the spectrum become somewhat confused. The results of Tien Shan (Kirov et al 1981) appear to join smoothly onto the lowest energy points of Haverah Park (Bower et al 1981), whilst earlier measurements, e.g. Vernov and Khristiansen (1967), La Pointe (1968), Efimov and Sokurov (1979), indicate that the spectrum may dip somewhat more

steeply after the knee before rising up to meet the Haverah Park data. It is unfortunate that no experimental data seems to exist to cover the gap between the lowest of the Haverah Park points and the highest of the Tien Shan.

The most comprehensive data on the energy spectrum at the highest energies comes from the large arrays of Haverah Park (Bower et al 1981) and Yakutsk (Efimov 1981). Data from the Sydney group has not been included as a problem exists in the energy assignment of their showers (Bray et al 1981). The Yakutsk data is also somewhat below that of Haverah Park ($\sim$1.25x in energy) and does not seem to show the complex character apparently observed at Haverah Park, possible sources of this discrepancy are currently under investigation (Bower et al 1983). The mere existence of cosmic rays with energy in excess of $\sim 5.10^{10}$ Gev is also somewhat puzzling. Shortly after the discovery of the Universal 2.7 K black-body radiation, it was realised by Greisen (1966) and Zatsepin and Kuzmin (1966) that unless particles with energy in excess of $\sim 5.10^{10}$ Gev originate within $\sim$200Mpc of the solar system, they must be destroyed in interactions with this Universal field of photons.

Data on the composition of primary cosmic rays with energies in excess of $\sim 10^{7}$ Gev must also come from indirect methods, most of which, e.g. Walker and Watson (1981, 1982), Coy et al (1982), Barrett et al (1977), would tend to imply a beam enriched to contain at least 65% protons.

Again we defer discussion on the results of atmospheric Cherenkov studies until a later stage.

1.3.2 ISOTROPY OF PRIMARY COSMIC RAYS

As a nucleus of charge Z moving in a uniform magnetic field of strength, B microgauss has a Larmor radius R given by

$R \sim E/ZB$ E = energy in electron volts/10^{15}

R = Larmor radius in parsec

it is apparent that a galactic magnetic field with a strength of a few microgauss will ensure that, for the bulk of primary cosmic rays, their arrival direction bears little relation to the direction of their source. This precludes a straightforward answer to the fundamental question: are the sources of cosmic rays galactic of extra-galactic?

The detection of a gradient of cosmic rays within the galaxy should provide evidence of a galactic origin, extra-galactic anisotropies having been smeared out within the residence time (Király 1979). Studies of the intensity of gamma-rays with energies ∿100Mev, which are thought to be produced by the nuclear interactions of primary cosmic rays with energy ∿1-10 Gev have been interpreted as implying the existence of such a gradient (Wolfendale 1980) and a consequent galactic origin for these particles. At higher primary energies where arrival directions are still confused by the magnetic field, this technique cannot be employed and the cosmic ray gradient, if it exists, must be searched for as a sideral variation in the intensity of the primary cosmic ray flux observed on earth.

In the case of a galactic origin, it can be shown (e.g. Hillas 1982a) that an estimate of the magnitude of the observed anisotropy (δ) is given by:

$$\delta = \frac{(\text{maximum intensity} - \text{minimum intensity})}{(\text{maximum intensity} + \text{minimum intensity})}$$

$$\sim \frac{\text{time for direct exit}}{\text{confinement time}} \qquad ..(1.1)$$

That is, the magnitude of the anisotropy is inversely proportional to the confinement time of the primary particles. As more energetic particles are expected to be less well contained in the 'magnetic box' of the galaxy, the magnitude of the anisotropy should increase with primary energy for a galactic origin.

The most comprehensive data on the measured anisotropy of primary cosmic rays at all energies in excess of $\sim 5.10^2$ Gev are contained in a series of recent papers by Lloyd-Evans and Watson (1982), Watson (1981) and Linsley and Watson (1977), figure 1.5 is reproduced from Watson (1981). We noted previously (section 1.2.1) that at energies $\lesssim$100 Gev/nucleon direct observations indicate that the mean amount of interstellar material traversed by primary cosmic rays, and hence their confinement time, falls approximately as $E^{-0.4}$. The associated rise in anisotropy (equation 1.1) does not appear to continue to EAS energies for the anisotropy as measured by small EAS experiments is remarkably constant from $\sim 10^2$-10^5 Gev/nucleus (figure 1.5) implying a more efficient confinement mechanism and a nearly constant primary lifetime in this region. Király and Kóta (1979) have interpreted this as even stronger confirmation of a galactic origin for cosmic rays of these energies.

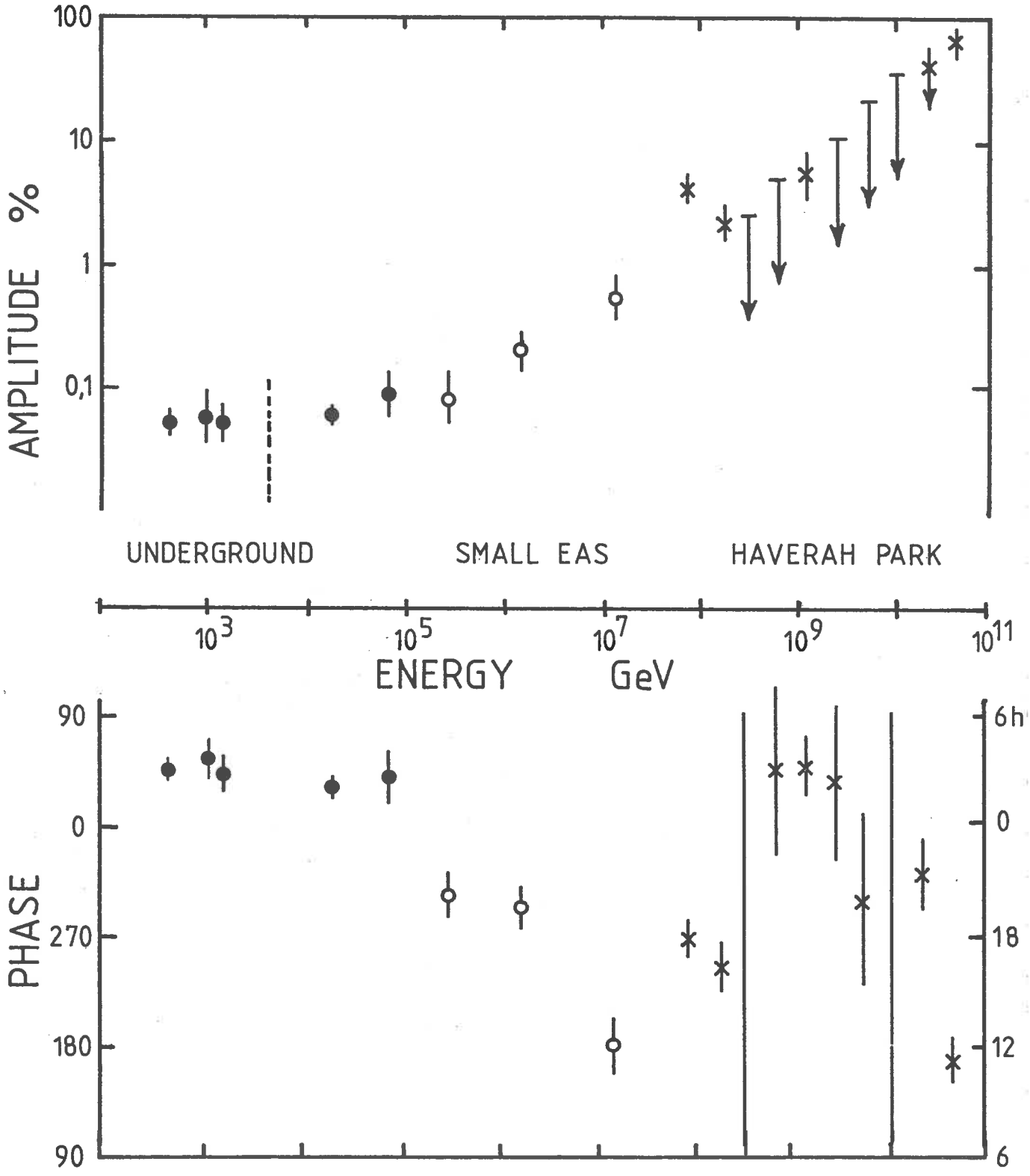

Figure 1.5: The amplitude and phase of the observed anisotropy of primary cosmic rays (after Watson 1981)

Above $\sim 10^5$ Gev/nucleus, in almost the same place as the all-particle energy spectrum shows it marked steepening (figure 1.1), the anisotropy begins to increase with primary energy, again roughly as $E^{0.5}$. The coincidence of these phenomena has often been explained as the result of a sudden decrease in the trapping eficiency of the galaxy as simple diffusive propagation breaks down (Peters 1961, Bell et al 1974), although Hillas (1979a, 1982a) has pointed out that the current implied composition in this energy region (section 1.2.1) does not accord with this simple mechanism. Nuclei of different masses should begin to escape from the galaxy at different values of energy/nucleus and produce a knee with a shape more complex than that observed. Despite the undertainity as to the cause of the anisotropy, its continued rise up to $\sim 10^8$ Gev and the strong constancy of phase amongst independent experiments (e.g. Lloyd-Evans and Watson 1982) argue in favour of a galactic origin up to at least $\sim 10^8$ Gev.

At energies in excess of $\sim 2\text{-}3.10^8$ Gev the Larmor radii of the primary particles are sufficiently large that their paths are not significantly altered by the large scale irregularities of the galactic magnetic field and the interpretation of arrival directions becomes a little more straightforward, although clouded by lack of knowledge of the magnetic field outside the galactic plane. Astley et al (1981) have demonstrated the existence of a significant bias of arrival directions towards southern galactic latitudes

for primary cosmic rays of energy $\sim 5.10^8$-5.10^9 Gev. Assuming that the magnetic field outside the galactic plane is as strong and extensive as evidence by electron synchrotron emission, Hillas (1982a) has shown that the particles are galactic in origin and have a radial density gradient of $\sim$30%/kpc. Alternatively if, as Astley et al (1981) propose, the field is weak, then the particles must originate outside the galaxy and be accelerated in the region of the local group of galaxies. Only a primary beam composed entirely of iron nuclei would be able to satisfy observations if the primaries are galactic in origin and the halo field weak. Above $\sim 3.10^{10}$ Gev, where the influence of the galactic magnetic field is even less, there is increasing evidence of an excess of events from high galactic latitudes and the general consensus is that these particles cannot originate within the galaxy and must originate somewhere within the Virgo Supercluster (see e.g. Watson 1981).

The main weakness in the preceding arguments lies in our lack of knowledge of the structure of the magnetic field over the scale of the galaxy and the uncertainity of the mass of the initiating particle. Current observations in this energy range ($\gtrsim 10^8$ Gev) are not inconsistent with a mixed composition containing up to $\sim$30% iron nuclei (e.g. Chantler et al 1982), consequently it is possible to speculate (Watson 1981) that the currently observed anisotropy is caused by an anisotropic iron component (galactic) mixed with a possibly extra-galactic, isotropic

proton component originating within the Virgo Supercluster. To date no techniques are available to test this hypothesis.

1.4 COSMIC RAY SOURCES AND ACCELERATION MECHANISMS

There is no general agreement on the source of the observed cosmic rays. At the lowest energies ($\sim$1-10 Gev) gamma ray and anisotropy measurements suggest they are probably of galactic origin. At the highest energies, $\gtrsim 10^{10}$ Gev, anisotropy measurements are more consistent with an extra-galactic source. In the intermediate energy range (almost the entire cosmic ray spectrum), there is no clear-cut evidence for either of these two categories. Simple energy considerations suggest that the bulk of these 'intermediate' cosmic rays are unlikely to be of extra-galactic origin, although there are a limited number of extremely energetic objects within the Virgo Supercluster capable of providing an extra-galactic component at these and higher energies (e.g. Silberg and Shapiro 1981). Consequently there is a degree of arbitrariness when deciding which energy regions one considers to be galactic and extra-galactic. With this in mind it is possible to make some tentative suggestions as to the sources and acceleration mechanisms within these two broad categories.

1.4.1 GALACTIC SOURCES AND MECHANISMS

Galactic cosmic rays are assumed to arise from sources within the galactic plane and are confined and isotropised by diffusive scattering off magnetic irregularities

in the interstellar medium. The observed energy variation of the mean path length arises naturally from considerations of an energy-dependent leakage from this galactic 'leaky-box'. However it is also possible to consider that the observed variation is the result of more efficient trapping of low energy particles near their source, before they finally escape into the galactic plane. The so-called 'nested leaky-box' model (Cowsik and Wilson 1973, 1975). In principle it is possible to distinguish between these two major alternatives by examining the actual distribution of observed path-lengths; trapping of all particles for some time near the source region results in a deficiency of short path-lengths in the nested leaky-box model (Cowsik and Wilson 1975). At present, uncertainties in the spallation and destruction cross-sections prevent such a distinction being made (Raisbeck 1979).

Almost every acceleration mechanism proposed for cosmic rays is dependent on the original Fermi (1949) idea of the gradual acquisition of energy by cosmic rays in collisions with more massive, more slowly moving objects. Two variants of this idea are now recognised; that originally proposed by Fermi (Second Order Fermi Mechanism) where the cosmic ray suffers both head-on and overtaking collisions with the other objects and its more efficient refinement, First Order Fermi Mechanism, in which only head-on collisions occur. The recognition that astrophysical shock fronts, such as found at the boundary of a supernova remnant or at

the termination of a super-sonic stellar wind, are capable of trapping and accelerating particles via the efficient First Order Fermi Mechanism has prompted considerable recent theoretical interest in the study of shock front acceleration processes (e.g. Bell 1978a,b, Blandford and Ostriker 1978, 1980, Cassé and Paul 1980).

The underlying idea of shock front acceleration is that sufficiently energetic cosmic rays will be undeflected by the shock itself and are able to 'bounce' freely between approaching scattering centres on either side of the shock and hence undergo first order Fermi acceleration. Particles ahead of the shock will always be overtaken by it as they are constrained, by scattering off self-induced Alfvén Waves (Wentzel 1974), to travel at a velocity very much less than that of the shock. Once behind the shock, the particles are scattered by the turbulent wake of the front and may or may not recross it to gain more energy. The finite probability of not recrossing the front has been shown (Bell 1978a, Blandford and Ostriker 1980) to give rise to a simple power law energy dependence of particles emerging from the shock. Although the idea of acceleration of particles in astrophysical shock fronts is relatively new and lacks strong experimental verification, the notion may be considered as a relatively natural extension of previously observed particle acceleration in interplanetary shock waves, e.g. Earth's Bow-Shock, as recently reviewed by Pesses et al (1982).

The major problems associated with shock acceleration are: a source of 'sufficiently energetic particles' to inject into the mechanism; and the ensuring of prompt acceleration of particles once injected. If the particles are not promptly accelerated, they are subject to significant ionization losses with a consequent distortion of abundance ratios. Also the particles must not suffer so much reacceleration (and consequent spallation) that they cease to accord with the observed secondary to primary ratios (Eichler 1979, 1980). Most authors (Bell 1978b, Blandford and Ostriker 1980, Eichler 1980) seem to agree that sufficient 'suprathermal' particles are generated by the shocks themselves from the surrounding ISM to provide a suitable pool of 'sufficiently energetic particles' whilst ionization losses and excessive production of secondaries can be avoided if the particles are confined mainly to the hot, low density 'coronal' gas phase of the ISM and suffer only occasional reacceleration.

Such conditions are satisfied in the 'Local Superbubble' model of cosmic ray origin of Streitmatter et al (1983), in which the particles reside mainly in the hot phase of the ISM (Superbubble interior) and only those in the region of the walls suffer acceleration due to the occasional collision of a supernova shell with it. Similar models involving the injection of particles from the supersonic stellar winds of clusters of hot, massive, rapidly evolving stars (OB associations) or individual active stars,

and their subsequent acceleration in either standing or propagating shocks associated with the star(s) have been invoked to account for the striking similarity observed between the source abundance patterns of cosmic rays and the abundance patterns of energetic particles found in the corona of solar-like stars (section 1.2.1). Cassé (1982) has also employed these ideas in an attempt to account for some of the isotopic anomalies observed in the source abundance patterns (section 1.2.1). In the model of Cassé a subset of stars (Wolf-Rayet) known to be both rich in ^{22}Ne and ^{12}C and suffering a large mass loss via a strong super-sonic stellar wind are proposed as injectors for these nuclides. Other, minor, variations on this basic theme have been recently summarised by Cassé (1981).

Unfortunately, shock fronts cannot accelerate particles to arbitrarily high energies. Efficient scattering ceases once the Larmor radius of the particle is less than its diffusion mean free path and adiabatic losses become significant if the shock radius and diffusion mean free path are comparable (Cesarsky and Lagage 1981). It seems unlikely that propagating shocks can accelerate a nucleus of charge Z to an energy greatly in excess of $\sim Z.10^5$ Gev and stationary shocks to much in excess of $\sim 2.Z10^6$ Gev, depending on shock life, radius of curvature, etc. (Cesarsky and Lagage 1981). It is interesting that the limiting energy is both charge dependent and occurs in the same energy region as the all-particle spectrum steepens.

As mentioned previously, it has usually been assumed that the energy spectrum knee is associated with some decrease in the ability of the galaxy to contain such energetic particles or some characteristic of the source (e.g. Hillas 1979a). Perhaps it is just where cosmic rays cease to be efficiently accelerated by the Fermi process.

Although shock waves seem a promising means of accelerating galactic particles up to energies $\sim 10^6$-10^7 Gev they appear incapable of producing the highest energy particles required for some models of galactic origin (e.g. Hillas 1982a). Mechanisms which are capable of accelerating particles to these energies have been postulated, but as they are also capable of accelerating particles to the highest observed energies (at which the particles are presumably extra-galactic in origin), they shall be discussed as such.

1.4.2 EXTRA-GALACTIC SOURCES AND MECHANISMS

Considerations of the Larmor radius of a charged particle moving in a magnetic field lead Hillas (1982a) to conclude that few currently known astrophysical objects are capable of satisfying a fundamental limit imposed on all acceleration mechanisms, whether 'one-shot' or statistical processes, namely:

$$BL >> E/ZC$$

B=magnetic field strength(μg), L=size of accelerating region(Kpc)

E=energy of particle/10^{18}ev, Z=charge of particle.

He concludes that we are limited to two basic classes of

objects in which to search for possible accelerators of the highest energy cosmic rays; small highly collapsed objects with intense magnetic fields (e.g. pulsars, active galactic nuclei) or large ($\sim$ mega-parsecs) objects with weak ($\sim$ micro-gauss) magnetic fields, e.g. shock front acceleration in the inter-galactic medium in the turbulent wake of galaxies. In neither class of object does he find a particularly convincing accelerator.

Colgate (1981a,b) is still of the opinion (Colgate and Johnson 1960, Colgate and White 1966) that the explosions of type one supernova are sufficient to account for the entire observed spectrum of cosmic rays.

In any of these extremely energetic processes our lack of detailed understanding of the processes involved limits the discussion of possible mechanisms to debates concerning feasibility alone: pulsars may have a large enough magnetic field to accelerate particles to $\sim 10^{11}$ Gev (e.g. Michel and Dessler 1981) but a layer of ionized gas may short this out first, alternatively the accelerated particles may lose all their energy by synchrotron emission (Hillas 1982a and references therein). Consequently the sources and acceleration mechanisms of cosmic rays of these energies are still very much open questions.

1.5 SCOPE OF THE CURRENT WORK

From the foregoing sections it is apparent that lack of reliable knowledge of the primary composition at energies in excess of $\sim 10^5$ Gev is a source of considerable

uncertainity in our attempts to locate the sources and accelerators of primary cosmic rays. In the remaining chapters we discuss how the observed features of an air shower, in particular the duration of the pulse of Cherenkov radiation produced by its passage through the atmosphere, may be used to draw conclusions about the mass and nuclear interactions of the initiating particle. An experiment to examine this parameter for EAS with vertical sea-level sizes in the range $\sim 10^5$-10^7 electrons is described and analysed with the aid of calculations employing contemporary nuclear physics models. The results of this analysis are compared with those of other similar experiments, where they overlap, and also with the results of other experiments employing considerably different techniques.

CHAPTER TWO

EXTENSIVE AIR SHOWERS

2.1 INTRODUCTION

At the top of the terrestrial atmosphere the integral flux of cosmic rays with energy in excess of 10^5 Gev is approximately one particle per square metre per hour. Therefore, since the integral energy spectrum is steep (figure 1.1), statistically significant direct observations of primary cosmic ray properties and interactions are not possible at energies much in excess of this. Instead observations must be made of the extensive air shower (EAS) of secondary particles produced by the nuclear interactions of the primary particle as it traverses the atmosphere.

In this chapter we first discuss the broad features and currently accepted theories of the nuclear interactions of the primary cosmic ray and examine the behaviour of the main secondary hadrons produced in them. Particular attention is paid to the details of the electromagnetic cascade produced by the decay of secondary neutral pions. The chapter concludes with a discussion of the usefulness of the depth of maximum of the electron cascade and its intrinsic fluctuations as an indicator of the properties of the underlying primary.

2.2 THE MAJOR COMPONENTS

It has long been known from cosmic ray studies that primary cosmic rays incident on our atmosphere do not suffer a single catastrophic collision with another nucleus, instead each primary is involved in a number of inelastic collisions in which it expends an approximately constant fraction of its energy (defined by its inelasticity, $K<1$) in the production of secondary hadrons and usually emerges from the collision as the most energetic or 'leading' particle. The total number of particles produced in each collision is defined as the multiplicity of that interaction. The most populous and important types of secondary hadrons produced in the interactions of the leading particle are the three pions π^+, π^-, π^0 (kaons, nucleons and antinucleons are also produced) which are responsible, via their decays, for the production of the muon (hard) and electromagnetic (soft) components of EAS. The relevant decay modes and half lifes are:

$$\begin{aligned} \pi^0 &\rightarrow \gamma+\gamma \quad T_{\frac{1}{2}} = 7.6.10^{-17} \text{ secs} \quad \text{produces the soft component} \\ \pi^+ &\rightarrow \mu^+ + \nu_\mu \\ & \qquad\qquad T_{\frac{1}{2}} = 2.6.10^{-8} \text{ secs} \quad \text{produces the hard component} \\ \pi^- &\rightarrow \mu^- + \nu_\mu \end{aligned} \qquad \ldots(2.1)$$

The finite lifetime of the muon, 2.2μs, produces an additional contribution to the soft component via the decays:

$$\mu^+ \rightarrow e^+ + \nu_e + \bar{\nu}\mu$$

$$\mu^- \rightarrow e^- + \bar{\nu}_e + \nu\mu$$

These major interactions are illustrated schematically in figure 2.1.

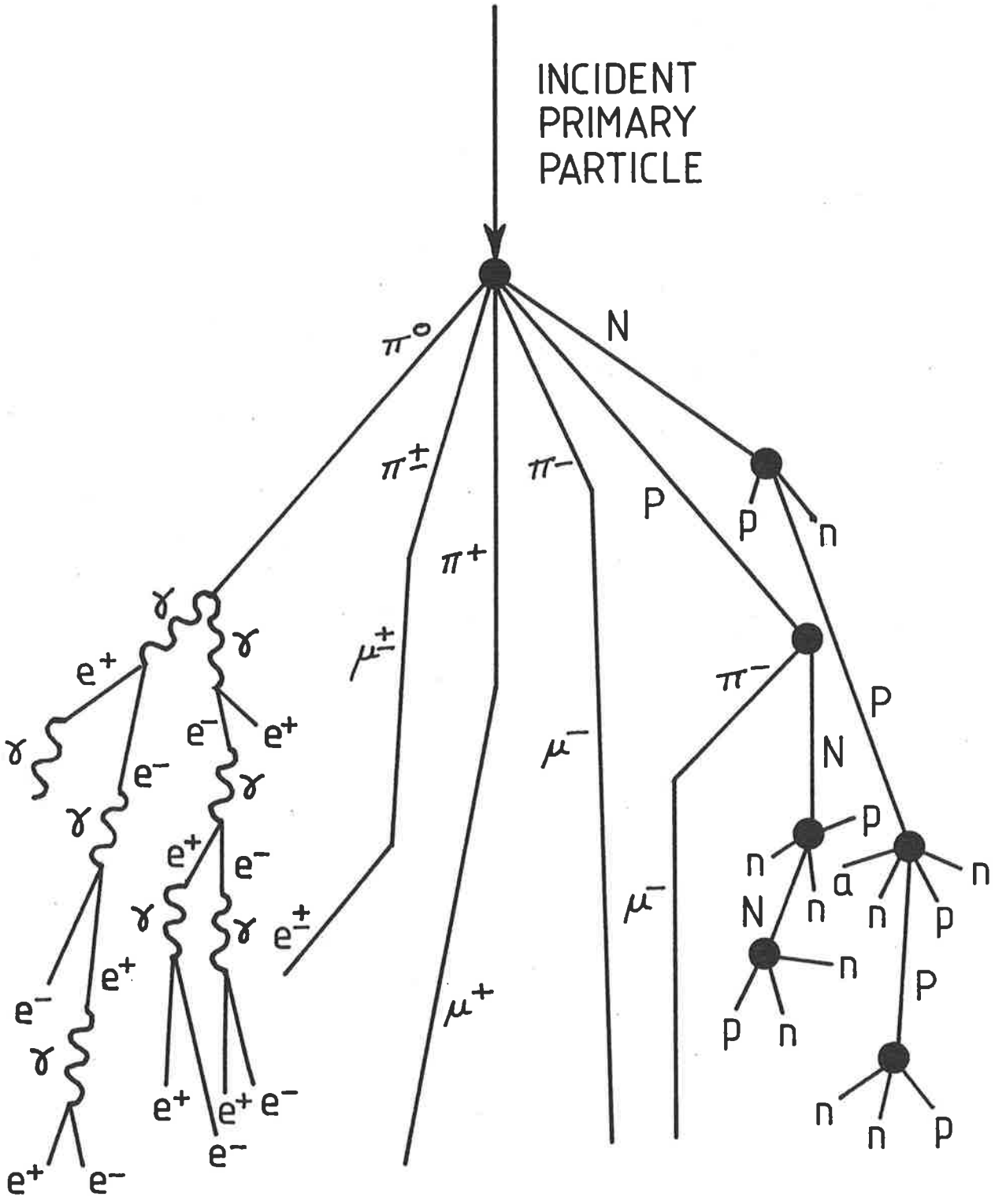

Figure 2.1: Schematic illustration of the major processes occurring in an extensive air shower (after Pomerantz 1971)

The overall growth and decay of the hard and soft components is controlled by the frequency, inelasticity and multiplicity of the interactions of the leading particle. Whilst the energy of this particle is high, large amounts of energy are transformed into secondary particles, and their numbers increase. Eventually however, the energy of the leading particle falls below that necessary to maintain the secondaries in face of their own energy losses and their number, after reaching a maximum, decreases. We might therefore expect a form of equilibrium to be established eventually between the nuclear and secondary cascades. Allan (1971) cites the similarity between the observed decay rate of the soft component (attenuation length) and the rate of energy loss by the leading particle as an example of this.

We now examine each of the three major shower components in turn.

2.2.1 THE NUCLEAR CASCADE

As outlined above, an understanding of the interactions occurring in the nuclear core of an EAS is crucial to the interpretation of EAS experiments. All the observed EAS parameters ultimately derive from these. The very great energy typical of even the smallest EAS, $\sim 10^5$-10^6 Gev, has necessitated the extrapolation of trends in accelerator data to energies two to three orders of magnitude in excess of those at which they were measured. The advent of the new colliding beam machines (e.g., Kalmus 1982) will, for the first time, provide direct measurements

of the relevant parameters at air shower energies and should considerably reduce the uncertainity in current interpretations of EAS experiments.

Some of the most basic features of high energy hadronic interactions had been deduced from cosmic ray studies many years before the arrival of controlled experiments of similar energy (see Feinberg (1972) for a discussion). One most noticeable characteristic was the inhomogeneity of the energy spectrum of the secondary particles: there were a large number ($\sim$80% of all secondaries) of comparatively low energy particles (mainly pions) and a few particles, 'fragments', of much higher energy.

The current convential interpretation of these and more detailed accelerator studies (Laboratory energy $\lesssim 10^3$ Gev) is basically that due to Feynman (1969) where it was proposed, on the basis of electron scattering studies, that nuclear matter was composed of discrete constituent parts or 'partons', now commonly equated with quarks. In analogy with electromagnetic bremsstrahlung Feynman suggested that the passage of a particle through nuclear matter would result in the radiation of particles (pionization) and the possible excitation and fragmentation of the target and projectile. This process is illustrated diagramatically in figure 2.2. Two important predictions

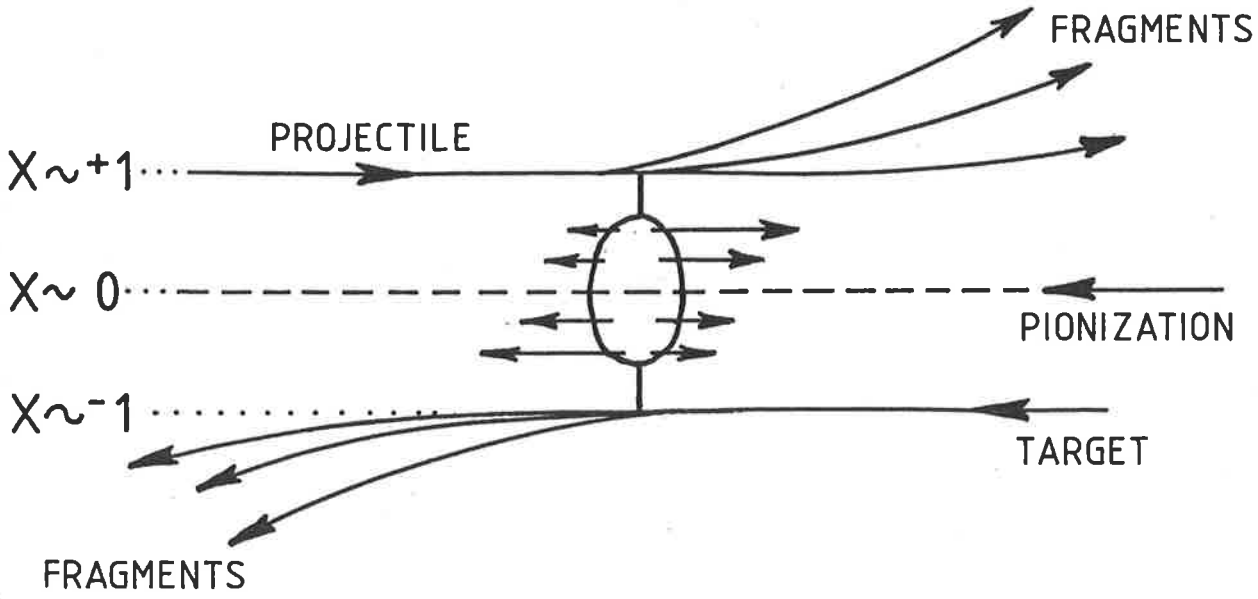

Figure 2.2: Schematic representation of a nuclear interaction as viewed by Feynman (1969) (after Morrison 1973)

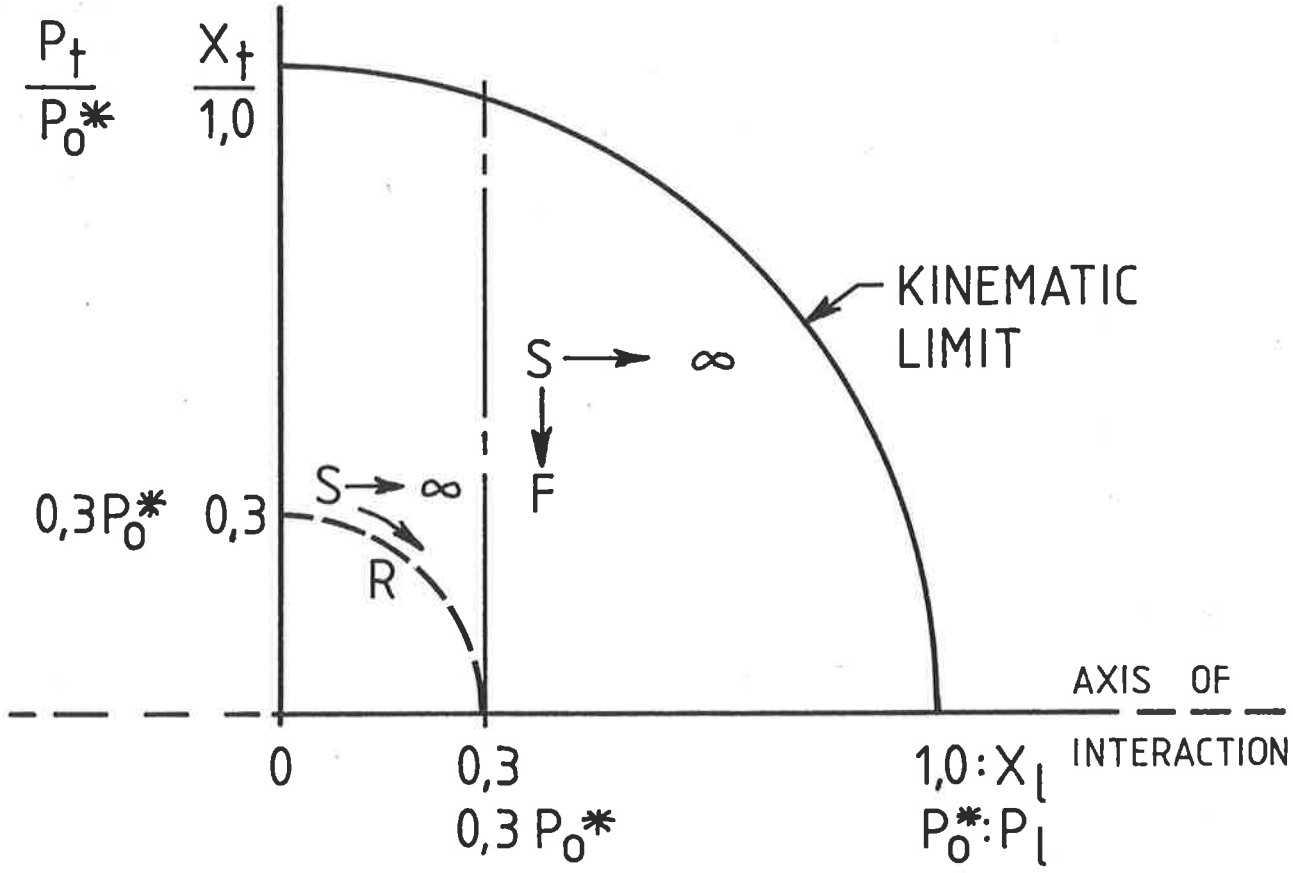

Figure 2.3: The variation of the Feynman scaling variable (F) and the radial scaling variable (R) in momentum space with CM energy (S). (after Taylor 1976)

of the Feynman hypothesis are:

(1) The multiplicity of an interaction, $\langle n \rangle$, should increase in direct proportion to the natural logarithm of the square of the centre of mass (CM) energy (S)

i.e. $\langle n \rangle = a + b\ln(S)$ (a,b constants)

(2) The cross-section for the production of a particle, type C say, in an interaction of the type:

$a+b \rightarrow c+$anything (denoted an inclusive interaction)

should eventually become independent of energy (approach a limiting distribution) as is true of conventional electromagnetic bremsstrahlung. This 'inclusive cross-section' would then be a function only of the transverse momentum (P_t) acquired by C in the interaction and Feynman's scaling variable:

$X^*_\ell = P^*_\ell / P^*_\circ$

P^*_ℓ = longitudinal momentum of C in the CM system

$P^*_\circ$ = maximum available momentum in the CM system

(These variables and the variation of X^*_ℓ with CM energy are illustrated in figure 2.3.)

Hence once the production cross-section for a given interaction had been reliably determined in terms of X_ℓ and P_t in accelerator experiments, it could be 'scaled' to calculate the production cross-section at EAS energies.

The model of Benecke et al (1969) and its associated hypothesis of 'Limiting Fragmentation' implies similar

conclusions to those of Feynman (1969) but is restricted to the fragmentation region of phase space ($X_\ell \sim \pm 1$), i.e. the fragments of the target and projectile should approach limiting distributions as the CM energy increases. The hypothesis of Limiting Fragmentation would form a complete description of an inclusive interaction only if no pionization occurred and the process was completely described by the distribution of the target and projectile fragments.

Some physical basis for these notions arises from accelerator studies of the degree of correlation between the momenta of secondary particles produced in high energy collisions. For such studies, secondary particles are usually characterized by their 'rapidity', y, a generalized velocity defined by:

$$y = \tfrac{1}{2}\mathrm{Ln}([E+P_\ell c]/[E-P_\ell c]) \qquad ..(2.2)$$

E = total energy of particle

c = velocity of light

Figure 2.4 illustrates a 'typical' distribution of the number of particles produced per unit of rapidity in such collisions. The Kinematic limit imposed on P_ℓ by the total energy of the system introduces the notion of a 'maximum' rapidity gap', Y, defined by:

$$Y = y_{max} - y_{min}$$

$$\propto \mathrm{Ln}(S)$$

Rapidity correlation studies (e.g. Amendolia et al 1974) suggest that collisions proceed via the formation of

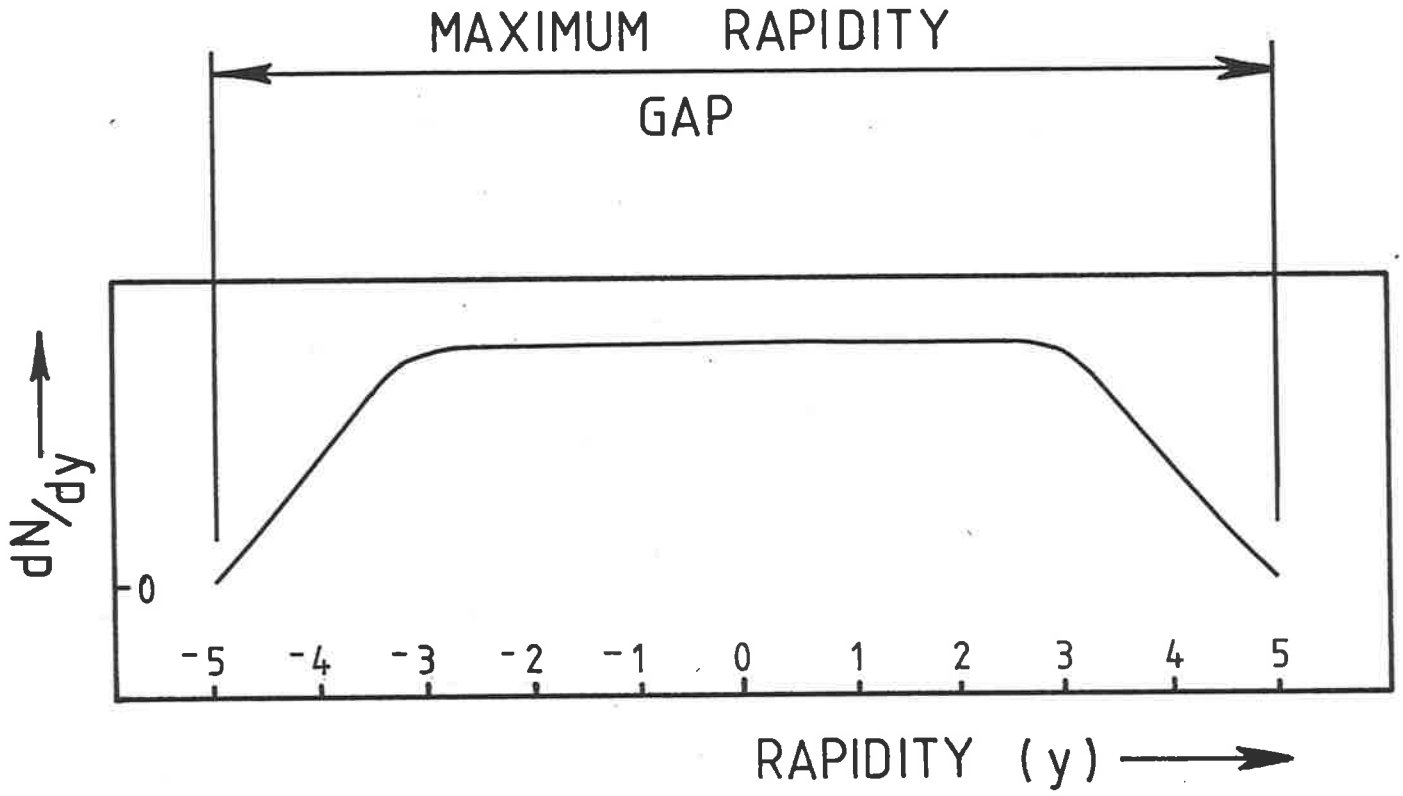

Figure 2.4: Sketch illustrating the main features of the rapidity distribution of particles produced in a 'typical' nuclear interaction. Note, as discussed in the text, that the maximum rapidity gap is energy dependent.

clusters of partons, distributed approximately uniformly over the allowed rapidity range, each of which subsequently decays into $\sim$3 mesons of small relative momenta, typically $\pm$1 unit of rapidity. Thus particles produced with rapidities differing by more than $\sim$2 units are unlikely to be correlated in momentum and vice-versa. In terms of hadronic interactions we see that at low CM energies, where the maximum rapidity gap is small, the produced particles will be highly correlated with both the target and projectile. As the CM energy increases, the maximum rapidity gap exceeds the rapidity correlation length and the particles produced with extreme rapidities (fragments) cease to be correlated and limiting fragmentation is expected. Further increases in the energy of the system result in particles nearer the central region becoming uncorrelated, until finally the whole spectrum approaches a limiting distribution (Feynman scaling).

Although Feynman scaling would appear to have been achieved and verified in the fragmentation region at accelerator energies $\lesssim 10^3$ Gev Lab (e.g. Albrow et al 1974), there exists evidence of a substantial and continuing violation in the central region up to the highest energies so far achieved ($\sim 2.10^5$ Gev Lab), e.g. Guettler, K. et al (1976), Thomé et al (1977), Yamdagni (1982). Feinberg (1972) suggests, on physical grounds, that such a violation is perhaps not unexpected, whilst Taylor et al (1976) note that

some energy dependence of cross-sections is implicit in the choice of X_ℓ as a scaling variable, and find that a better representation of the available CERN ISR data, particularly in the region $X \lesssim 0.2$, is obtained by employing 'radial scaling' (Kinoshita and Noda, 1971, 1973a,b, Yen 1974) wherein cross-sections are parameterized in terms of P_t, X_r, S and X_r is defined by

$$X_r = E^*/E^*_o$$

E^* = energy of particle in CM system

E^*_o = total energy available in CM system.

As $S \to \infty$, $X_r \to X_\ell$ (see figure 2.3) and one expects radial scaling to approach Feynman scaling as the system energy increases, this is indeed observed, although as mentioned previously, in some cases this limit is not achieved at either CERN ISR or $P\bar{P}$ energies.

Although Feynman scaling provides a good description of the observed production cross-sections in the region most relevant to studies of the electromagnetic component of EAS (fragmentation region (see section 2.3)), it is unable to provide a satisfactory description of nuclear interactions in the region most significant to studies of the low energy muon flux (central), e.g. Gaisser et al (1978) and only data from the new accelerators will place the description of nuclear interactions at EAS energies on a firm foundation. Current attempts to deduce the validity of scaling at EAS energies using cosmic ray data are hampered by the uncertainity in the primary mass composition

at these energies. It would seem to be generally agreed that EAS with primary energy in the region 10^5-10^8 Gev develop too rapidly to be compatible with a combination of a pure proton composition and scaling (Tonwar 1981). Reconciliation between experiment and theory is achievable by assuming a combination of either: the continuation of scaling (at least in the fragmentation region) to EAS energies, a continuing rise in total inelastic nuclear cross-sections (Amaldi et al 1977) and a dominance of heavy nuclei ($\sim$40-50% Fe) at $\sim 10^6$ Gev, e.g. Gaisser and Yodh (1980); or the violation of scaling and a composition similar to that determined at lower energies, e.g. Olejniczak et al (1977). Unfortunately it seems as though neither of the above assumptions can explain all the available experimental data, especially those from studies of the hadronic core of EAS (Hillas 1979b, Tonwar 1982).

Models which incorporate scaling violation usually do so by the assumption of a multiplicity which increases more rapidly with energy than the logarithmic increase allowed by scaling, e.g. de Beer et al (1966). The division of energy amongst many low energy particles results in a rapid degradation of the primary energy and enables the shower to reach maximum at a depth consistent with observations. Accelerator results are, as yet, incapable of disproving the assumption of a rapidly increasing multiplicity, although early results from the CERN proton-antiproton collider, $E_{lab} \sim 2.10^5$ Gev, suggest

that models which assume a multiplicity increasing as, or more, rapidly than $E^{0.25}$ are excluded (Alpgard et al 1981). There is also evidence of possible slight violation of scaling in the fragmentation region at these energies (Yamdagni 1982). Gaisser (1982) argues that the effect of the latter, if proven, would be insignificant at energies less than $\sim 10^9$ Gev.

It has been suggested that the occurrence of 'Centauro' events (Lattes et al 1973, Lattes et al 1980) in cosmic ray interactions of energy $\sim 10^5$ Gev indicates the onset of some new nuclear phenomenon. The excess production of charged hadrons typical of these events (e.g. $\sim$50 charged hadrons and at most one neutral pion) could mimic an air shower initiated by a massive primary nucleus. To date the cross-section for Centauro events has yet to be reliably determined, but their absence in the CERN proton-anitproton collider to date (Yamdagni 1982) would seem to imply that they are perhaps characteristic of some exotic nucleus-nucleus interaction (e.g. Gaisser and Yodh 1980).

An interesting topical speculation is that of Cleymans et al (1982). It is not expected that quarks should remain confined to individual nucleons in nuclei once their energy densities exceed that of a single quark inside a nucleon, resulting in the appearance of quark matter. In a conservative analysis Cleymans et al (1982) suggest that sufficiently high energy densities are achieved in heavy ion collisions of energy $\gtrsim 10^5$ Gev. The consequent

appearance of quark matter in the primary cosmic ray beam provides, in their analysis, a consistent explanation of several well-known cosmic ray anomalies, each with a threshold of $\sim 10^5$ Gev, e.g. Centauro events (Lattes et al 1973), the rapid development of EAS (e.g. Wdowczyk and Wolfendale 1972), Tien Shan 'Long-flying Component' (Yakovlev et al 1979), etc. A necessary adjoint of their analysis is the assumption of a significant proportion of heavy nuclei, in excess of 10%, in the primary mass spectrum at $\sim 10^5$-10^6 Gev.

The conservative point of view would favour models which employed the continuation of scaling, at least in the fragmentation region, rising nuclear cross-sections and an increasing proportion of iron in the primary beam. These assumptions agree with what has been directly determined at low energies and do not require any new assumptions. Hillas (1979b) has demonstrated reasonable agreement between such models, incorporating radial scaling, and a range of EAS observations. A similar conservative approach has been adopted by the Durham group who find best agreement for a wide range of EAS measurements, e.g. Gaisser et al (1978), Chantler et al (1983), by employing a 'two component' model to describe the multiplicity distribution. Feynman scaling is assumed to apply in the fragmentation region, but in the central region multiplicity is allowed to rise as $E^{0.25-0.33}$, a predicition not inconsistent with available data. The model also requires an increasing proportion of heavy nuclei and a continued rise in nuclear cross-sections.

Nucleus-Nucleus collisions

At high energies very little accelerator data is available on the mechanics of nucleus-nucleus collisions. In most EAS simulations (e.g. Protheroe 1977) it is usual to assume that a primary nucleus of total energy E and mass number A breaks up completely in its first collision into A nucleons of energy E/A, each of which initiates its own individual air shower. Dixon et al (1974) showed that this 'superposition model', whilst predicting the mean depth of maximum reliably, underestimates the shower to shower variation of depth of maximum. More realistic fragmentation models, incorporating details of nucleus-nucleus interactions observed in emulsion champters at $\sim$20 Gev/nucleon (Gaisser et al 1982) have shown that the relative width of the distribution of depth of maximum is approximately twice that estimated from simulations employing the superposition model. It is noted that these models (Gaisser et al 1982) are in accord with the estimate of mean depth of maximum deduced using the superposition theorem.

2.2.2 MUON COMPONENT

The charged pions produced in the nuclear cascade may either decay into the appropriate muon/neutrino combination (equation 2.1) or participate in further hadronic interactions. The competition between decay and interaction is mediated by the relativistic lifetime (i.e. energy) of the pion and local air density. Protheroe

(1977) indicates that, at a typical production height of ∿5km, pions of energy less than 30 Gev are more likely to decay than interact. At greater altitudes (lower densities) this threshold shifts to higher energies.

Muons may interact with matter by means of either the electromagnetic or weak interactions. Their relatively large mass ensures a negligibly small cross-section for bremsstrahlung and thus once formed they traverse the atmosphere, losing energy only by ionization and Cherenkov emission, to reach the observer unaffected by the cascading processes inherent in the nuclear and electromagnetic components. Consequently the total flux of muons observed at sea-level is an integral of the muon production over the entire length of the shower and contains information on the development of the nuclear cascade. This is in contrast to the electromagnetic component (section 2.2.3) where the sea-level particles are the products of relatively recent, local interactions, not strongly related to the overall EAS development. Also of particular interest are the high energy muons ($\gtrsim$100 Gev) produced at great altitudes in the early nuclear interactions where low air density ensures that few pions have a chance to interact before decaying into muons; these carry relatively direct information on the parent nucleus and its interactions (e.g. Yodh et al 1982).

The sensitivity of the muon flux to details of the nuclear cascade has prompted the development of a variety

of techniques aimed at extracting this information. A number of such techniques, sensitive to primary energies $\sim 10^5$-10^7 Gev, have been discussed previously (in chapter one, section 3.1). Studies of the muon flux associated with EAS induced by primary particles with energies in excess of $\sim 10^7$ Gev are almost entirely the province of groups involved in the Haverah Park collaboration. Here numerous techniques have been applied to examine the sea-level muon flux of EAS with primary energy in excess of $\sim 10^8$ Gev in an effort to resolve the uncertainity in primary composition at these energies, e.g. Earnshaw et al (1973), Gibson et al (1981), McComb and Turver (1982d), Blake et al (1982), Watson and Walker (1981), (1982).

2.2.3 ELECTROMAGNETIC COMPONENT

The half life of the neutral pions produced in the nuclear cascade is so short (equation 2.1) that virtually all neutral pions decay before suffering further hadronic interactions. The high energy gamma-rays produced in this decay may interact with the surrounding matter and transfer their energy to electrons by any of three processes: ejection of a bound electron via the photo-electric effect; scattering off an essentially free electron (Compton interaction); or, if their energy is in excess of $\sim$1Mev, production of a positive and a negative electron (pair-production). The individual cross-sections for these three processes and their sum is illustrated in figure 2.5, from which it can be seen

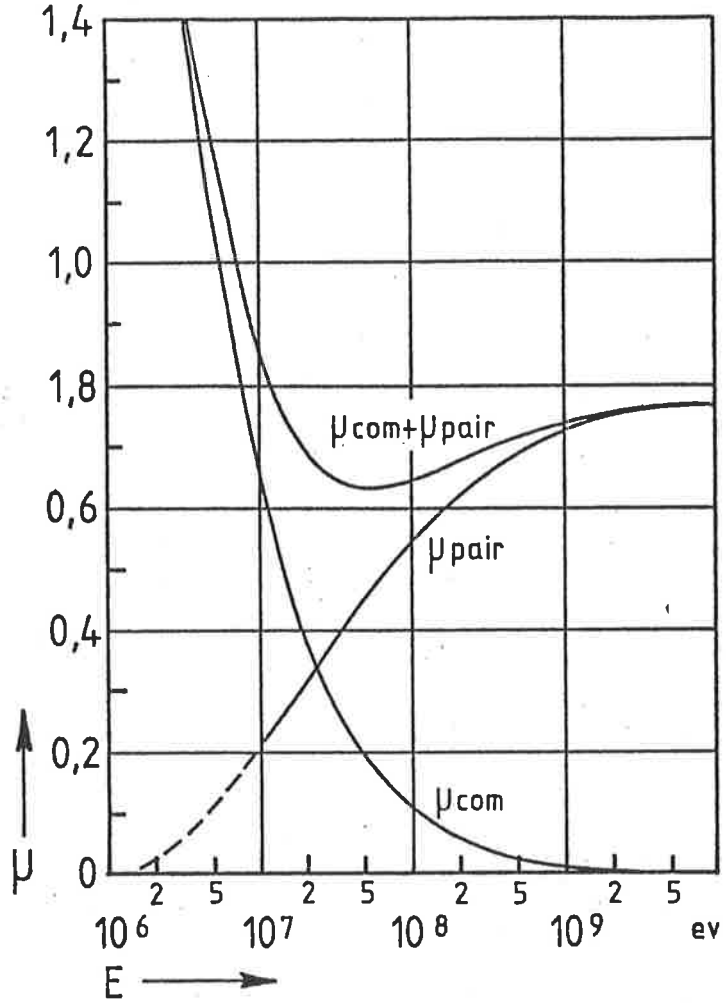

Figure 2.5: The total probability per radiation length for air for Compton scattering, for pair production and for either (after Rossi and Greisen 1941). The photoelectric effect is not significant on this scale.

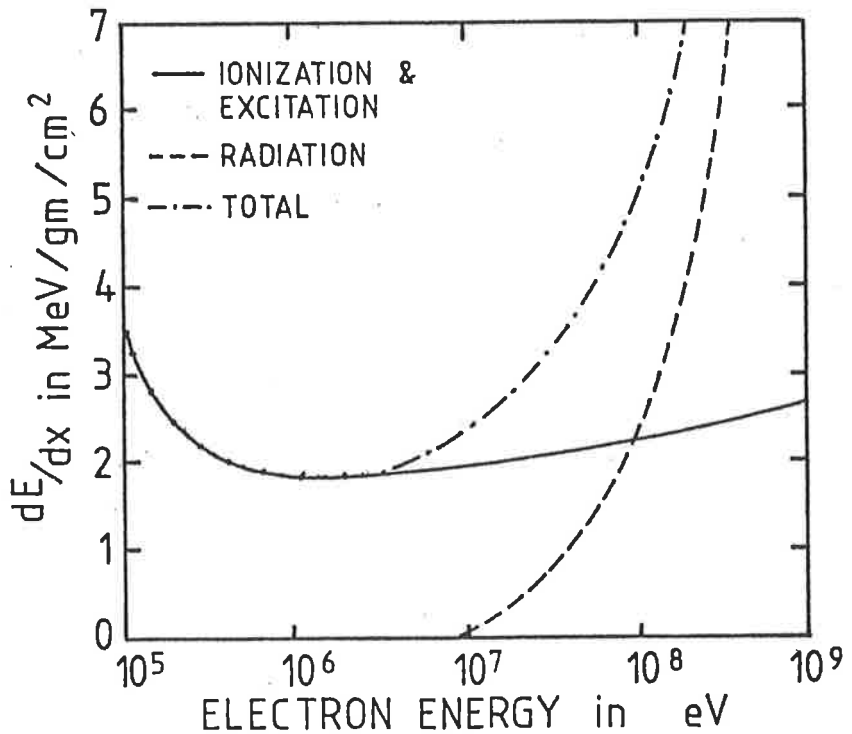

Figure 2.6: The energy dependence of the rate of energy loss of an electron in air by ionization, by radiation and their sum (after Pomerantz 1971)

that high energy gamma-rays will favour the production of energetic electron pairs whilst lower energy gamma-rays will transfer their energy to electrons mainly by Compton and photoelectric interactions.

The electrons produced in the above processes interact with their surroundings mainly by ionizing and exciting atoms they pass or by emitting a photon as they are decellerated in the electric field of a nucleus (bremsstrahlung). From figure 2.6 it is apparent that at high energies one process, bremsstrahlung, is dominant whilst the other dominates at low energies. The dividing line between the two regimes, where an electron loses energy at equal rates by both ionization and bremsstrahlung is the critical energy (E_c) and for air is approximately 77 Mev. Thus at energies in excess of 77 Mev interactions of the soft component are dominated by pair-production and bremsstrahlung and we may write (approximately):

$$\gamma \underset{\text{bremsstrahlung}}{\overset{\text{pair production}}{\rightleftharpoons}} e^+ + e^-$$

Each process has associated with it a characteristic length, of meanfree path, X_c, defined by the equation:

$$\frac{dE}{dX} = \frac{E}{X_c}$$

$$\equiv E = E_o e^{-X/X_c}$$

E = energy of particle (electron or gamma-ray)

X = amount of matter (g cm^{-2}) traversed

For bremsstrahlung this length is the radiation length (X_o). Linsley (1981) gives 36.1 g cm^{-2} as the best estimate of

its value for air. At high energies ($>>E_c$) the mean free path for pair-production is also approximately this value:

$$X_{p-p} = \frac{9}{7} X_o$$

The average distance traversed by a particle before losing half its energy by one of these processes (assuming $X_o \sim X_{p-p}$) is termed a shower unit, R:

$$R = X_o \mathrm{Ln}(2)$$

The concept and basic features of an electromagnetic cascade follow naturally from the preceeding ideas (e.g. Allan 1971).

Assume, as a first approximation, that pair-production and bremsstrahlung are the only significant processes for particles with energy in excess of the critical energy and the interaction length of both processes is one radiation length. The initial gamma-ray (from π^0 decay) of energy E_o will then, on average, interact after one shower unit to produce a positive and a negative electron, each of energy $E_o/2$. On shower unit later, on average, each electron will expend half its energy in the production of a gamma-ray of energy $E_o/4$. This process in which the number of particles is doubled and the energy per particle halved every shower unit is termed an electromagnetic cascade and is illustrated, schematically, in figure 2.7. In this simple model the energy per particle continues to decrease exponentially until it reaches the critical energy where ionization and other energy loss mechanisms are assumed to become effective.

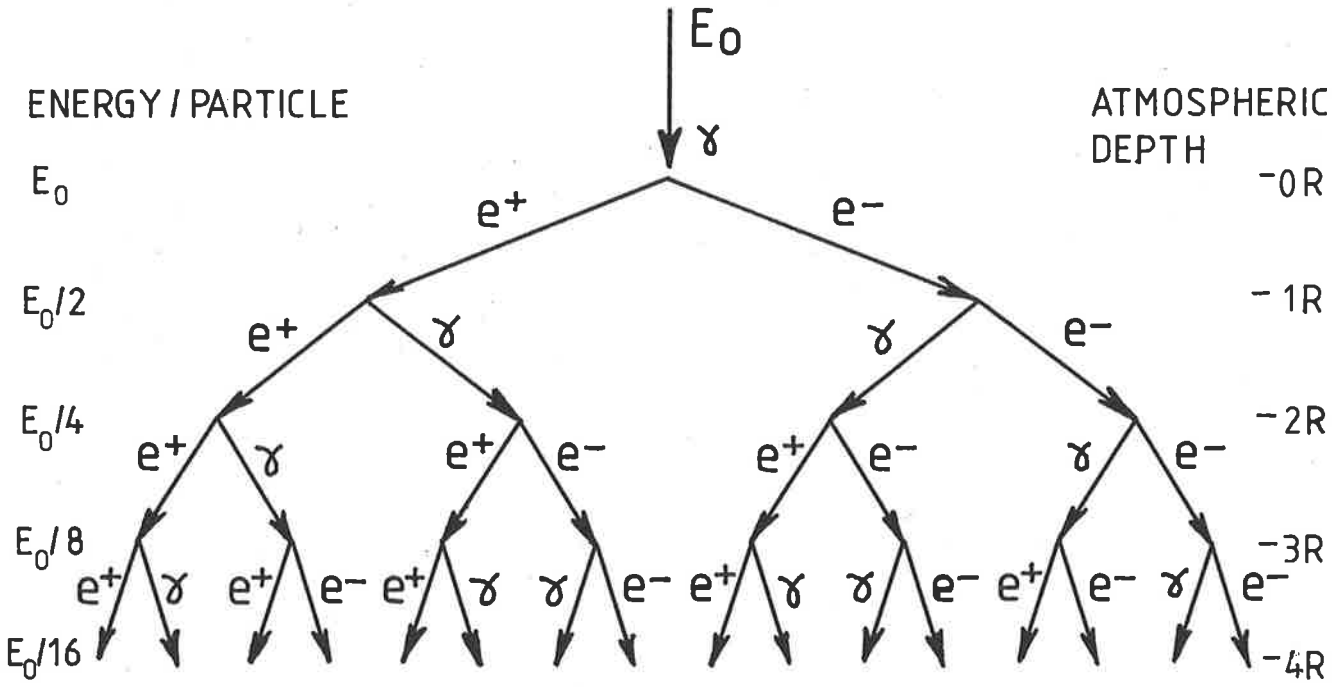

Figure 2.7: Schematic illustration of the initial stages of an electromagnetic cascade.

These prevent further increases in particle numbers and the cascade, in this picture, ceases after a further ~ 40 g cm^{-2} as the particles lose their energy by ionization of the medium.

From the above discussion we conclude that a cascade initiated by a particle of energy E_o and reaching maximum after n shower units has the following properties.

Number of particles at maximum $(e^+, e^-, \gamma) = (E_o/E_c)$ ..(2.4)

$= 2^n$ ..(2.5)

Depth (g cm^{-2}) to maximum $X_{max} = nR$

$= nX_o \ln(2)$ ..(2.6)

Combining 2.5 and 2.6 $X_{max} = X_o \ln(E_o/E_c)$ ..(2.7)

In this simple model all particles at a given depth have the same energy, which decreases with depth as 2^n. Thus the integral energy spectrum, averaged over the whole cascade is:

$$N(>E) = \int_o^{n(E)} 2^n \, dn$$

$$\sim e^{\ln(E_o/E)} / \ln(2)$$

$$\sim \text{constant}/E \qquad ..(2.8)$$

where $n(E) = \ln(E_o/E)$; n = number of shower units

The main results of this simple model are:

(a) Number of particles at maximum is proportional to E_o.

(b) Depth of maximum (g cm^{-2}) is proportional to $X_o \ln(E_o)$.

(c) The integral energy spectrum, for $E > E_c$, averaged over the entire cascade is approximately the same for electrons and photons and is inversely proportional to E.

These results are not in serious conflict with those of more accurate treatments (Rossi and Greisen 1941, Richards and Nordheim 1948, Roberg and Nordheim 1949).

Unlike the other components of an EAS the electrons produced in electromagnetic cascades are subject to significant Coulomb scattering which introduces a significant lateral and longitudinal dispersion into the soft component of an EAS. Roberg and Nordheim (1949) calculate that electrons of energy E(Mev) have an rms angular spread given approximately by:

$$\theta_{rms} \sim 0.66(1+E_s/E)$$

E_s = scattering energy $\sim$ 21 Mev

Consequently 'typical' electrons in an EAS with energies $\sim$30 Mev have an angular spread of a few degrees resulting in electromagneticcomponent spreading out into a thin curved disc, approximately three metres thick and some hundreds of metres in diameter, with the higher energy electrons concentrated towards the centre and front of the disc.

The number density of the electromagnetic component in an EAS, ρ, decreases with distance from the centre of the disc in a manner reasonably well-fitted by the 'NKG distribution' (Greisen 1956):

$$\rho(N,R) = \frac{C(s).N}{R_o}.(R/R_o)^{S-2}\ (1+R/R_o)^{S-4.5} \qquad ..(2.10)$$

N = total number of electrons in disc

R = distance from core

$$C(S) = \frac{\Gamma(4.5-S)}{2\pi\Gamma(S)\Gamma(4.5-2S)}$$

R_o = Moliere radius

$= X_o(Ec/Es)$

The parameter, S, is a measure of the 'age' of the electromagnetic component and equation 2.10 is only strictly defined for a pure electron-photon cascade where S is a monotonic function of the stage of development of the cascade; $0 \leq S < 1$ before maximum, S = 1 at maximum and $1 < S < 2$ after maximum (see figure 2.8) The NKG distribution was originally developed to provide a convenient description of the results of analytical calculations of the lateral distribution of an electron-photon cascade (Nishimura and Kamata 1951). Recently it has become apparent that the lateral distributions observed in Monte-Carlo simulations of electron-photon cascades are, for a given stage of longitudinal development, considerably narrower than those predicted by the NKG formula (Allan et al 1975, Hillas and Lapikens 1977). Thus the properties of an electron-photon cascade, at any stage of development, are no longer adequately described by a unique value of S. Instead an accurate description of the Monte-Carlo simulations requires the assumption of a 'lateral' age parameter ~ 0.2 units less than that predicted by the stage of longitudinal development. Additionally this lateral age parameter must be allowed to vary slightly with radius as illustrated in figure 2.9 (Capdevielle and Garwin 1982). We note, however,

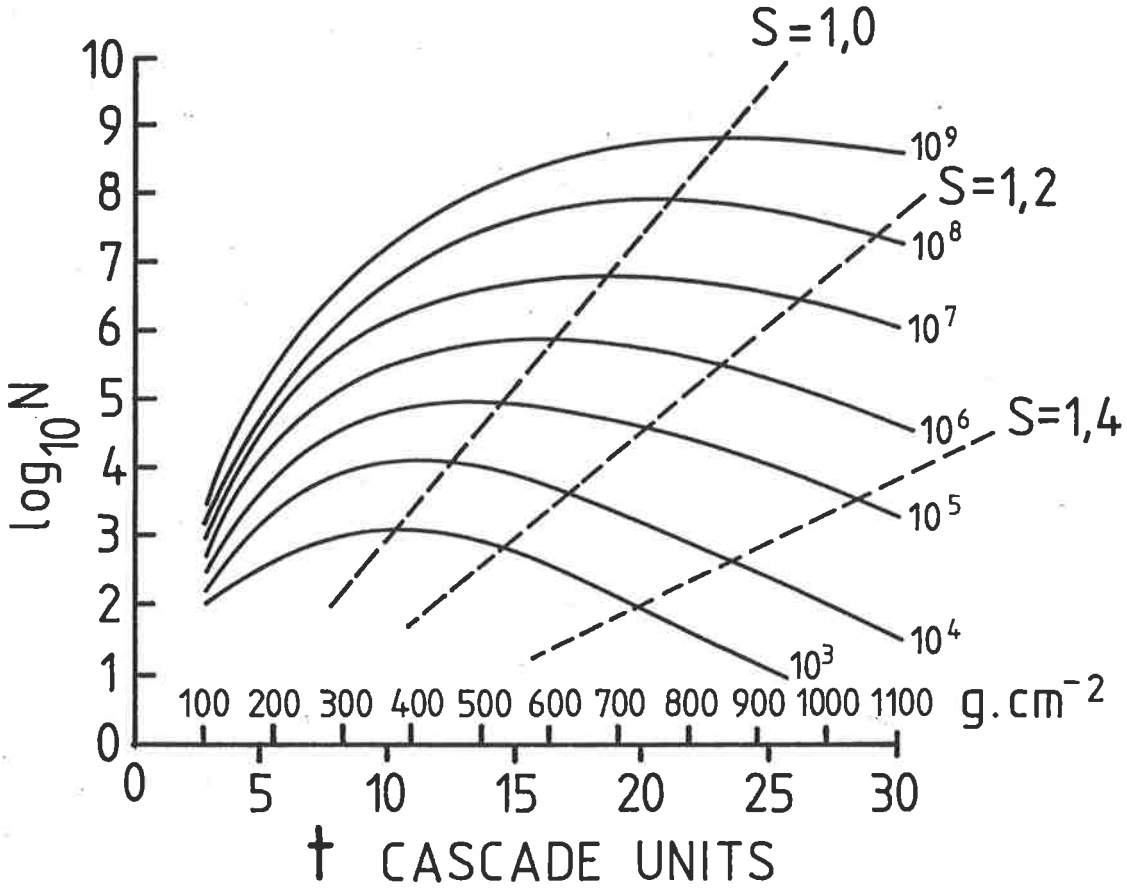

Figure 2.8: Graphical representation of the results of analytical calculations of the number of particles (N) in an electromagnetic cascade as a function of atmospheric depth. The numerals attached to each curve indicate the energy (Gev) of the initiating particle and the dashed lines points of equal age (S). (after Snyder 1949)

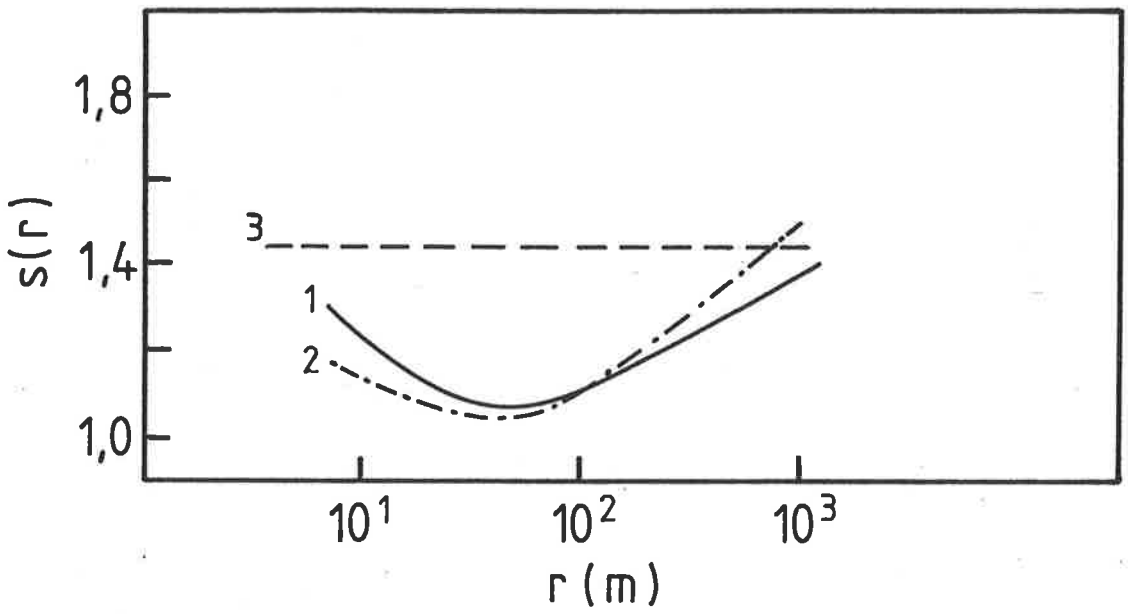

Figure 2.9: Variation of the lateral age parameter in a pure electromagnetic cascade as computed by various authors: (1) Uchaikin et al (1979); (2) Hillas and Lapikens (1977); (3) theoretical age parameter.
(after Capdevielle and Gawin 1982)

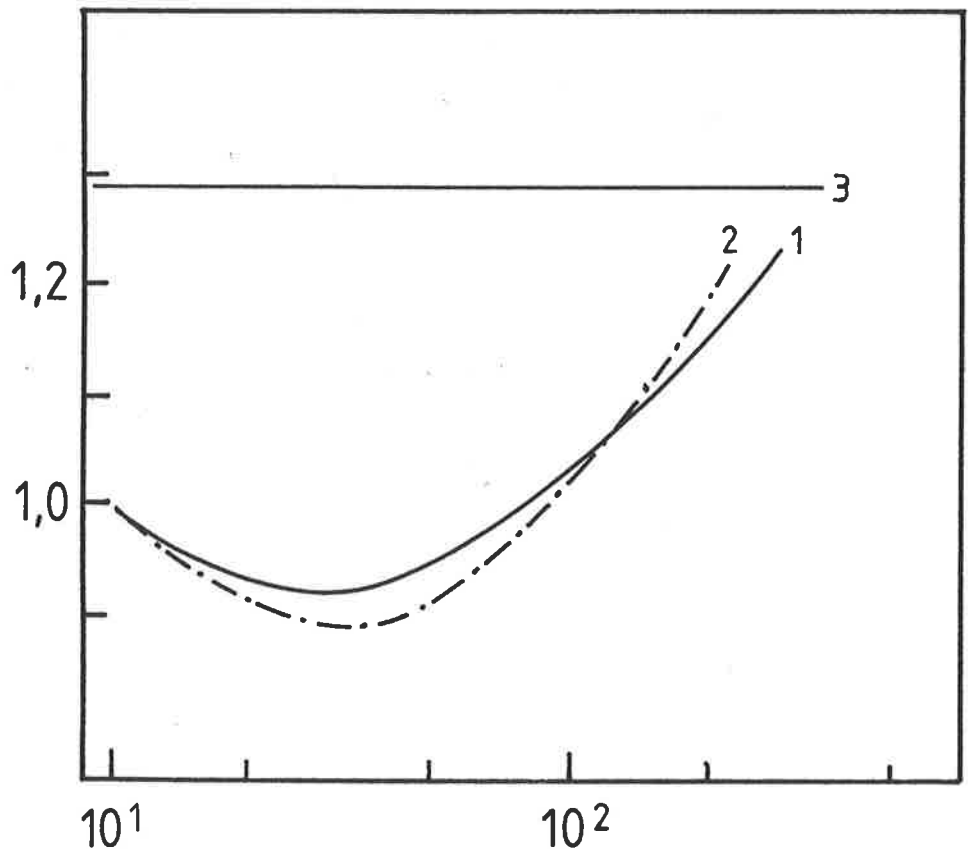

Figure 2.10: The lateral age parameter in EAS for different assumptions of the radial distribution of electrons in an electromagnetic cascade: (1) Uchaikin et al (1979); (2) Hillas and Lapikens (1977); (3) theoretical age parameter.
(after Capdevielle and Gawin 1982)

that the mean value of the lateral age parameter, averaged over radius, is still expected to be a monotic function of the stage of development of the cascade.

In an extensive air shower which is a superposition of many cascades at various stages of development, such a simple relationship would not be expected to persist, although it would be reasonable to expect an EAS observed near maximum development to appear 'younger' than one observed at a later stage of development where it is composed of mainly older, decaying cascades, e.g. Gerhardy et al (1981), Miyake (1981), Asakimori (1981), Abdullah (1981). Tonwar (1981) and Capdevielle and Gawin (1982) caution that selection effects, due to the variation of the lateral age parameter with core distance (see figure 2.10) may affect some of the above experimenters' conclusions.

2.3 DEPTH OF MAXIMUM OF THE ELECTROMAGNETIC COMPONENT

It has already been noted (section 2.2) that the growth and decay of the electromagnetic component of an EAS should contain information on the underlying nuclear interactions; the dependence of one particular parameter, depth of maximum development of the electromagnetic component, on these interactions is now discussed. We restrict our discussion to the two most representative nuclei, those of hydrogen and iron.

2.3.1 FACTORS INFLUENCING THE DEPTH OF MAXIMUM

The depth of maximum development of the electromagnetic component and its shower-to-shower fluctuations

are determined by the mass, energy per nucleon and mean free path of theinitiating nucleus and the multiplicity and inelasticity of its interactions. The superposition model of nucleus-nucleus collisions (section 2.2.1) implies that all EAS initiated by primary particles of the same energy per nucleon will have the same depth of maximum. For a given primary species this depth will fluctuate from shower to shower by an amount determined by the mass and mean free path of the species. Extrapolations of current accelerator data predict that the mean free path of a 10^6 Gev proton in air is expected to be $\sim$60g cm^{-2} (e.g. Hillas 1979b, Yodh et al 1982) whereas that of an iron nucleus should be considerably smaller $\sim$14g cm^{-2} (e.g. Westfall et al 1979). As there is a significant chance ($\sim$5%) of the leading particle surviving three interaction lengths without interacting, the major hadronic interactions of the leading particle, which provide the observed secondary particles, will be subject to a much greater variation in atmospheric depth in proton induced EAS ($\sim$3x60g cm^{-2}) than in iron induced EAS ($\sim$3x14g cm^{-2}). Variations in the depth of first interaction will be most significant in determining the depth of maximum development. The effect of subsequent fluctuations in the depth of π^0 production is smoothed somewhat by the slow growth of the initial energetic electromagnetic cascades (equation 2.7 implies that a 100 Gev cascade reaches maximum development

after $\sim$260g cm^{-2}, c.f. nuclear mean free path $\lesssim$60g cm^{-2}). Fluctuations are further reduced for showers initiated by heavy nuclei by the averaging effects of the superposition on many (e.g. 56 for Fe) equal energy showers. For reasons analogous to the above, nuclear physics models which share the available interaction energy amongst a large number of secondary pions, e.g. CKP, will predict, for a given primary species, a smaller depth of maximum, less subject to fluctuations than those models which share it amongst relatively few, e.g. Scaling. In conclusion we see that we expect showers induced by heavy nuclei to reach maximum at smaller mean atmospheric depths and to fluctuate less about this mean than those induced by light nuclei; the differences in mean depth of maximum and degree of fluctuation will be determined by the nature of the nuclear interactions of the primary particle.

The first efforts to quantify these effects were made by Linsley (1977) who introduced the term 'elongation rate' to describe the rate of increase of depth of maximum with primary energy. This attempt was modified and improved by Hillas (1978), Gaisser et al (1978), Gaisser et al (1979). The salient features of these papers are summarised below.

In the event of an energy independent composition and nuclear mean free path Linsley (1977) noted, as previously discussed, that the depth of maximum was primarily

controlled by a few major interactions occurring at fixed locations in the atmosphere. The sole cause of the increase of depth of maximum with energy was just the lengthening (elongation) of these early cascades as the energy of the neutral pions producing them increased. Hence one might expect on the basis of equation (2.7):

$$X_{max} = X_o \, Ln(E_{\pi^0 \ eff}) + \text{constant} \qquad ..(2.11)$$

Where $E_{\pi^0 \ eff}$ is the energy of those neutral pions most effective in elongating the electromagnetic cascade, i.e. those produced in the fragmentation regions. If we assume that the available energy is distributed uniformly amongst the relevant secondary pions, we have:

$$E_{\pi^0 \ eff} = E_o/\langle n \rangle \qquad ..(2.12)$$

$\langle n \rangle$ = multiplicity in fragmentation region

$= K \, E_o^{\alpha}$

$\neq$ total secondary multiplicity

combining 2.11 and 2.12 we have:

$$X_{max} = (1-\alpha) X_o \ln(E_o) + \text{constant}$$

which generalises, via the superposition theorem, to:

$$X_{max} = (1-\alpha) X_o Ln(E_o/A) + \text{constant} \qquad ..(2.13)$$

E_o = total energy of nucleus

A = mass number of nucleus

hence:

$$\left.\frac{dX_{max}}{d\ln(E)}\right|_{A = \text{const}} = (1-\alpha) X_o \qquad ..(2.14)$$

where α = logarithmic derivative of secondary multiplicity in the fragmentation region

$\alpha_{min} = 0$ (scaling models)

$\alpha_{max} = \frac{1}{2}$ (determined by energy conservation)

Gaisser et al (1979) estimate $\alpha \sim .23 \pm .11$ for most realistic models of nuclear interactions. Equation 2.14 is the result of Linsley (1977). 'In the event of energy independent cross-sections and composition the elongation rate is bounded above by X_o' (and below by $X_o/2$).

Hillas (1978) noted that energy was first carried as part of the hadronic cascade and then as part of the pion cascade before entering an electromagnetic cascade, thus any energy dependence of nuclear of pionic mean free paths would be expected to alter the elongation rate, e.g. increasing nuclear cross-sections would reduce the elongation rate. Allowing for these effects we arrive at the 'complete' expression for the elongation rate, in the event of energy dependent composition and interaction lengths, as expressed by Gaisser et al (1979), in more practical units:

$$\frac{dXmax}{d\log_{10}E_o} \sim 85(1-\alpha)\left[1-\frac{d\log_{10}A}{d\log_{10}E_o}\right]+ k\,\frac{d(\lambda_\pi+\lambda_n)}{d\log_{10}E_o} \qquad ..(2.15)$$

where $k \gtrsim 1$; λ_π, λ_n are nuclear and pion interaction lengths respectively. The effect of energy dependent interaction lengths (last term equation 2.15) has been estimated at -20 ± 10g cm^{-2} (Gaisser et al 1979). We note that scaling always produces the maximum elongation rate and that a

'violation' of Linsley (1977), i.e. an elongation rate in excess of $\sim$85g cm^{-2} per decade of primary energy, necessitates a mean primary mass that decreases with energy; regardless of the model of nuclear interactions. Table 2.1 lists values of the elongation rate predicted by this equation for various combinations of composition and nuclear interaction.

The accuracy of equation 2.15 has been examined by several authors (see Linsley and Hillas 1981, McComb and Turver 1982a) who find, for simple scaling models with energy independent cross-sections and composition, elongation rates in excess of that predicted by equation 2.15 (viz. $\sim$97g cm^{-2} per decade). Hillas (1981c) has demonstrated this to be due to the neglect of the energy dependent decay of the charged pions in the nuclear cascade. As the primary energy increases, a smaller fraction of these pions decay into muons, instead they participate in further interactions, lengthening the 'pion cascade' (Hillas 1978) and consequently the overall electromagnetic cascade. Thus, in the event of energy independent nuclear cross-sections and composition the depth of maximum, is expected to increase more rapidly with energy than predicted by Linsley (1977).

McComb and Turver (1982a) have computed the expected elongation rates for a variety of models of nuclear interactions and find, in addition to the above, that the model which best fits their EAS observations (Chantler et al 1983) predicts a variation in the elongation rate with energy from $\sim$90g cm^{-2} per decade at $\sim 10^5$ Gev/nucleon to $\sim$50g cm^{-2} at $\sim 10^9$ Gev/nucleon, with no associated

composition	nuclear physics model	elongation rate
energy independent	energy independent cross-sections + scaling	85 g cm^{-2}/decade
energy independent	energy independent cross-sections + extreme scaling violation ($\alpha=\frac{1}{2}$)	42.5 g cm^{-2}/decade
changes from Fe to Protons over one decade of energy	energy independent cross-sections + scaling	234 g cm^{-2}/decade
changes from Fe to Protons over one decade of energy	energy independent cross-sections + extreme scaling violation ($\alpha=\frac{1}{2}$)	117 g cm^{-2}/decade

Table 2.1: Elongation rates according to equation (2.15). The effect of rising nuclear cross-sections would be to reduce each of the above by $\sim$20g cm^{-2}

change in composition - in distinct contrast to the early Linsley (1977) suggestion.

2.3.2 FLUCTUATIONS IN THE DEPTH OF MAXIMUM

For a given primary energy and nuclear species the depth of maximum of the electromagnetic component will fluctuate from shower to shower as a result of three major effects: variation in the depth of the initial interaction; fluctuations in the development of the shower; and, in the case of massive primary nuclei, fluctuations in the break-up of the primary particle.

If only the first of these effects was significant the depth of maximum, at fixed primary energy for a given nuclide, would be exponentially distributed and the width of the distribution characterized by the mean-free path of the primary. As the mean depth of energy deposition in an air shower, $\langle X \rangle$, is given by:

$$\langle X \rangle = \langle X \rangle_n + \langle X \rangle_\pi + \langle X \rangle_{em}$$

where $\langle X \rangle_{n,\pi,\ em}$ refer to the mean depths of energy deposition of the nucleonic, pionic and electromagnetic components and $\langle X \rangle \propto X_{max}$ (Hillas 1978) this exponential distribution of depth of maximum will be broadened by any in-shower fluctuations of $\langle X \rangle_n$, $\langle X \rangle_\pi$ and $\langle X \rangle_{em}$. Walker and Watson (1982) argue that the relatively large numbers of energetic particles present in both the pionic and electromagnetic components will ensure that development fluctuations are dominated by fluctuations in the nuclear core, i.e. $\langle X \rangle_n$, and that these fluctuations should also scale with the

mean free path of the primary. This conclusion is supported by the calculations of Ellsworth et al (1982) who find that fluctuations in the pionic and electromagnetic components of proton initiated air showers are insignificant if the mean free of the proton is $\gtrsim$15g cm^{-2}.

For massive nuclei, where the distribution of initial starting points is much less than that of a proton, it is thought that fluctuations in the depth of maximum development result mainly from variations in the initial break-up of the primary and fluctuations in the development of the shower (e.g. Gaisser et al 1982, Watson 1982). It would also seem, at least near $\sim 10^8$ Gev, that for iron nuclei the fluctuations are dominated by variations in break-up and change only slowly with energy (mean free path) (Watson 1982).

The paucity of available data has restricted most experimental examinations of the depth of maximum distribution to simple determinations of its width (standard deviation), e.g. Walker and Watson (1982), Chantler et al (1982). Even so, such measurements, when combined with the previously determined mean depth of maximum at a given primary energy, are capable of providing reasonably good constraints on the mass of the primary particle and the nature of its nuclear interactions (e.g. Chantler et al 1983). Recently, attention has been directed to measurements of the actual shape of the depth of maximum distribution (Stanev et al 1982, Ellsworth et al 1982). These authors

note that even in the presence of a mixed primary beam the tail (large X_{max}) of the depth of maximum distribution arises mainly from proton interactions and as such the slope of the distribution in this region is characteristic of the proton mean free path. Preliminary results of experimental determinations of the proton-air mean free path at $\sim 2.10^8$ Gev employing this technique have been reported recently (Coy et al 1982, Cassidy et al 1982).

C H A P T E R T H R E E

CHERENKOV RADIATION FROM EXTENSIVE AIR SHOWERS

3.1 INTRODUCTION

In this chapter we first discuss the production mechanism and general properties of Cherenkov radiation, then examine details of the Cherenkov radiation produced in the atmosphere by cosmic ray air showers. The usefulness of this radiation as a tracer of the development of the electron component of individual air showers is discussed in detail. Particular emphasis is placed on measurements of the arrival time distribution of the Cherenkov flux.

3.2 PROPERTIES OF CHERENKOV RADIATION

The properties of Cherenkov radiation are consistent with the theory proposed by Frank and Tamm (1937) and Tamm (1939), shortly after the pioneering investigations of Pavel Cherenkov (see e.g. Cherenkov 1958). Although based on classical electromagnetism, the theory of Frank and Tamm is little altered by consideration of quantum effects (Ginsburg 1940, Cox 1944) as Cherenkov radiation is the result of a large number of relatively minor long-range interactions between a charged particle and atomic electron clouds in which quantum effects are negligible.

The passage of a charged particle near an atom induces a time varying polarization of the atomic electron

cloud (figure 3.1) resulting in the emission of electromagnetic radiation which propagates through the medium with a phase velocity, c/n, (here, in a convention assumed for the remainder of the chapter, c represents the velocity of light in vacuo and n the refractive index of the medium). If the velocity of the charged particle is less than that of the electromagnetic radiation, the Huygens wavelets produced by individual atoms will, on average, interfere destructively and there will be no resultant electromagnetic field at distances in excess of a few wavelengths. If, however, the velocity of the particle is greater than the wave-front velocity, individual Huygens wavelets will interfere constructively to produce a conical wavefront (see figure 3.3). The wavefront travels at an angle θ_c to the path of the particle where, for a particle of velocity v, θ_c is given by the relation:

$$\cos(\theta_c) = \frac{c/n}{v} = 1/\beta n \qquad ..(3.1)$$

Equation 3.1 implies the existence of a velocity threshold, determined by the refractive index of the medium, below which no Cherenkov emission is possible and above which radiation is emitted at a velocity-dependent angle, also dependent on the refractive index of the medium. Specifically we have, from equation 3.1, for a particle of rest mass m_o

threshold velocity: $(\theta_c=0)\ \beta = \frac{1}{n}$

$$\therefore E_t = m_o c^2 (1-1/n^2)^{-\frac{1}{2}} \qquad ..(3.2)$$

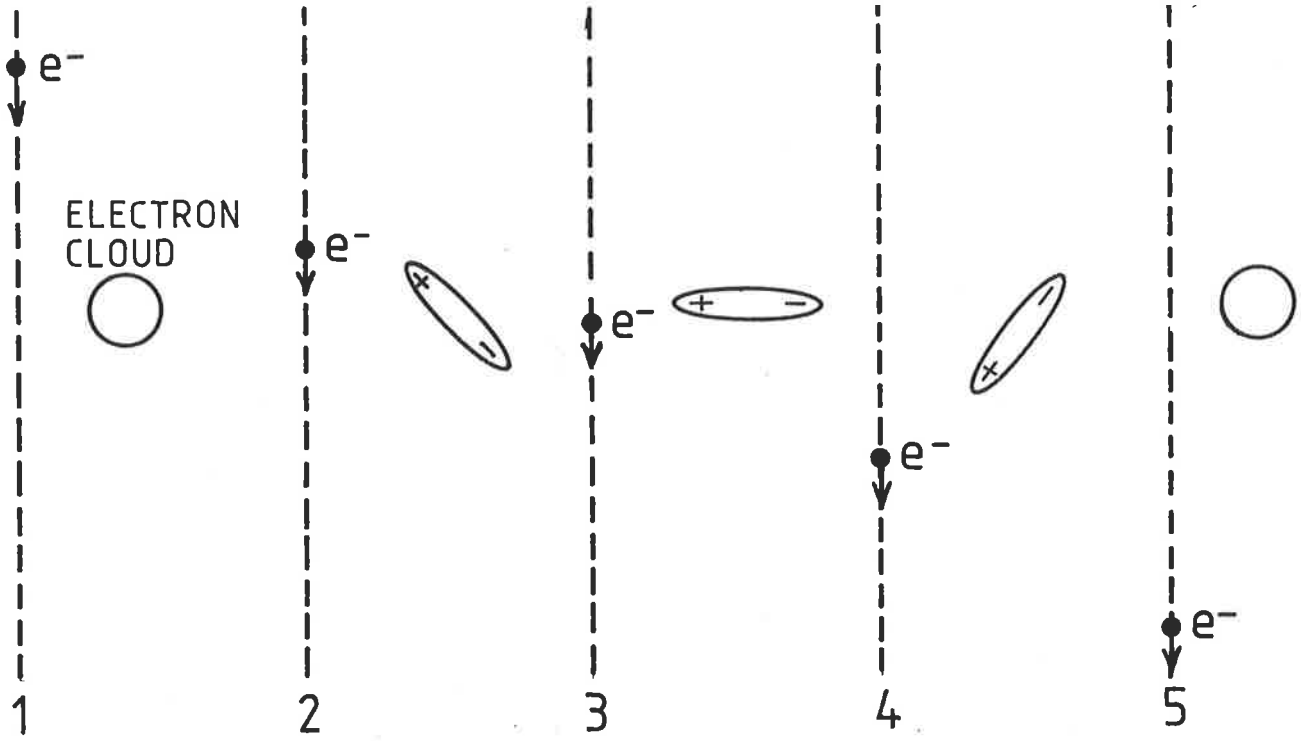

Figure 3.1: Sketch illustrating the time dependent polarization of an atomic electron cloud induced by the passage of a charged particle.

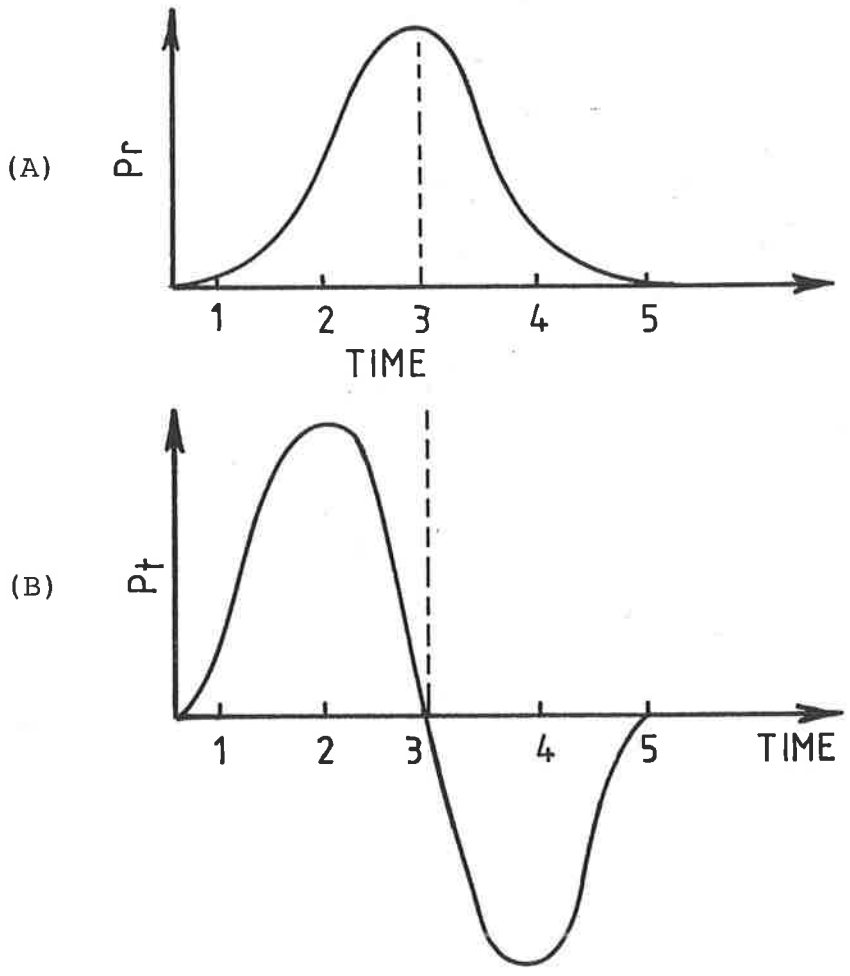

Figure 3.2: Sketch of the radial (a) and longitudinal (b) polarization of the atomic electron cloud in figure 3.1 as function of time. The numerals indicate the corresponding phases in figure 3.1. (after Jelley 1982)

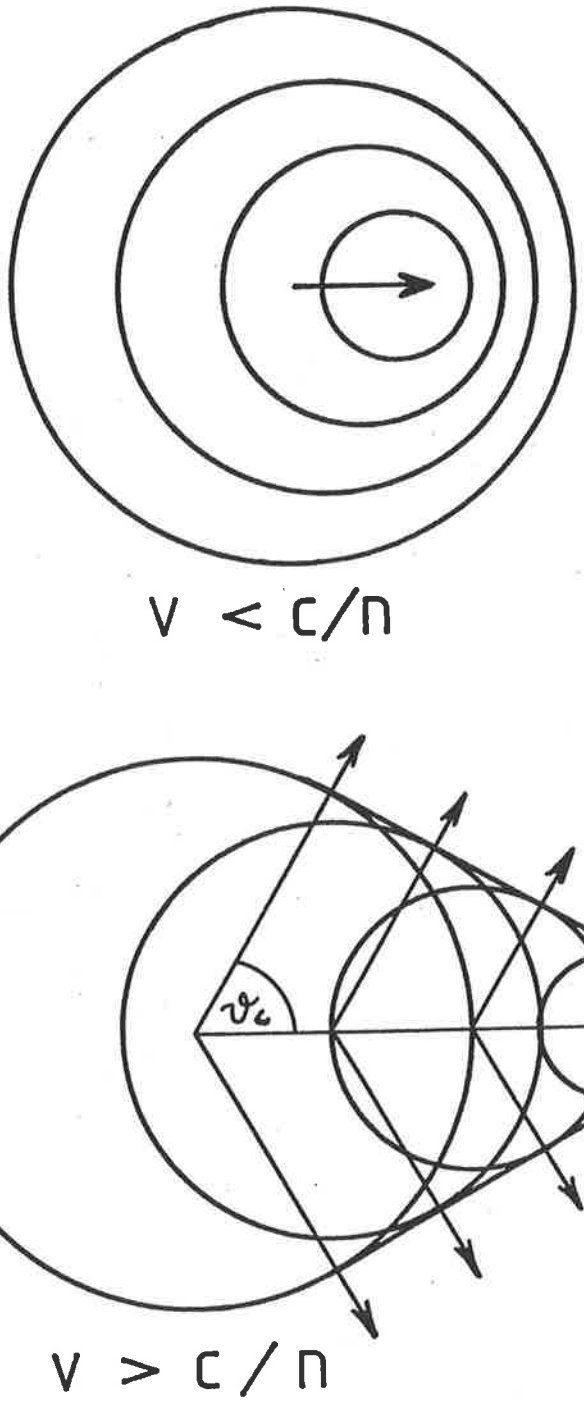

Figure 3.3: Huygens construction illustrating the production of Cherenkov radiation in a medium of refractive index n by a particle of velocity v.

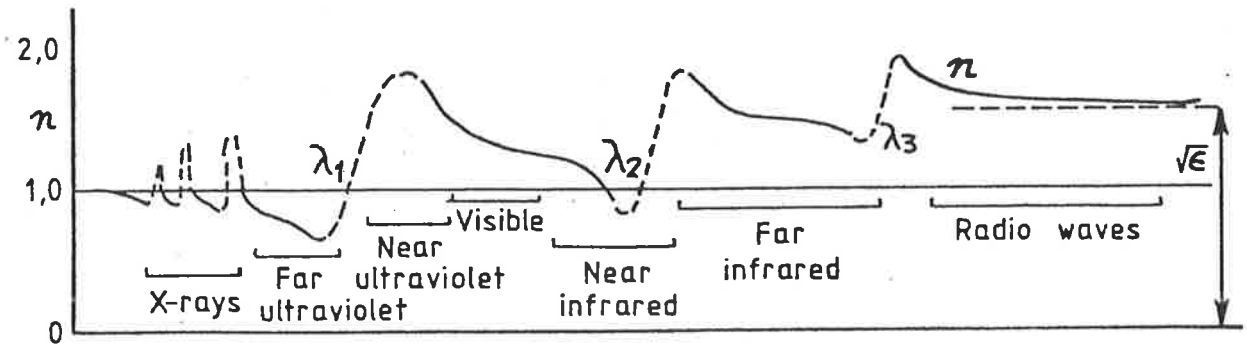

Figure 3.4: Refractive index (n) of a typical transparent medium as a function of wavelength (from Jenkins and White 1950). Cherenkov emission is possible wherever n>1.

where E_t is the threshold kinetic energy of the particle.

limiting angle: ($\beta \sim 1$) $\theta_c = \arccos(1/n)$ ..(3.3)

Passage of a charged particle past an atom as in figure 3.1 causes a nett variation of polarization in only the longitudinal direction (figure 3.2). After Jelley (1982) we may approximate this variation as two oppositely directed impulses and consequently, the frequency spectrum of the emitted Cherenkov radiation (fourier transform of figure 3.2(b)) will be a continuous spectrum of the form $\nu d\nu$ (ν=frequency), limited only by the requirement that $\beta n > 1$. Thus, in a typical transparent medium (e.g. figure 3.4) we expect Cherenkov radiation to be emitted at wavelengths ranging from radio through to the near ultra-violet. Specifically we have:

Energy/unit pathlength: $$\frac{dE}{dL} = \frac{\pi (Ze)^2}{\varepsilon} \int_{\beta n > 1} \left(1 - \frac{1}{\beta^2 n^2}\right) \frac{d\lambda}{\lambda^3}$$ ..(MKSA

or, assuming that the medium is non-dispersive over the wavelength range of interest,

Number of photons/unit pathlength: $$\frac{dN}{dL} = \frac{\pi (Ze)^2}{hc\ \varepsilon} \sin^2(\theta_c) \left(\frac{1}{\lambda_2} - \frac{1}{\lambda_1}\right)$$

$$\sim \frac{K \Delta\lambda}{\lambda^2}$$ ..(3.4)

3.3 CHERENKOV RADIATION FROM EAS

3.3.1 DISCOVERY AND INITIAL INVESTIGATIONS

It is believed that Blackett (1948), in a discussion on possible contributions to the general night sky illumination, was the first to suggest that Cherenkov radiation would be

produced in the atmosphere by cosmic rays. The realization that in addition to the flux of Cherenkov radiation produced by the passage of many uncorrelated particles, extensive air showers should produce a component of relatively brief, $\sim 10^{-8}$ sec, intense pulses which might therefore be observable above the background fluctuations lead Galbraith and Jelley (1953) to conduct a successful search for such pulses. In a series of pioneering experiments in England and at the Pic du Midi in France (Jelley and Galbraith 1953, Galbraith and Jelley 1955, Jelley and Galbraith 1955, Barclay and Jelley 1955), they established that the observed pulses were indeed consistent with their having been produced in extensive air showers by the Cherenkov mechanism. Similar investigations were soon underway elsewhere, most noticeably in the Pamir Mountains (Nesterova and Chudakov 1955, Chudakov and Nesterova 1958).

3.3.2 PROPERTIES OF EAS INDUCED CHERENKOV RADIATION

The refractive index, n, of a medium of density, ρ, is given by the Lorentz-Lorenz formula.

$$\frac{n^2-1}{n^2+2} = K\rho = \frac{(n+1)(n-1)}{n^2+2} \qquad ..(3.5)$$

K = constant

For air as $n \sim 1$ we may approximate equation 3.5 as

$$\eta = n-1 = (3/2)K\rho$$

Also, assuming an exponential atmosphere of density scale height h_o, we have

$$\eta = \eta_o e^{-h/h_o} \qquad ..(3.6)$$

$$\eta_o = 2.9 \times 10^{-4}$$

As $\eta << 1$ equations 3.2 and 3.1 become

$$E_t \sim m_o c^2/\sqrt{(2\eta)} \qquad ..(3.7)$$

$$\theta_c \sim \sqrt{2\eta}\ (1-(E_t/E)^2)^{\frac{1}{2}} \qquad ..(3.8)$$

$$\theta_{max} \sim \sqrt{2\eta}$$

$$\sim 1.3° \text{ at sea level}$$

Figure 3.5 displays the variation of threshold energy with altitude for an electron. For all other charged species this diagram may be scaled according to rest mass (equation 3.7). Any sufficiently energetic particle in an EAS may, of course, emit Cherenkov radiation but from table 3.1 we see that under most circumstances the observed Cherenkov flux will be dominantly produced by the electrons of the soft component. Under particular viewing conditions, it may be possible to distinguish those photons produced by the energetic hadrons and muons near the core (Grindlay 1971) or by heavy primaries (Sood 1983).

Once produced, Cherenkov photons are subject only to atmospheric transmission losses and provide relatively direct information on their parent electrons. We have seen previously (chapter two) that the variation of the electromagnetic cascade with atmospheric depth, or even just the depth of maximum development and its variation, are capable of providing information on the properties and interactions of the primary particle. Given that the Cherenkov flux observed at sea-level is made up of light produced over the entire development of the shower, it is reasonable to

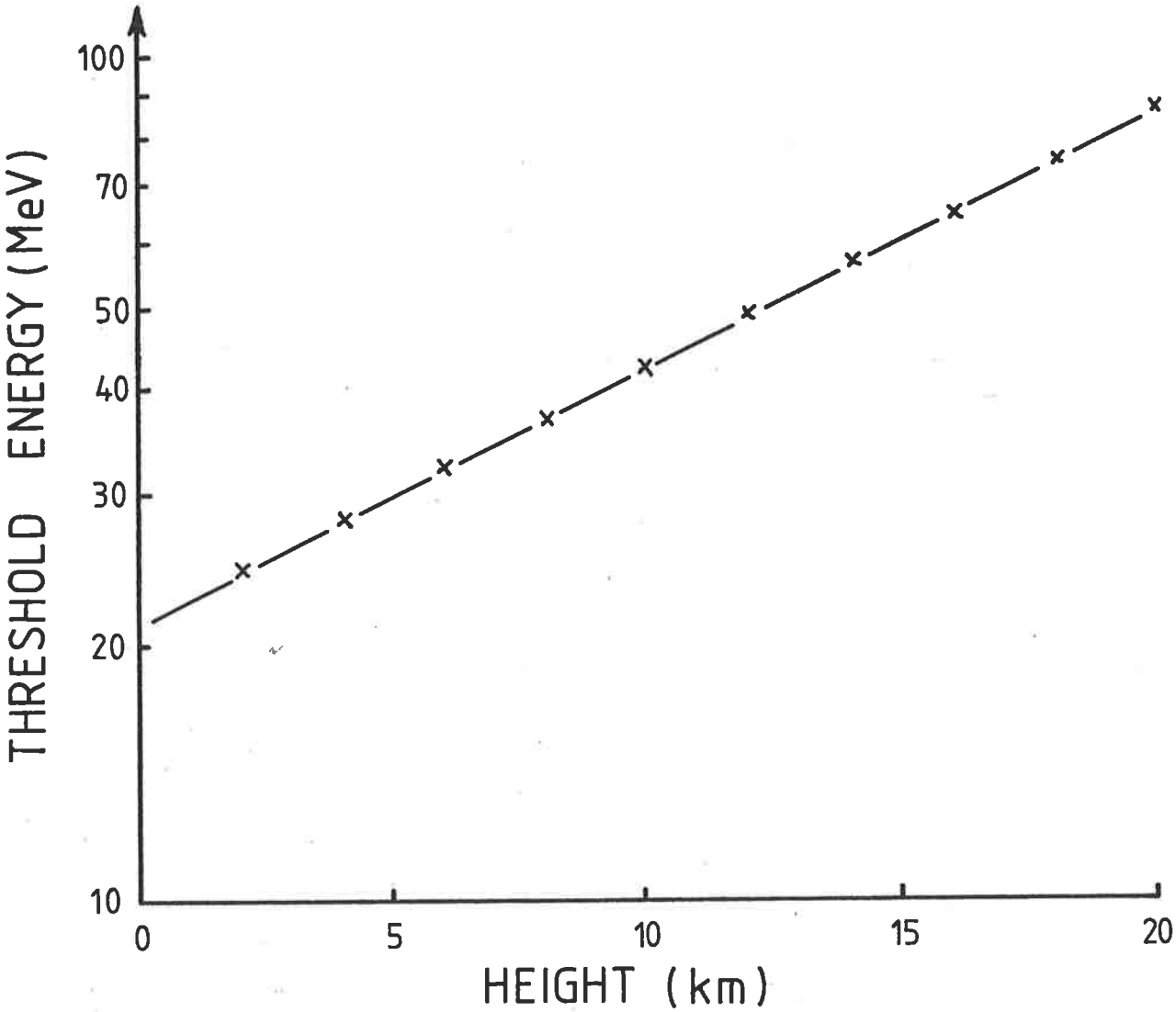

Figure 3.5: Altitude dependence of the threshold energy for the production of Cherenkov radiation by an electron in the atmosphere. A refractive index model, similar to that discussed in the text, with a density scale height of 7.1km, has been assumed.

Particle	Rest mass	Threshold energy	Percentage
electron	.5 Mev	21 Mev	∿90%
muon	∿104 Mev	∿4.4 Gev	∿10%
nucleon	∿ 1 Gev	∿4 Gev	∿1%

Table 3.1: Threshold energy for Cherenkov production and relative abundance of the major components of an EAS at sea-level.

question whether either or both of the above parameters may be derived from sea-level measurements of the Cherenkov flux. We now address ourselves to this question.

3.4 RELATIONSHIP BETWEEN CHERENKOV FLUX AND ELECTRON DEVELOPMENT

3.4.1 EARLY INVESTIGATIONS

The precise details of the total Cherenkov flux and its arrival time distribution are determined by a number of parameters: the variation of electron number with atmospheric depth; energy spectrum and angular distribution of those electrons with energy in excess of the Cherenkov threshold; the altitude variation of these two distributions; lateral and longitudinal dispersion of the electrons about the shower core; atmospheric transmission and density profile between production and detection levels; and, finally, the optical response and location (with respect to shower axis and core) of the detection system. Of these, the first is to be determined and the remaining effects must either be minimized or sufficiently well understood to enable unambiguous extraction of the required parameter from the observed flux.

In an effort to maximise the detected signal, many early experiments were conducted with the aid of a Cherenkov 'telescope' in which a parabolic reflector and photomultiplier were combined to provide an efficient

large area collecting system (see reviews by Boley 1964 and Jelley 1967). Similarly, systems employing optical filters and wavelength 'shifters' to concentrate observations in the near-middle ultra-violet region of the spectrum were suggested and tried, e.g. White et al (1961), Castagnoli et al (1967), Bosia et al (1972a). The latter experiments aspired to take advantage of the strength of the Cherenkov spectrum, relative to the night sky background in this wavelength region (figure 3.6). Charman (1965) even discussed the possibility of making daylight observations of Cherenkov radiation by restricting measurements to the wavelength region 200-280 nanometre where ozone absorption would ensure the virtual elimination of all background radiation. Unfortunately both of these 'improvements' make interpretation of the observed flux in terms of the longitudinal development of the shower more difficult.

Light is attenuated in the atmosphere in both a wavelength and altitude dependent manner as a result of three main processes: Rayleigh (molecular) scattering; aerosol (1-10μm particles) scattering; and ozone absorption. The attenuation lengths for each of these processes, at various altitudes, are displayed as a function of wavelength in figure 3.7. These data are taken directly from the publication of Elterman (1968). Near sea-level, aerosol scattering is seen to be the dominant process at most wavelengths, but its influence decreases rapidly with

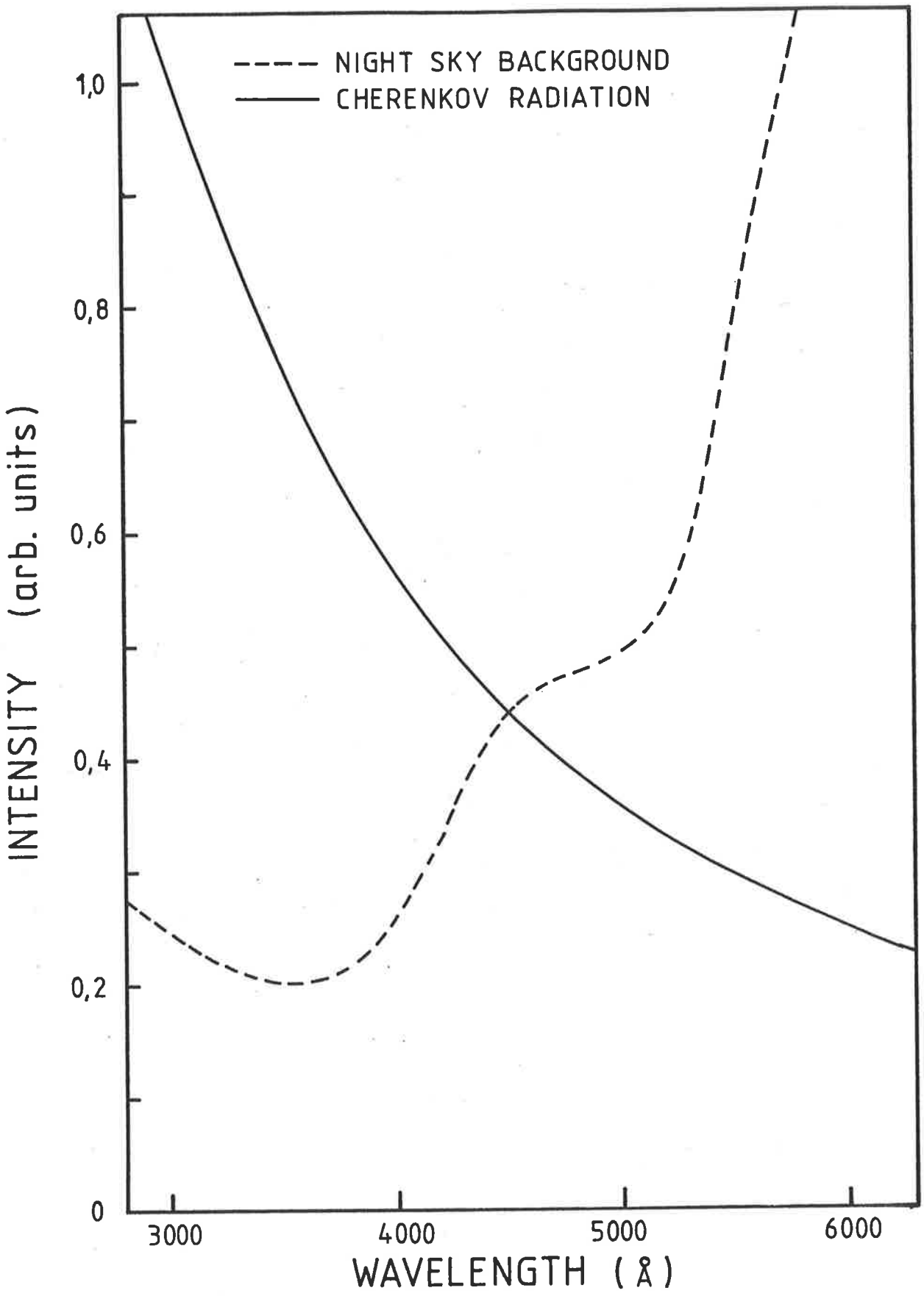

Figure 3.6: Relative intensities of the atmospheric Cherenkov and night-sky background spectra (after Bosia et al 1972a)

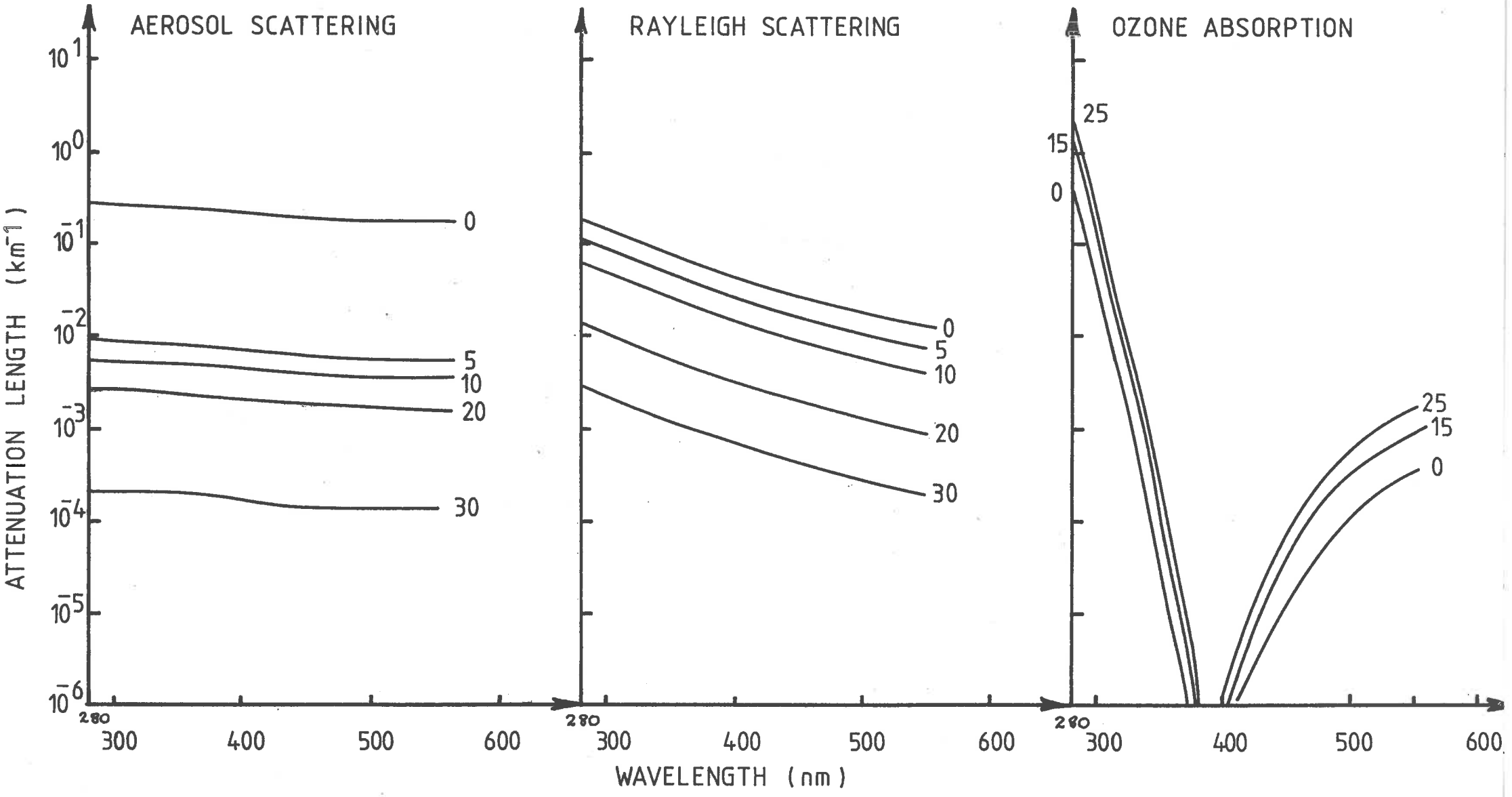

Figure 3.7: The attenuation length (reciprocal of distance over which light is attenuated by a factor of e) for each of the three major attenuation processes. Note that the curves refer to horizontal propagation at an altitude (km) indicated by the numerals attached to each curve.

altitude and Rayleigh scattering becomes the dominant attenuation mechanism for altitudes in excess of $\sim$2-3km and wavelengths $\gtrsim$290 nanometre. For near and middle ultraviolet wavelengths ($\lesssim$290nm), ozone absorption is dominant at all altitudes causing severe attenuation. Figure 3.8 illustrates the combined effect of all three processes on light of various wavelengths originating at different heights in the atmosphere. We note that atmospheric Cherenkov measurements made primarily in the ultraviolet region of the spectrum will not be equally sensitive to all altitudes due to the severe attenuation of these wavelengths by ozone absorption. Clearly, in order to receive light from a relatively unbiased range of altitudes measurements, should be restricted to wavelengths $\gtrsim$350 nanometre.

The narrow angular acceptance, typically $\sim$0.5°-2.0° associated with an isolated Cherenkov 'telescope' was a source of bias and confusion (Boley 1964). For inclined showers, the photons detected by such a system arise from a relatively brief phase of the entire development of the shower, namely that period when the shower core passes through, or makes it closest approach to, the acceptance cone of the telescope (Malos et al 1962, Sitte 1962). Consequently, the observed flux bears little relation to the overall electron development. If, however, measurements are made on vertical showers, at small core

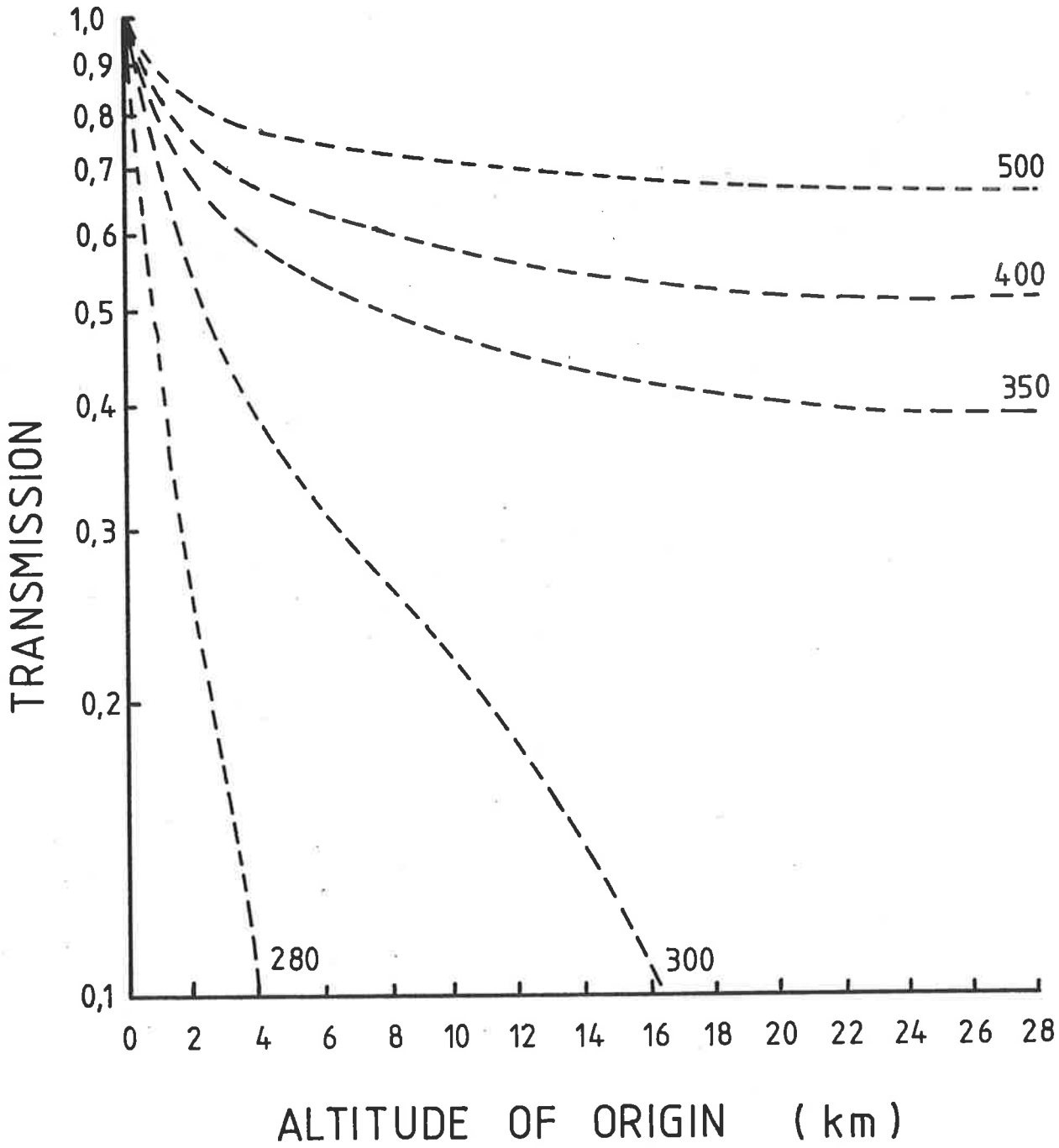

Figure 3.8: Fraction of light surviving vertical propagation from a given altitude to sea-level as a function of wavelength. The numerals attached to each curve indicate the wavelength (nm) under consideration. (from the data of Elterman 1968)

distances, $\lesssim$tens of metres, and the field of view is small enough to ensure that all the light produced in the acceptance cone at a given altitude arrives simultaneously, then the time structure of the pulse may be related to the longitudinal development of the shower (Bosia et al 1972b, Galkin et al 1979). However, for a 'typical' air shower installation in which Cherenkov observations are triggered by the arrival of the particle front, the vast majority of showers viewed by vertical narrow angle detectors would not be vertical and the former situation would apply. Bosia et al (1977, 1980) have demonstrated that under such circumstances the arrival time distribution of the Cherenkov photons provides information on the lateral distribution of the electron component, the telescope effectively scanning across the disc as it passes through the field ov view.

3.4.2 CURRENT INVESTIGATIONS

From the above it is apparent that in order to receive a relatively unbiased flux of Cherenkov light from a wide range of zenith angles, it is best to make observations in the blue-green region of the visible spectrum with a detector of large angular aperture. If, in addition, the detector is sufficiently remote from the axis of the shower (so that only the total number of electrons at any atmospheric depth, not their lateral and longitudinal dispersion, is important) the interpretation

of the arrival time distribution of Cherenkov light is much simplified (Fomin and Khristiansen 1971, Guzhavin 1975, Orford and Turver 1976, Hillas 1982c). Before discussing these interpretations we briefly examine the main features of the distribution of total Cherenkov light intensity with core distance (lateral distribution).

Lateral Distribution of Cherenkov Radiation

Consider an idealised one-dimensional vertical shower in which all the disc electrons are constrained to a point on the axis. Assume, to a first approximation, that the entire Cherenkov flux originates at the point of maximum development. The angular distribution of the Cherenkov light emitted from this point will then be determined solely by the angular distribution of those electrons with energy in excess of the Cherenkov threshold at shower maximum and therefore relatively independent of primary energy, nuclear interactions or depth of maximum.

Showers of equal energy but different depths of maximum will thus emit approximately equal amounts of Cherenkov radiation, but its lateral distribution will depend on the depth of maximum development or, more generally, the height of maximum, i.e. the geometric distance, along the shower axis between the observation plane and the point of maximum development (figure 3.9). From figure 3.10 we see that showers reaching maximum at large distances from the observation plane spread their

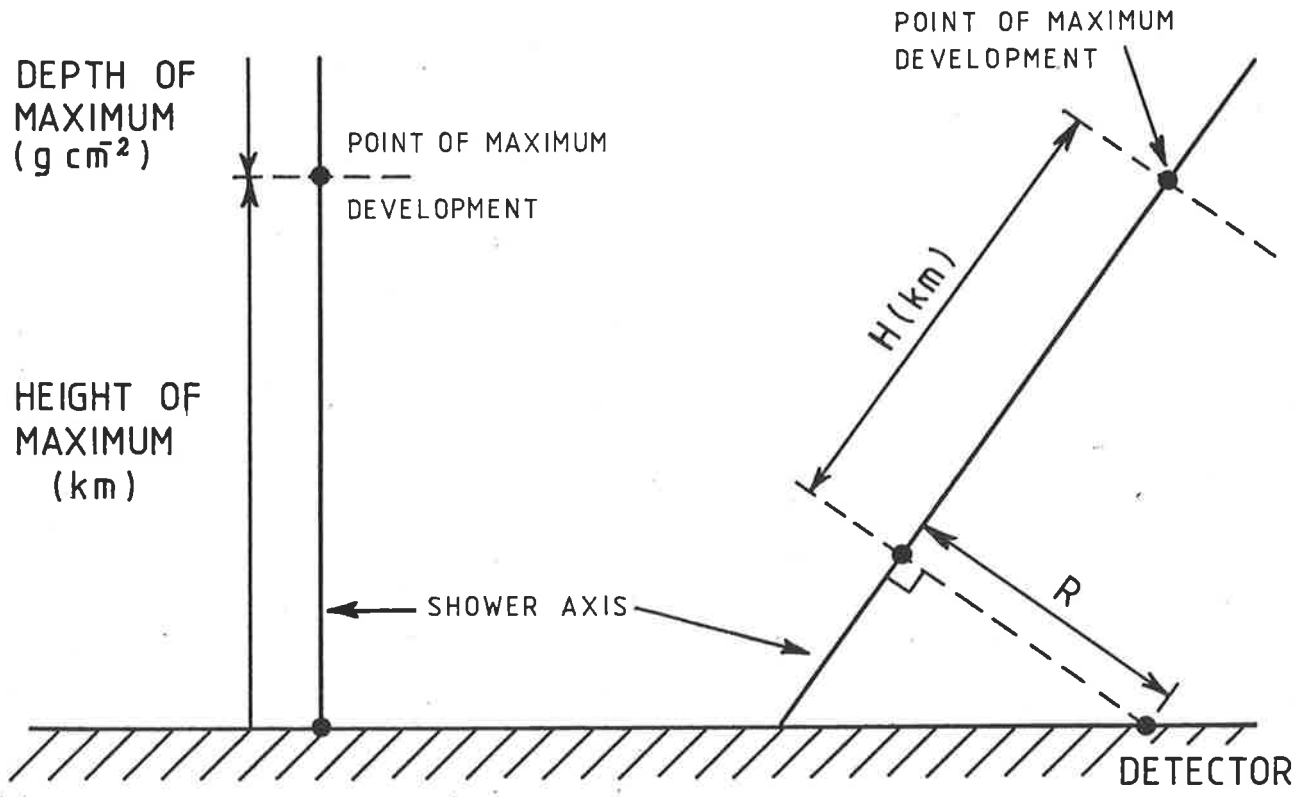

Figure 3.9: Sketch illustrating the definition of the term 'height of maximum'.

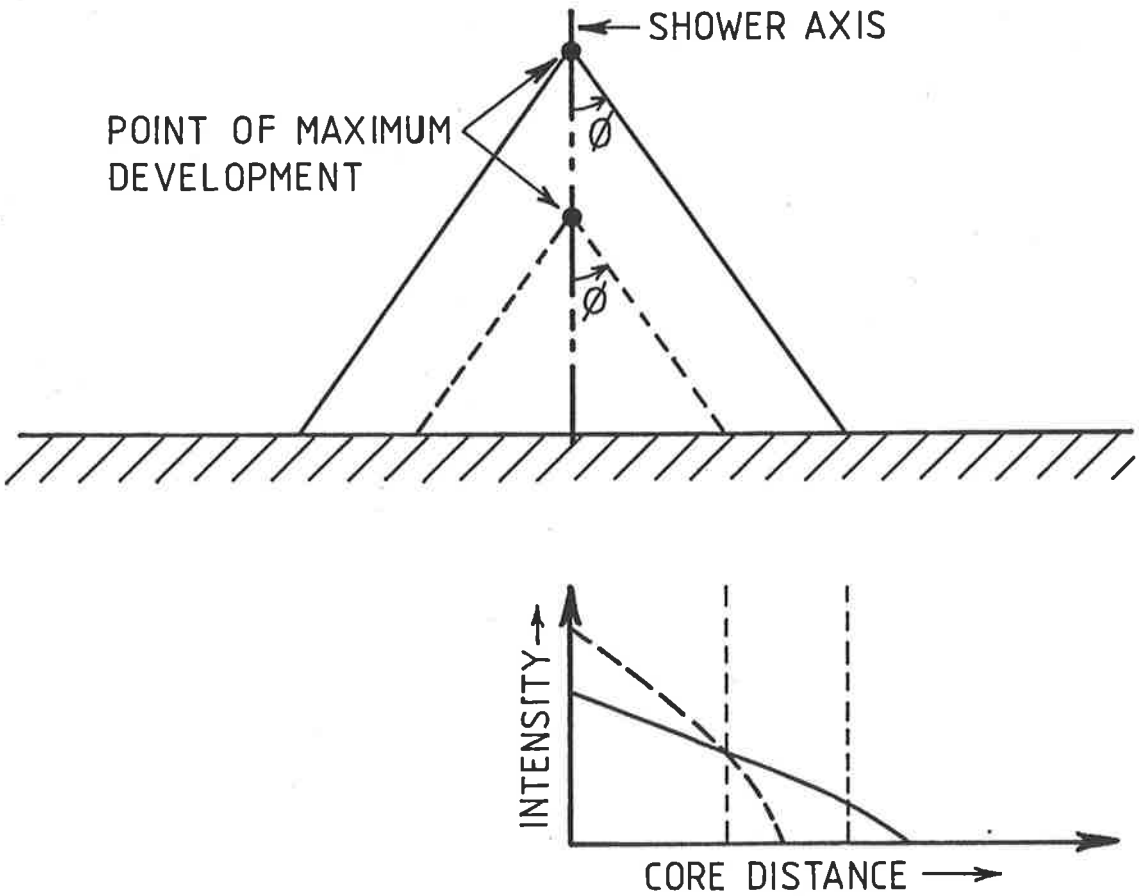

Figure 3.10: Much simplified model of the development of an EAS illustrating the formation of 'steep' and 'flat' lateral distributions of Cherenkov radiation by late and early developing showers respectively.

Cherenkov radiation out over a larger area than those which develop at low altitudes. Consequently, although the areas under both lateral distributions are equal, the rapidly developing shower has a lateral distribution which varies more slowly with core distance than that of the late-developing shower, i.e. the 'steepness' of the lateral distribution is a measure of the depth of maximum development.

A more realistic approach would note that Cherenkov radiation is produced along the entire length of the shower axis and that the angular distribution of the relevant electrons differs markedly from the Gaussian distribution assumed in some analytical calculations (e.g. Zatsepin and Chudakov 1962). Hillas (1982b,c) notes the existence of a significant number of high-energy electrons moving almost parallel to the shower axis. Fortuitous variation of the Cherenkov angle with altitude results in these unscattered electrons producing a distinct 'shoulder' in the lateral distribution at a core distance of $\sim$125 metres. Either side of this region, the 'slope' of the lateral distribution is observed to vary with altitude in the manner outlined above (Patterson and Hillas 1983b).

Although based on a highly idealised model of electron development, the principle of steep lateral distributions correlating with late-developing showers and vice-versa, is supported by the results of detailed

calculations (e.g. Ivanenko et al 1977, Protheroe 1977). As the variation of the lateral distribution function with height of maximum is a purely geometric effect, one might expect that showers incident from angles other than the zenith should have lateral distributions similar to vertical showers if the height of maximum is the same in each case, this would appear to be so, Kalmykov et al (1979), Makarov et al (1981), Patterson and Hillas (1983b).

Arrival Time Distribution of Cherenkov Radiation

A closer examination of the above one-dimensional model reveals, as demonstrated by Fomin and Khristiansen (1971), a relatively straightforward relationship between the evolution of the soft component of an air shower and the arrival time distribution of the Cherenkov light at sea-level.

We no longer assume that the entire Cherenkov flux originates at the point of maximum development, instead it is assumed produced along the entire axis at an intensity proportional to the number of electrons with energy in excess of the Cherenkov threshold. Light originating on the axis at some altitude, H metres say, will form an approximately spherical wavefront which arrives at a point a distance R metres from the axis a time T after the 'tangent plane' (figure 3.11) of its producing electrons given by (in the case of a vertical shower):

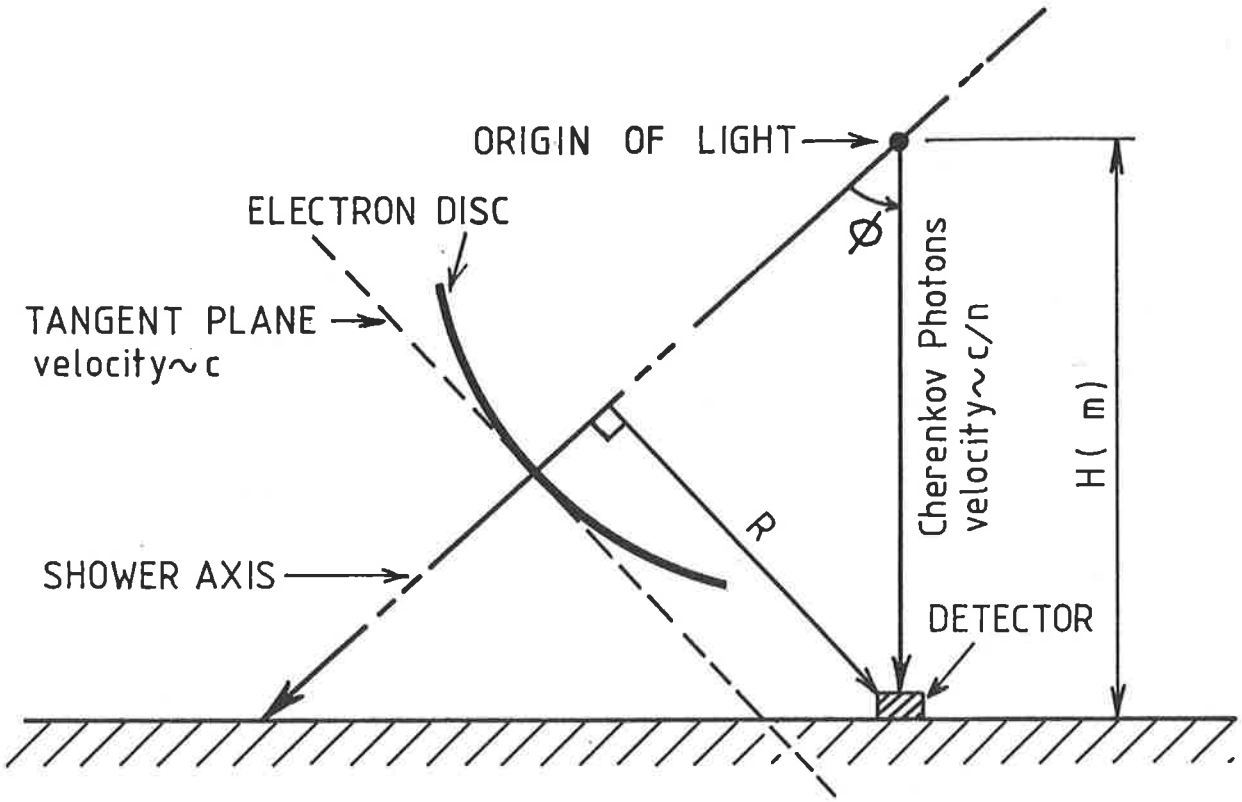

Figure 3.11: Sketch illustrating definition of the term 'tangent plane'.

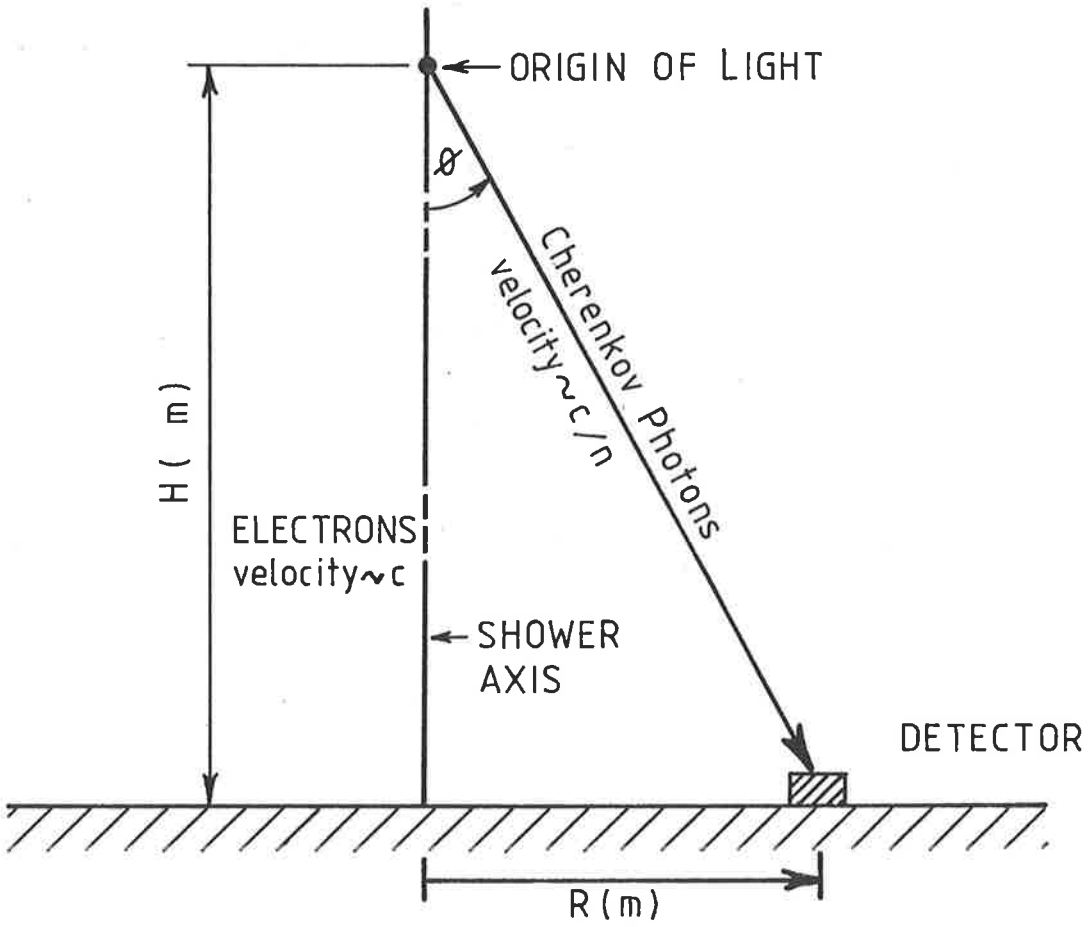

Figure 3.11a: Sketch defining terms employed in the calculation of the delay behind the tangent plane of light from H metres (vertical shower).

$$T = \frac{\sec(\theta)}{c}\int_0^H n(h)\,dh - \frac{H}{c} \qquad ..(3.9)$$

(symbols defined in fig.3.11a)

$n(h)$ = refractive index

$= 1 + \eta_o e^{-h/h_o}$ (c.f.eqn.3.6)

Now as $\sec(\theta) \sim 1+R^2/2H^2$ equation 3.9 becomes (to sufficient accuracy)

$$T = \frac{H}{c} + \frac{R^2}{2cH} + \frac{\eta_o h_o}{c}\left(1 - e^{-H/h_o}\right) - \frac{H}{c} \qquad ..(3.10)$$

Thus, to a good approximation, the difference in arrival time for light produced at two different altitudes: H_1, H_2 $(H_1 > H_2)$ is:

$$\Delta T = \frac{\eta_o h_o}{c}\left(e^{-H_2/h_o} - e^{-H_1/h_o}\right) + \frac{H_2 - H_1}{2H_1H_2c}\,R^2 \qquad ..(3.11)$$

Equation 3.11 has been employed in figure 3.12 to illustrate the variation in arrival time difference with radial distance and altitude.

The ultra-relativistic nature of the Cherenkov emitting electrons ensures that the Cherenkov photons always travel more slowly than their production region. Consequently, on the axis of the shower, the most recently produced photons arrive first, before those originating at higher altitudes which have fallen behind the electrons. At larger radii the difference in geometrical path lengths between the two altitudes and the detector (AC - BC figure 3.13) decreases, compensating the above effect and allowing photons produced at high altitudes to 'catch-up' with those produced at lower altitudes. In this simple model the two effects become equal at a core distance of $\sim$60 metres and photons arrive approximately simultaneously; a

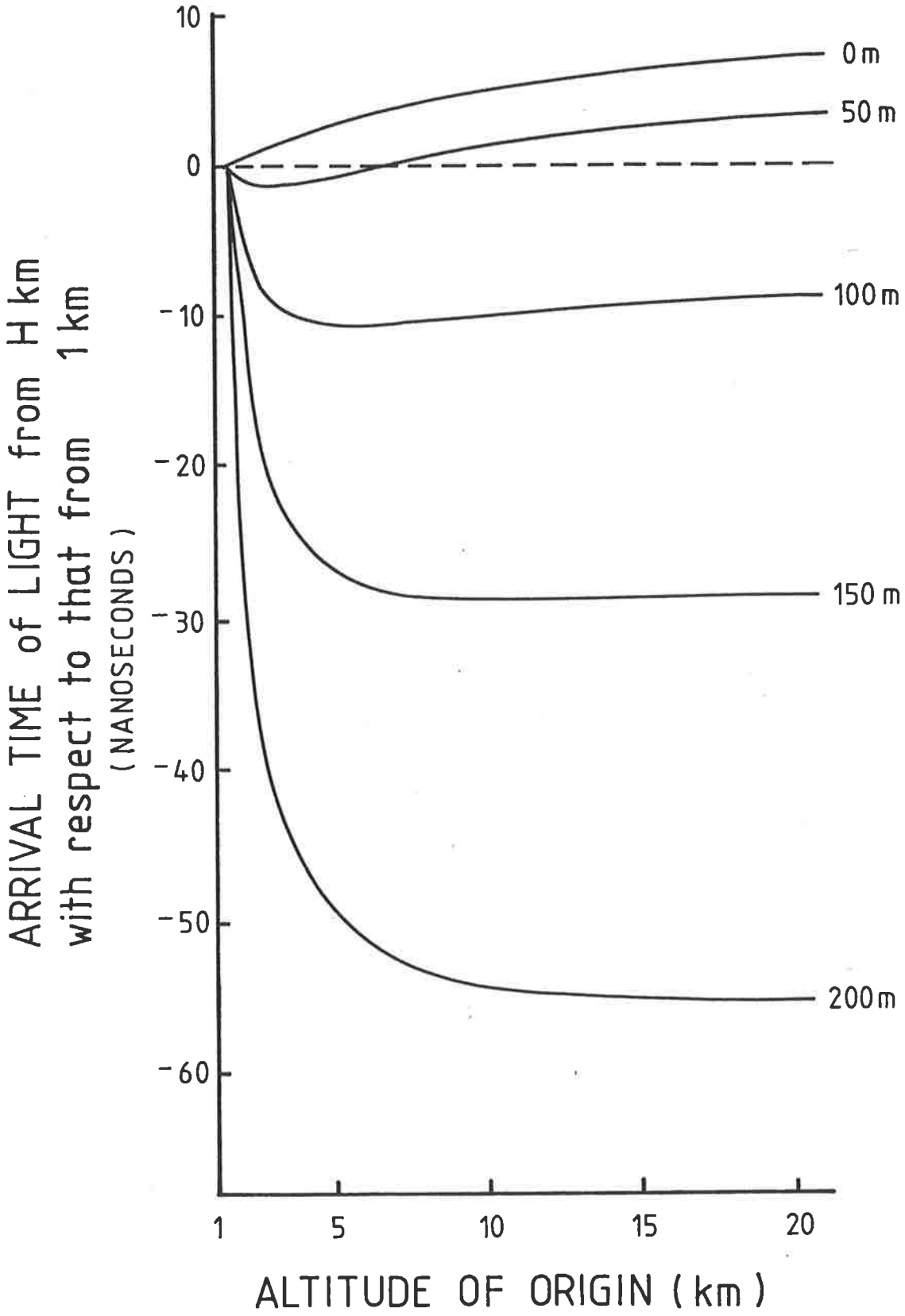

Figure 3.12: Arrival time of light produced at H kilometres, in a one-dimensional vertical shower, with respect to that from one kilometre as a function of core distance. Calculated according to equation 3.11 in the text.

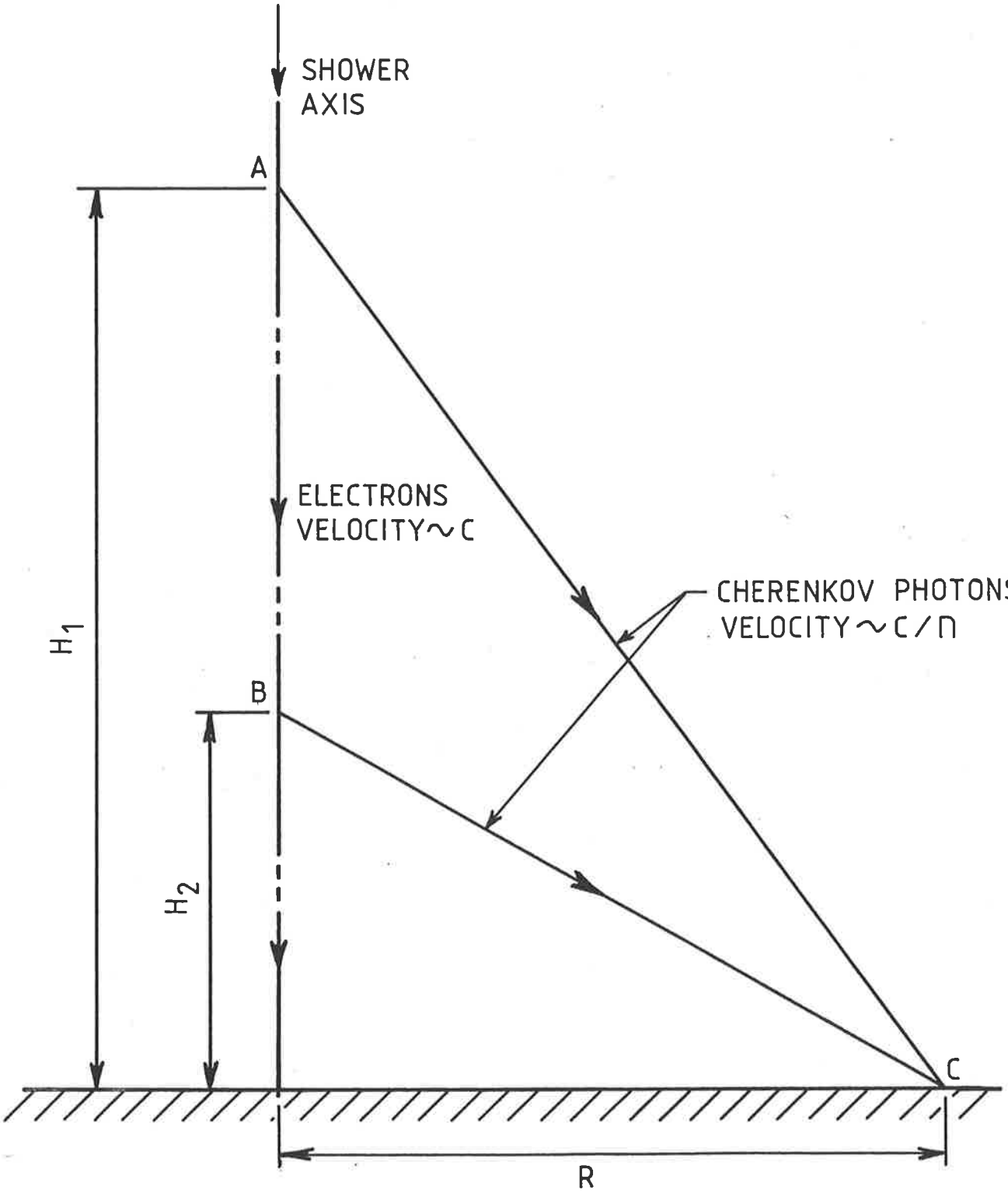

Figure 3.13: Sketch of the geometry assumed in the discussion of the difference in arrival time of light from two different altitudes for a simple one-dimensional model of shower development.

macroscopic Cherenkov effect. In reality the finite dimensions of the disc prohibit simultaneity and the pulse width merely reaches a minimum value of a few nanoseconds at core distances ∿80-100 metres (e.g. Makarov et al 1981).

At greater distances, perhaps ∿100-150 metres for real showers, refractive index effects become negligible, geometrical effects dominate and photons arrive in the time sequence in which they are produced. Photons arriving in the time interval $T \rightarrow T+dT$ have originated in the height interval $H \rightarrow H-dH$ thus, assuming an angular distribution function, $f(\theta)$, for the Cherenkov photons (θ defined as in figure 3.11a) and allowing for the inverse square law variation of intensity, we have for the number of photons, $d\phi$, detected in the time interval $T \rightarrow T+dT$

$$d\phi \propto \frac{N_H . f(\theta) . dH}{H^2}$$

where N_H is the number of Cherenkov emitting electrons at height H.

From equation 3.10 we have:

$$dT = \frac{-R^2}{2H^2 c} dH + \frac{\eta_0}{c} e^{-H/h_0} . dH$$

i.e. $$dT \sim \frac{R^2 dH}{2cH^2} \qquad (R \gtrsim 10 \text{ metre}) \qquad ..(3.12)$$

and so $$\frac{d\phi}{dT} \propto \frac{2cN_H . f(\theta)}{R^2}$$

Thus at large core distances not only does there exist a unique relationship between arrival time and height of origin, with photons arriving in the same time sequence as

they are produced, but the flux of photons at a given time depends on the product of the number of electrons and their angular distribution at the corresponding altitude. Clearly this provides, as first recognized by Fomin and Khristiansen in 1971, the opportunity to reconstruct the entire electromagnetic cascade for a large number of showers, unrestricted by the requirements of earlier suggestions employing narrow angle detectors (Bosia et al 1972b).

Calculations of the Cherenkov yield per electron as a function of atmospheric depth for a variety of models of nuclear interactions, primary energy and depth of maximum, have been performed by Ivanenko et al (1979) and Hillas (1982c). They find, due to the fortuitous cancellation of several effects, that the yield is relatively constant at depths $\lesssim$700-800g cm^{-2}. Thus, for depths less than this, the Cherenkov pulse (particularly its rising portion) is a relatively accurate mirror of the total electron number, below this the effect of the angular distribution of the emitted Cherenkov light is more pronounced and significant corrections are necessary to infer the electron number. Figure 3.14, reproduced from Hillas (1982c), illustrates this effect.

3.5 STUDIES OF THE ARRIVAL TIME DISTRIBUTION OF CHERENKOV RADIATION

3.5.1 CASCADE RECONSTRUCTION

Figures 3.15 and 3.16, reproduced from Hillas (1982c)

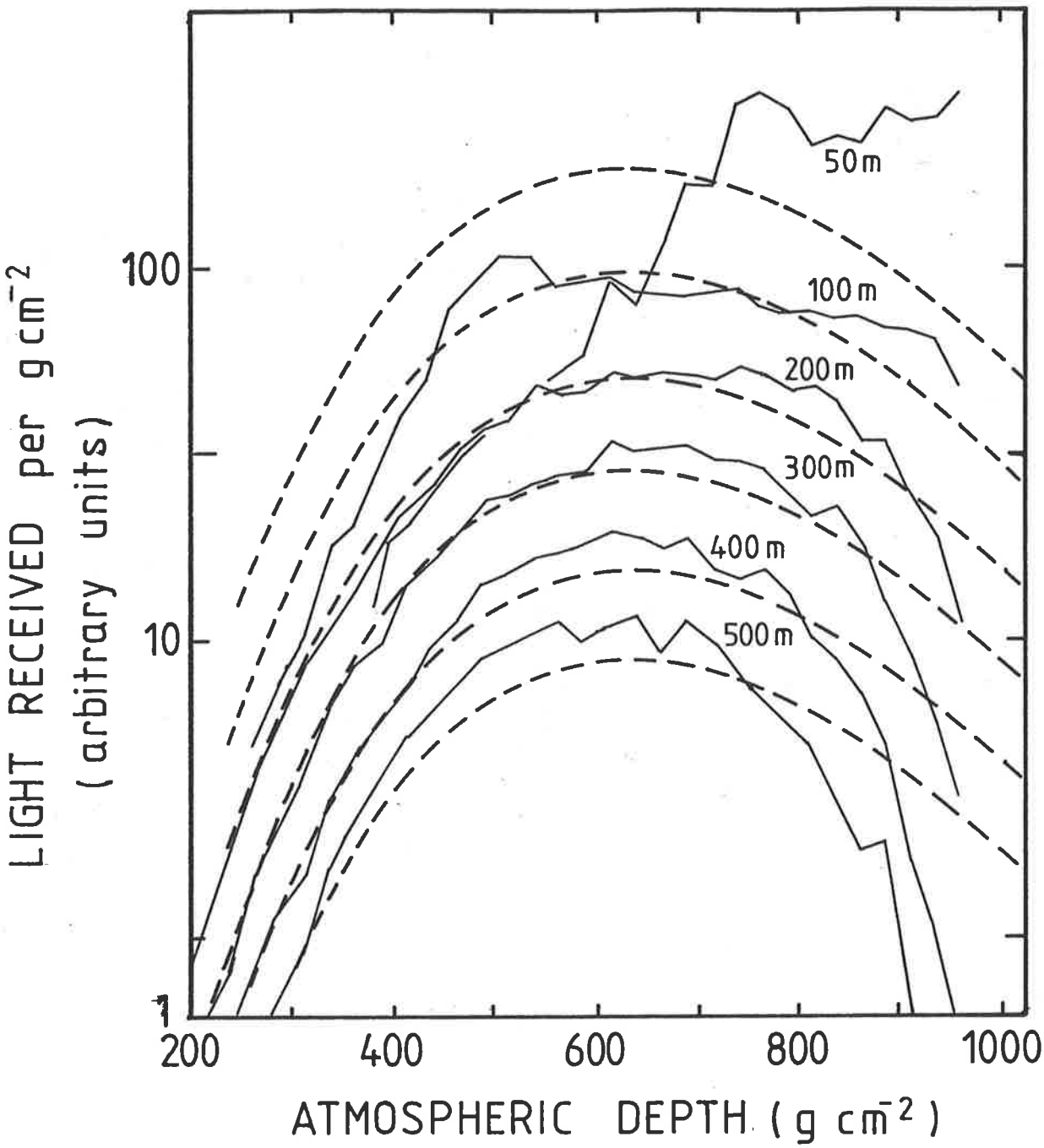

Figure 3.14: Relationship between the observed Cherenkov pulse shape at sea-level and the electron development of the air shower (from Hillas 1982c). The numbers attached to each curve indicate the core-distance at which the observation is made.

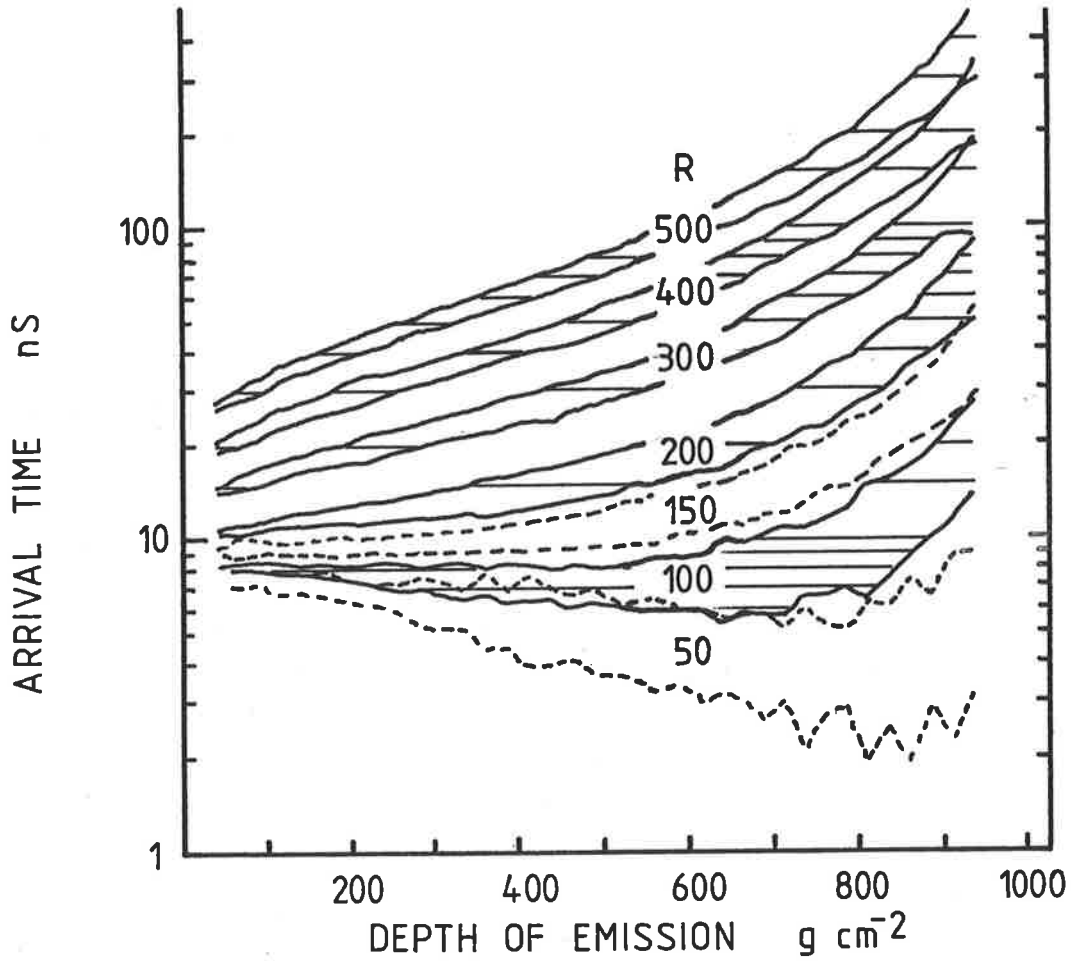

Figure 3.15: Spread in the arrival time of light from a given atmospheric depth for a realistic (three-dimensional) air shower (from Hillas 1982c) as a function of core distance (R)

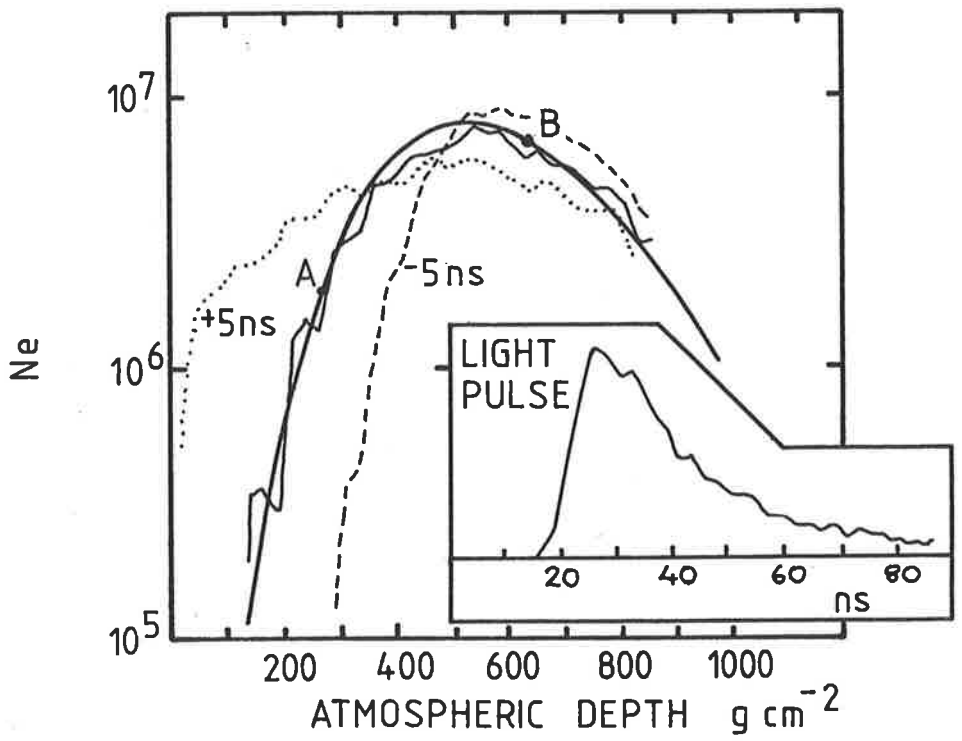

Figure 3.16: Development curves reconstructed from a theoretical Cherenkov pulse shape, illustrating the effect of errors in the measurement of the delay behind the tangent plane (from Hillas 1982c)

illustrate the major problems associated with attempting to reconstruct the cascade curve employing the above technique. The finite extent of the disc ensures that not all the light arriving at a given time had its origin at the same stage of development of the shower and although the dispersion introduced is only of the order of a few nanoseconds, the uncertainity in point of origin is quite marked at reasonable core distances, e.g. $\pm\sim$100g cm^{-2} at 200 metres for the light originating around $\sim$400g cm^{-2}. To ensure a reasonable approximation to a one-to-one relationship between production height and arrival time, measurements should probably be made at distances $\gtrsim$250-300 metres. The effect of errors in the measurement of the delay behind the tangent plate is illustrated in figure 3.16, even at three hundred metres measurements must be accurate to the order of one nanosecond in order not to distort the shape and depth of maximum of the cascade curve. In addition to the above, the relatively short duration of typical Cherenkov pulses ($\sim$10-20ns) means that most pulse shapes are significantly affected by the instrumental response (typical full width at half maximum $\sim$5ns) requiring either accurate deconvolution of the true pulse, a difficult problem, or the performance of observations at large radii ($\gtrsim$300 metres) where instrumental broadening is negligible.

The first efforts at reproducing a development curve were made by the Durham group (Orford and Turver 1976

and Hammond et al 1978). They assumed, supported by their simulations, that the light observed at specified fractions of the peak detected Cherenkov amplitude emanated as a sphere from one point on the shower axis. The centre of several spheres, each from a different point in the development of the shower, were located by measuring the Cherenkov pulse shape and its relative arrival time at several well spaced detectors, thus the trajectory and development of individual showers were mapped. As no allowance is made for the effect of the angular distribution of the Cherenkov light, this technique reproduces the 'Cherenkov development' rather than the electron development which, as remarked earlier, do not correspond well on the falling edge of the cascade curve. In addition to requiring rigorous computer simulations to relate the depth of Cherenkov maximum and its fluctuations to their related electron parameters, this method is also difficult to apply at energies $\lesssim 10^8$ Gev where the observation of a sufficient number of widely spaced pulses is not usually available (Andam et al 1981a).

In principle, only one Cherenkov pulse shape, its delay relative to the tangent plane, and a set of Cherenkov 'yield' curves (e.g. Ivanenko et al 1979, Hillas 1982c) are necessary to reconstruct the cascade curve and this has been attempted by the Moscow group Grigor'ev et al (1979), Kalmykov et al (1981), who have reconstructed the rising portion of the electron cascade

for several high energy showers, observed at large core distances to negate the effects of instrumental broadening. Their experimental arrangement does not allow them to measure the delay behind the tangent plane, rather it is inferred from measurements of the full width at half maximum of the pulse (see above references) and the curve, somewhat indirectly, reconstructed with assistance of data from the associated particle array.

Hara et al (1981) have adopted a unique approach to the determination of the electron development by Cherenkov techniques. Air showers incident on the Akeno array within $\sim 30°$ of the zenith are viewed from a distance of approximately two kilometres by a set of three large diameter parabolic mirrors, each equipped with a focal plane array of photomultipliers. Each mirror has a total field of view of $\sim 20°$, with each individual photomultiplier viewing $\sim 5° \times 5°$. In essence, each mirror is a combination of the isolated Cherenkov telescopes discussed in section 3.3.1, each telescope viewing a different portion of the development curve, with several mirrors being required to provide uniform coverage of the sky at all altitudes above the array in a manner analogous to the 'Fly's Eye' experiment (Cassidy et al 1982). Again, shower calculations are employed to deduce the depth of electron maximum from the observed Cherenkov maximum and some attempts have been made to reconstruct the Cherenkov development of individual showers.

Although these techniques offer, in principle, to reveal most of the information on the development of individual EAS, the problems discussed at the beginning of the section have resulted in relatively few showers, of restricted energy, being subject to such analyses. At the time of the most recent International Cosmic Ray Conference (Paris, 1981) results were presented for a total of sixty-nine showers for all three methods. Of these, fifty contained information only on the depth of maximum development, Andam (1981a); eleven had information of the rising portion of the cascade, Kalymkov et al (1981); and the remainder had some information on the late stages of Cherenkov development, Hara et al (1981). Clearly, it may be some time before individual cascade curves are measured routinely over a wide range of energy.

A less technically demanding, and unfortunately less informative, technique (but one with a wider range of applicability) is the measurement of the full width at half maximum (FWHM) of individual Cherenkov pulses.

3.5.2 MEASUREMENTS OF THE FULL WIDTH AT HALF MAXIMUM

Consider again equation 3.10 and figure 3.13. If H_1 and H_2 are the altitudes at which the Cherenkov emission is half its peak value, then ΔT in equation 3.11 will be the FWHM of the Cherenkov pulse and the height of electron maximum will lie somewhere between the two altitudes (unless the shower develops very close to the observation level). The relationship between the height of electron

maximum and H_1 and H_2 is not immediately obvious, being determined by, amongst other factors, the shape of the cascade curve (not symmetrical about point of maximum), Cherenkov threshold, and the angular distribution of the emitted photons. It would be reasonable though to assume that, to a first approximation, the atmospheric thickness (g cm^{-2}) between the two fifty percent points was independent of primary energy and depth of maximum, the width of the cascade curve increasing only slowly with energy (Gaisser 1981). Thus at a fixed core distance in excess of $\sim$150-200 metres, where geometrical effects are the dominant source of differences in arrival times, showers reaching maximum development at large altitudes, where the path length difference (AC-ABC figure 3.13) is small, will produce pulses with a smaller FWHM than late developing showers in which H_1 and H_2 are closer to the observer and the pathlength difference consequently larger. Although the distance (g cm^{-2}) between H_1 and H_2 is assumed constant, the decreasing atmospheric density implies than the geometric distance between H_1 and H_2 will increase with height, although not at a sufficient rate to alter the overall conclusion that for fixed core distance the FWHM of the Cherenkov pulse is a monotonically decreasing function of altitude.

The exact relationship between height of electron maximum and Cherenkov FWHM is likely to be determined by the interaction between several factors (see above). In

spite of this, it appears a relatively simple relationship exists between the Cherenkov FWHM and height of maximum (Kalmykov et al 1979, Patterson and Hillas 1983a) which is graphed in figure 3.17 for a core distance of 300 metres. The sea-level data of McComb and Turver (1982b), although not presented in this form, have also been plotted assuming a U.S. Standard Atmosphere to relate depth to height. Similar relationships exist for other core distances (e.g. Hillas and Patterson 1983a, Aliev et al 1981).

Although FWHM measurements and consequent depth of maximum determinations are less technically demanding than efforts to reproduce the entire cascade, the brevity of the Cherenkov pulse in comparison to typical instrumental response times requires that suitable allowance be made for the effect of experimental broadening on the relationship between FWHM and height of maximum. This is usually effected by either convolving the instrumental response in with the calculations used to determine the relationship between pulse duration and point of maximum, or attempting to eliminate instrumental effects from the observed pulse before comparing its width with calculations. Of the two, the former is preferable where suitable simulations are available, although not always the most feasible, in the absence of adequate simulations.

In conclusion, it would seem that a single measurement of the Cherenkov pulse duration, at any core distance in excess of $\sim$150-200 metres is sufficient to determine, with the aid of suitable calculations, the depth

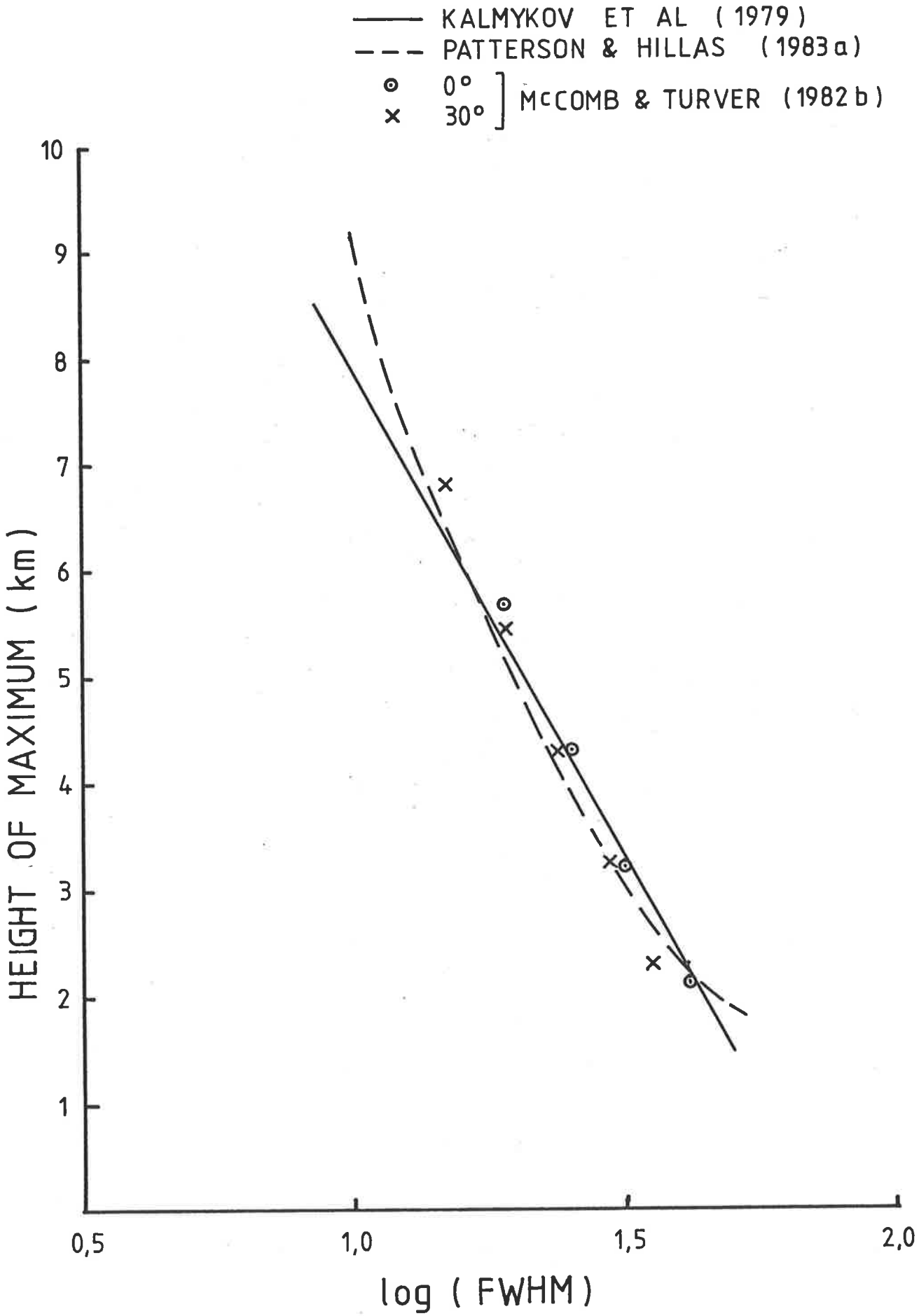

Figure 3.17: Relationship between the logarithm (base 10) of the Cherenkov pulse FWHM (ns) and the height of maximum (km) of the electromagnetic cascade of an EAS. Note that one curve is sufficient for all zenith angles.

of electron cascade maximum for that shower. This method, although providing less information than full cascade reconstruction, is simpler to apply and is suitable for a much wider range of EAS.

3.6 CURRENT STATUS OF FWHM OBSERVATIONS

To date, four groups have reported the results of experimental determinations of the depth of maximum by measurements of the Cherenkov pulse FWHM. The most comprehensive results to date are those of the Durham group who operated an 'all Cherenkov' array at Dugway in the USA (Chantler et al 1979). Details on the depth of maximum and its fluctuations in the energy range $\sim 6.10^6$-2.10^9 Gev were determined by a variety of techniques (Chantler et al 1983 and references therein). Aided by calculations incorporating their detector response, they have determined the variation of the mean depth of maximum with primary energy by the FWHM technique in the range $\sim 3.10^7$-10^9 Gev (Andam et al 1981b) and its fluctuations at primary energy $\sim 2.10^8$ Gev (Chantler et al 1982). Multiple measurements of the FWHM are made on individual showers enabling the interpretation of development fluctuations within and between showers.

The first reported determinations of the Cherenkov FWHM and its radial dependence at large core distances were those of the Moscow group (Gadalov et al 1972). Subsequent investigations by this group have concentrated

on the recording of multiple Cherenkov pulses, usually by means of a large number of photomultipliers operated in parallel at one or more locations, associated with air showers of energy $\gtrsim 2.10^7$ Gev incident on the Yakustk array. These have enabled the determination of the energy dependence of the mean depth of maximum for these showers and examination of the depth of maximum fluctuations for showers of energy $\sim 10^8$ Gev (e.g. Berezhko et al 1979, Grigor'ev et al 1978, Kalmykov et al 1979). Measurements have recently been extended to showers of smaller energy with the construction of an array designed to detect both the electron and Cherenkov flux for showers with primary energy in the range $\sim 3.10^6$-3.10^7 Gev (Makhmudov et al 1979). To date only preliminary results have been presented for this system (Aliev et al 1981). The calculations employed to relate the observed Cherenkov FWHM to the height of maximum (e.g. Ivanenko et al 1976) do not incorporate the instrumental response, rather it is 'subtracted out' - as their calculations indicate that the instrumental width and true width add in quadrature (e.g. Kalmykov et al 1979).

The Akeno group (Inoue 1981a,b) have conducted measurements of the Cherenkov FWHM with two large area fast time response (FWHM ~ 3.5ns [Tanahashi 1982]) detection systems based at the Akeno EAS array and Mount Chacaltya. To date they have reported measurements of the variation of the mean depth of maximum with energy for sea-level showers in the energy range $\sim 5.10^6$-10^8 Gev and the mean

duration of Cherenkov pulses observed at an altitude of 5200 metres initiated by primary particles of $\sim 10^8$ Gev. It is not apparent how instrumental effects are allowed for.

The Adelaide group has concentrated on making single detector measurements of the depth of maximum for showers with vertical sea-level sizes in the range 2.10^5-2.10^7 particles (e.g. Thornton and Clay 1979). Their analysis employed the relationship of Kalmykov et al (1979) and a modified version of the 'subtraction of squares' technique (Thornton 1983) to determine the variation of mean depth of maximum with sea-level size. Recently this system has been extended to permit up to three measurements per shower (Liebing et al 1981) and the analysis is now aided by the introduction of simulations incorporating their detector response (Liebing et al 1983).

CHAPTER FOUR

EXPERIMENTAL WORK

4.1 INTRODUCTION

The experiment described in this chapter was conducted at the extensive air shower array operated by the Physics Department of the University of Adelaide at Buckland Park. Only EAS successfully detected by this 'particle' array were examined for Cherenkov radiation. Consequently, the chapter commences with a discussion of some of the design features and associated performance characteristics of this array. This is followed by a description of the experimental system constructed to detect and record the shape of the pulse of Cherenkov radiation associated with these showers. The chapter concludes with a discussion of the calibration and routine operation of the Cherenkov system.

4.2 BUCKLAND PARK PARTICLE ARRAY

4.2.1 ROUTINE OPERATION

The Buckland Park EAS array is situated on a coastal plain, in rural surrounds, approximately 40 kilometres north of the city of Adelaide ($\sim$35°S) at a mean atmospheric depth of $\sim$1030g cm^{-2} (figure 4.1). The array, which currently encloses an area of $\sim 3.10^4 m^2$, is sensitive to EAS with vertical sea-level sizes in the range $\sim 10^5$-10^7 particles (equivalent vertical muons) and has undergone considerable evolution since it was first commissioned in 1972 (Crouch 1979, Gerhardy 1983, Prescott et al 1983).

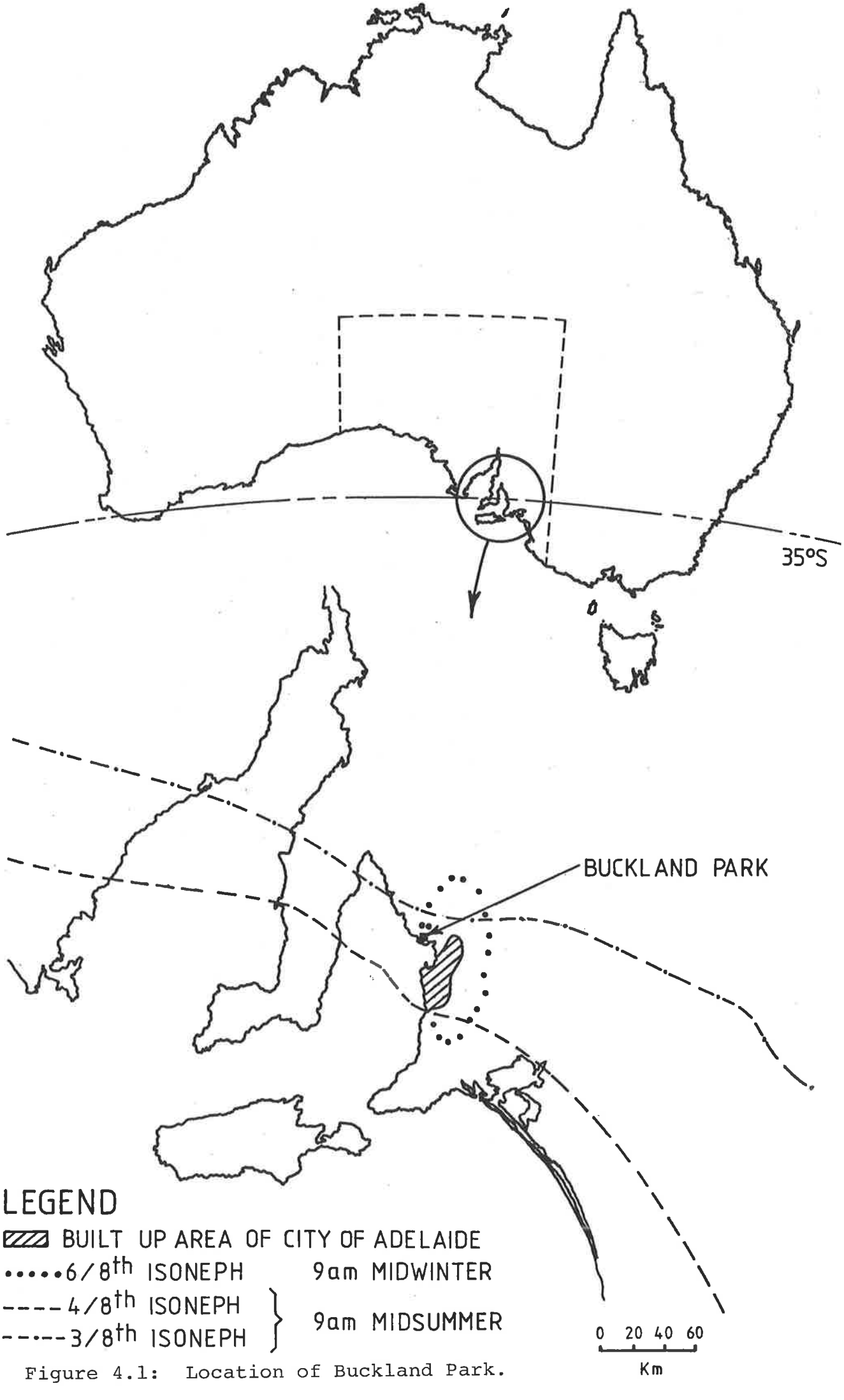

Figure 4.1: Location of Buckland Park.

For the majority of the experiment to be described (January 1979-April 1982), the array comprised eleven one metre squares of plastic scintillator disposed as in figure 4.2. A twelfth site (R) was operative from December 1980 onwards. Each scintillator was shielded by $\sim$4g cm^{-2} of material which provided thermal insulation and physical protection from the environment. Samples of the incident shower-front particle density were provided by all detectors in the array, while the inner four sites (A,B,D,E) also provided measurements of the arrival time (relative to C site) of the front. These raw data were recorded on a magnetic tape which was retrieved every $\sim$2-3 days for analysis at Adelaide. No on-site or real-time analysis of the raw data was possible. Data for subsidiary experiments, such as the one to be described, were recorded in the event of a suitable coincidence being detected between the main array and the subsidiary experiment. The two sets of data were then compared some three to four days later.

4.2.2 ARRAY PERFORMANCE

The main requirements of the particle array, for the experiment of concern, were that it provide a reliable, unbiased estimate of the size and core location of each shower detected by the array. Other simultaneous experiments (see Gerhardy 1983) placed other requirements on the performance of the array. Crouch (1979) analysed the behaviour of the above detector arrangement and

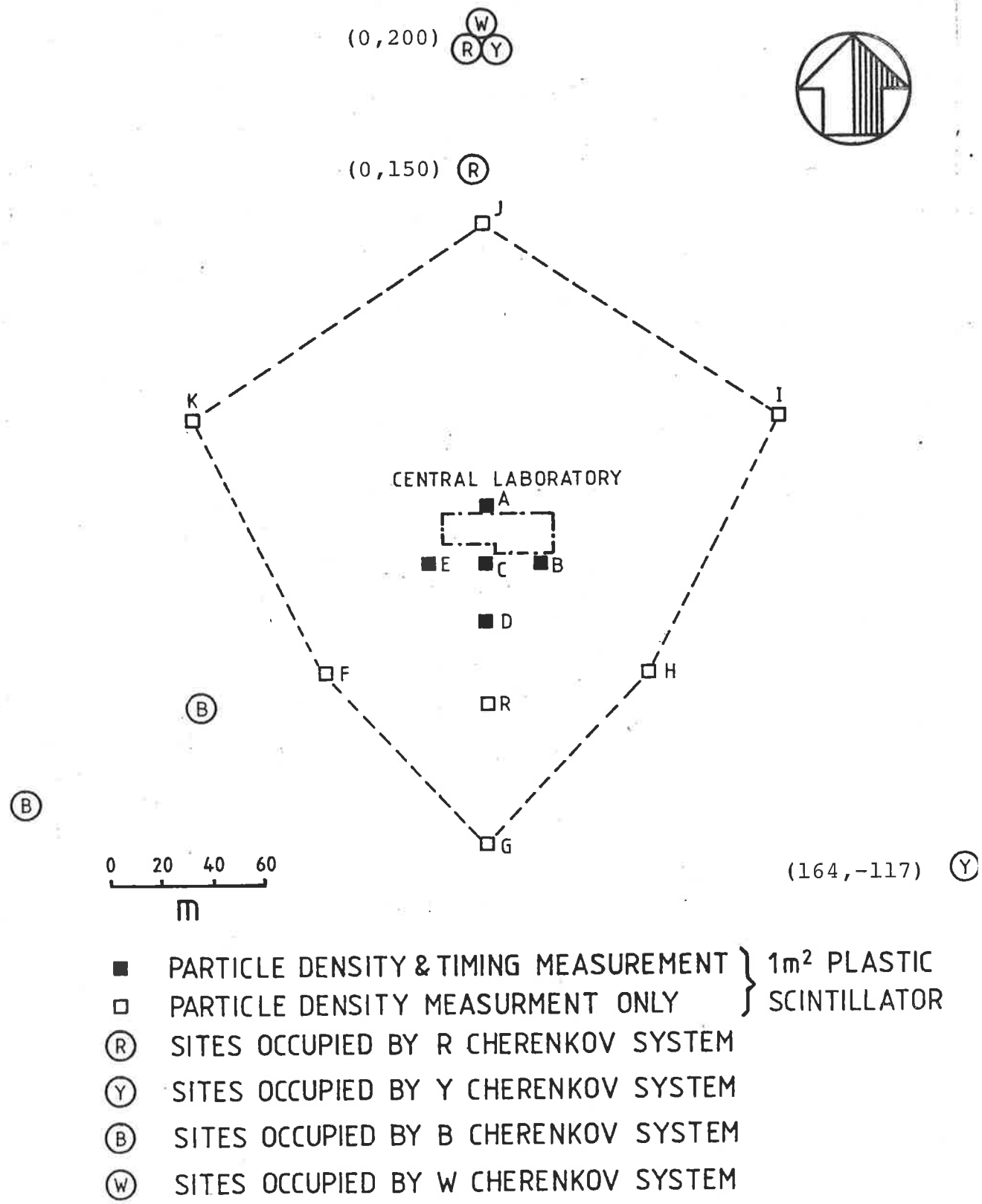

Figure 4.2: Map of the Buckland Park extensive air shower array indicating both particle and Cherenkov detectors. The co-ordinate system is centred on C site and the positive X and Y axes pass through the centres of site B and A respectively.

concluded that the required performance was best achieved if the recording system was triggered by the simultaneous observation of a relatively large number of particles in a few closely spaced detectors, other arrangements inducing significant bias. The typical core error and shower size estimate for the triggering arrangement employed during the course of the experiment, $\rho_A \geqq 6$ and $\rho_D \geqq 8$, (ρ_X: equivalent particles/m² at site X) appear in figures 4.3 and 4.4 (after Crouch 1979). In practice, an additional coincidence of $\rho_B \geqq 2$ and $\rho_E \geqq 2$ was also required to ensure adequate timing information. This was found to have negligible effect on the array characteristics (Crouch 1979).

Routine analysis of events detected by the array commenced with the determination of the direction of the shower axis by standard techniques to a typical accuracy of $\sim(2.5\sec\Theta)°$ (Gerhardy 1983). The size and core location of the shower were then determined by searching for the coordinates of the point at which the reduced chisquared variable, ψ_r^2, reached its minimum value.

$$\psi_r^2\Big|_{X,Y,N} = \sum_i \left(\frac{\rho_i - \rho_{oi}}{\rho_i}\right)^2 / (n-\nu) \qquad ..(4.1)$$

N = shower size

X,Y = coordinates of shower core

n = number of operative detectors

ν = number of degrees of freedom (3)

ρ_i = density measured at site i

ρ_{oi} = density predicted at site i

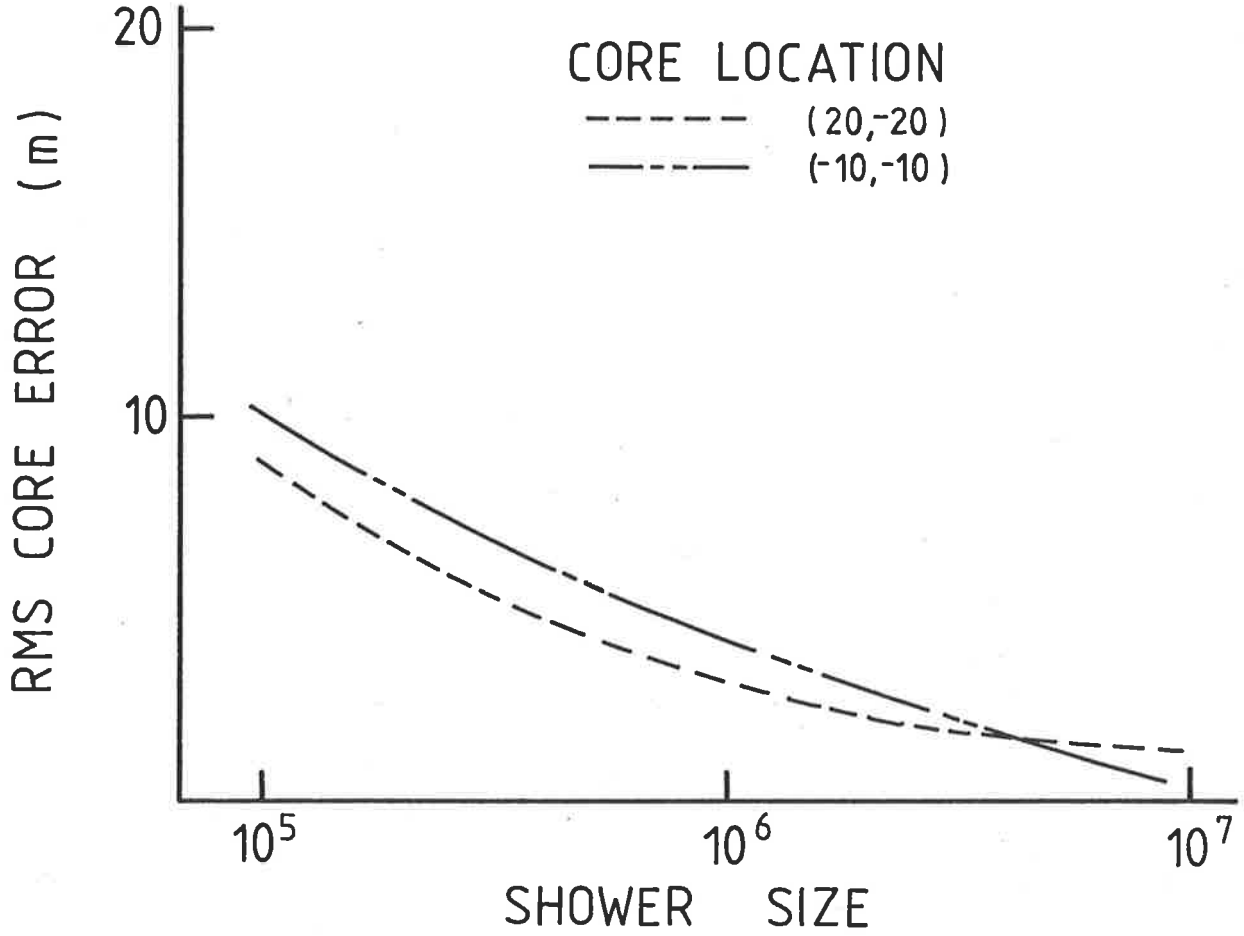

Figure 4.3: Typical core location errors for the Buckland Park array
(after Crouch 1979)

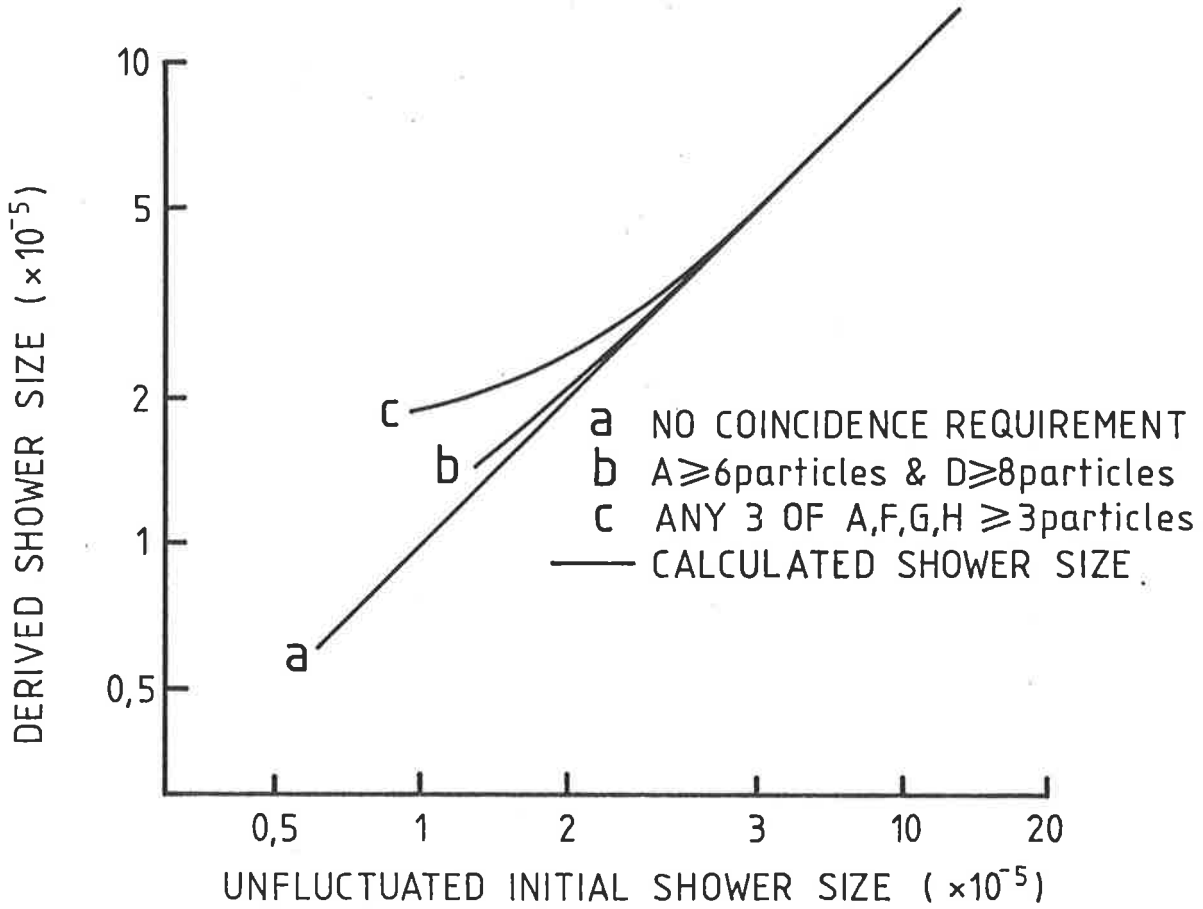

Figure 4.4: Comparison of shower size estimates deduced from Buckland Park array for different triggering criteria
(after Crouch 1979)

where $\rho_{oi} \propto (N/r_i).\exp(-r_i/r_o)$ ..(4.2)

r_i = perpendicular distance from shower axis to i^{th} detector

r_o = 60.00 metres

N = shower size

Greisen (1960) has shown that equation 4.2 provides an acceptable fit to the EAS scintillator densities observed within ∿200 metres of the shower core (as is typical at Buckland Park).

Throughout the entire period of the Cherenkov observations the particle array was employed to provide measurements of the isotropy, size spectrum and other characteristics of EAS in the size range $\sim 10^5$-10^7 particles. These experiments necessitated regular checks of both the calibration of individual detectors (for density and timing measurements) and the overall performance of the entire array (Gerhardy 1983). Naturally occasional 'anomalies' were detected in the system. These were corrected and their effects on previously recorded data, if significant, allowed for wherever possible. Sites unable to produce reliable data after this process were excluded from the analysis of EAS reported in this thesis. Such occasions were rare. Some general features of the showers detected and well-analysed by the particle array during the period of the Cherenkov observations appear in figures 4.5 and 4.6 (after Gerhardy 1983).

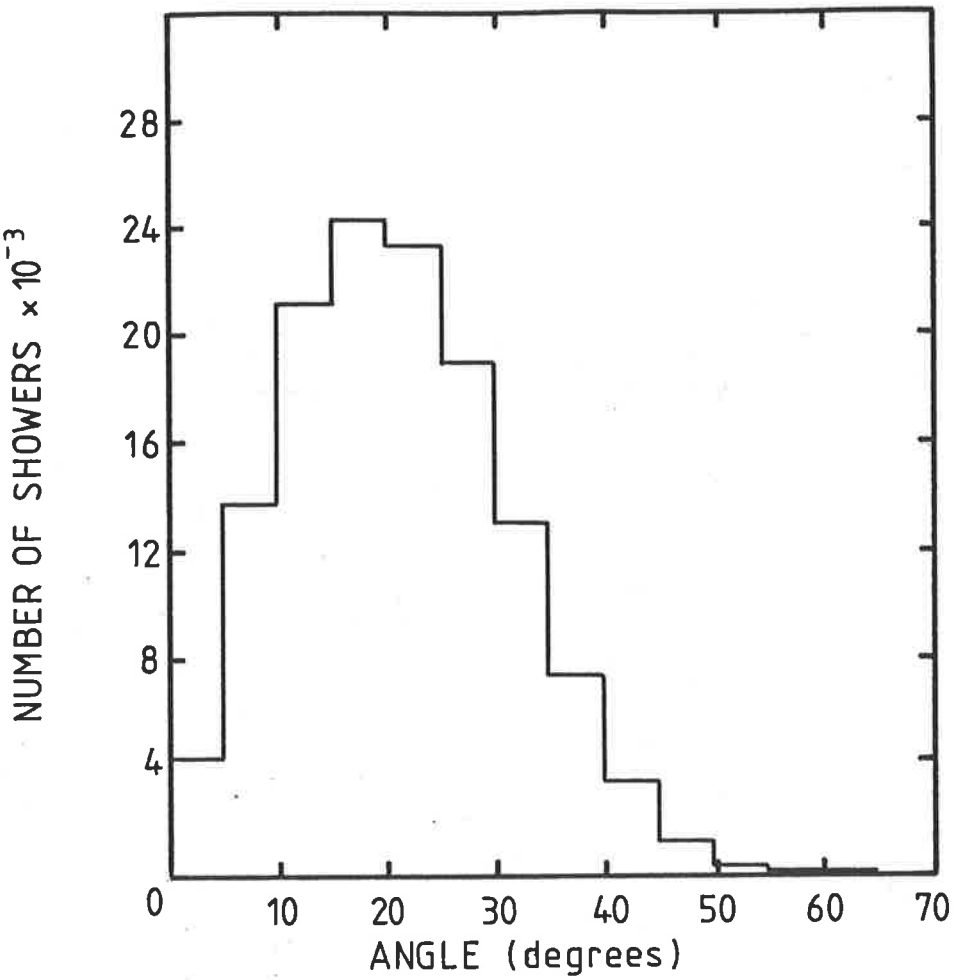

Figure 4.5: Zenith angle distribution of a large sample of showers detected by the particle array during the course of the experiment (from Gerhardy 1983)

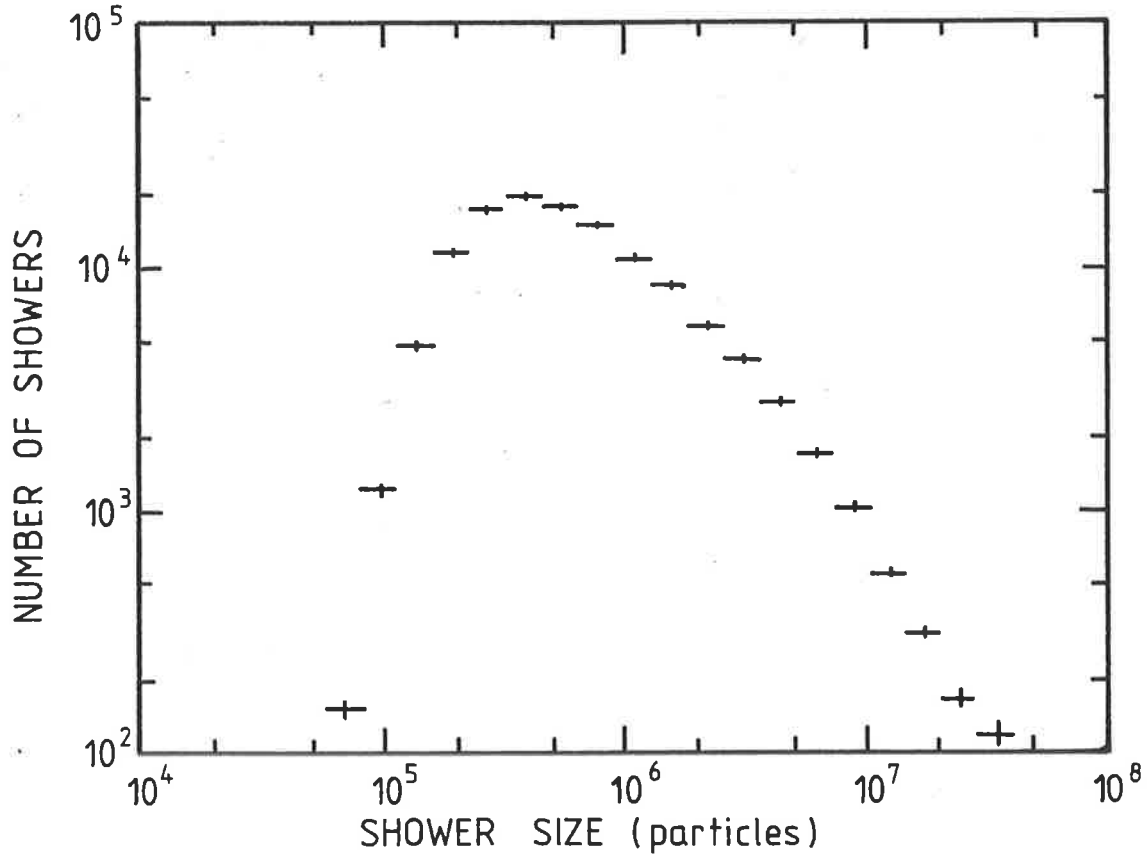

Figure 4.6: Spectrum of shower sizes detected at Buckland Park during the course of the experiment (from Gerhardy 1983)

4.2.3 PARTICLE DATA REANALYSIS

In addition to the above rigorous examination, each shower detected by the array during a Cherenkov 'run' was reanalysed by the author, assuming a more standard description of the electron lateral distribution (NKG function: chapter 2, section 2.2.3) and employing a more powerful routine to determine the coordinates of the point of minimum ψ_r^2 (MINUIT, James and Roos 1975). This was felt necessary as the core location procedure employed in routine analysis had been observed, under certain conditions, to become 'trapped' in a 'local' minimum of the ψ_r^2 function and be unable to reach the true or 'global' minimum of the function (Crouch 1977).

MINUIT is a very versatile minimizing routine which employs user supplied commands to locate the global minimum of a given function. The performance of MINUIT, and that of different command sets, was examined by employing the routine to analyse (i.e. deduce the core location and shower size) of a set of synthetic vertical showers of known sea-level properties 'detected' by the array. A computer program calculated the mean density expected at each detector for a given set of shower parameters (assuming an NKG lateral distribution function), then sampled from a poisson distribution of that mean to simulate the detection process. If these 'fluctuated' densities met the triggering criteria ($\rho_A \geq 6$ and $\rho_D \geq 8$) the shower was analysed by MINUIT and the resultant

parameters compared with those of the original shower. In this way a set of MINUIT commands capable of reliably and efficiently reproducing a wide range of input data was selected. It is noted that this is not a trivial exercise; some MINUIT command sets were observed to return distinctly more accurate and reliable approximations of the input data than others. Whether this was a feature of the MINUIT routine itself or something inherent to the problem is not known, nor was it investigated. It is sufficient that the set of commands employed in the final analysis had demonstrated its ability to analyse EAS with sizes in the range $\sim 10^5$-10^7 particles and NKG age parameters in the range 0.6-1.8, incident on the Buckland Park array accurately and reliably.

Figures 4.7 and 4.8 illustrate the major differences between the routine analysis of particle data and the analysis employing the NKG/MINUIT combination, here the same set of raw data (times and densities) has been analysed by both methods and the results compared. We note the greatly improved efficiency in locating the minimum value of ψ_r^2 and the slight reduction in shower size associated with employing the NKG function rather than the Moscow/MIT function (equation 4.2). The latter effect has been commented upon elsewhere (Gerhardy 1983).

A consequence of the above examination of the array response was the demonstration of a significant

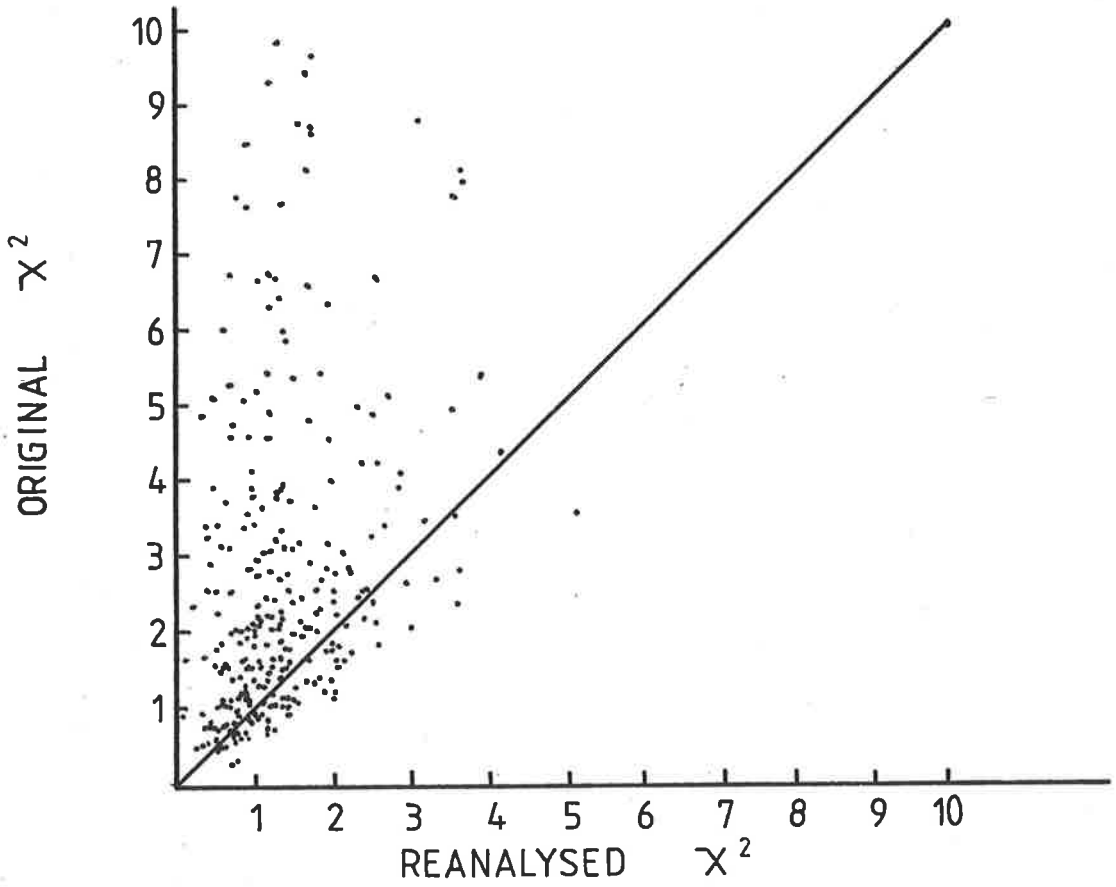

Figure 4.7.

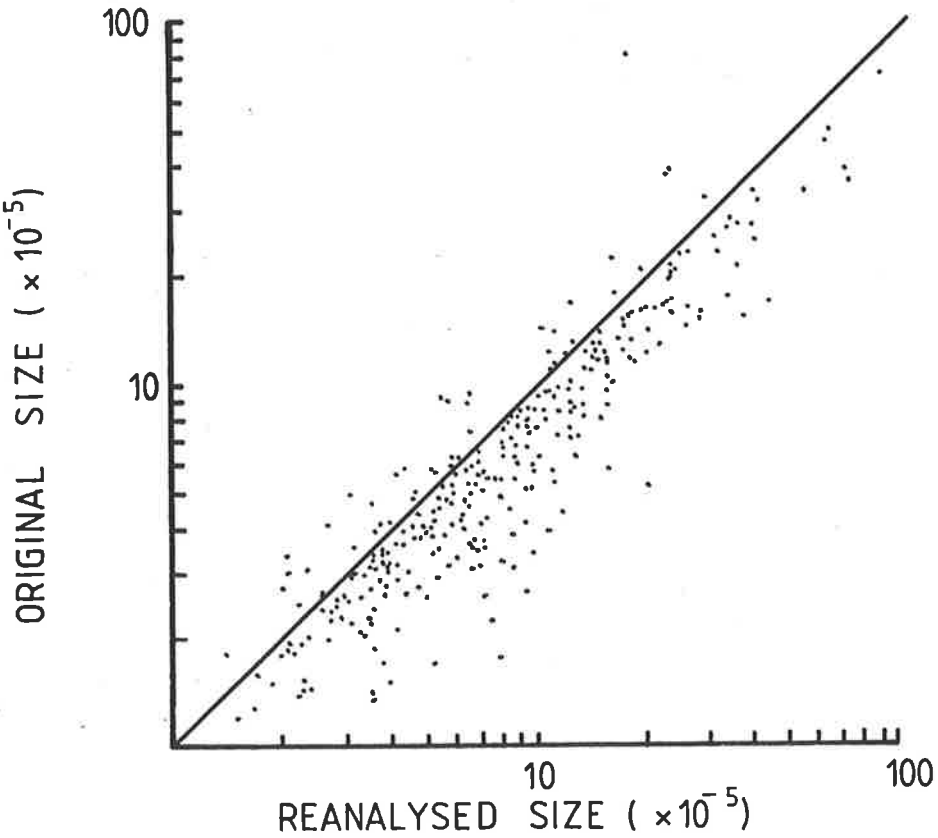

Figure 4.8: Comparison of sea-level size and value of ψ_r^2 for a sample of individual EAS analysed routinely (original) and analysed with the MINUIT/NKG combination discussed in the text (reanalysed).

bias towards the detection of young (small s) showers at small shower sizes, typically $\lesssim 5.10^5$ particles, due to the decreasing efficiency of the array in detecting showers in this region (Clay et al 1981). Above $\sim 5.10^5$ particles it would seem that the array detects showers of all ages with approximate equality.

We note in passing the recent work of Capdevielle and Gawin (1982) which demonstrated that the true electron lateral distribution is best fitted by a function in which the 'age' of the shower varies with core distance. This result is expected to have little application to the Buckland Park data, as the 'lateral age' parameter of Capdevielle and Gawin reaches a minimum value and varies only slowly over the range of core distances encompassed by typical Buckland Park measurements ($\sim$20-100 metres, figure 2.10).

4.3 THE CHERENKOV SYSTEM

4.3.1 GENERAL DESCRIPTION

The data reported in this thesis were obtained in the period January 1979 through to April 1982 from two independent Cherenkov light detectors constructed specifically for the project by the author. One system, R, was operative for the entire period, mainly at the most northerly of the sites indicated in figure 4.2, although some data was also taken at a site some fifty metres closer to the centre of the array (see figure 4.2).

The second system, Y, was operative from November 1979 onwards. Initially these two systems were operated simultaneously at the same site (the northernmost) before the second system was moved to the south-eastern position indicated in figure 4.2.

Each detector comprised a 5 inch diameter fast response photomultiplier (Philips XP2040) mechanically collimated and located on the roof of a small instrumentation caravan. Each caravan was supplied with three-phase mains power from the central compound to aircondition the caravan, provide lighting and power the experimental apparatus. A short length ($\sim$2-3 metres) of RG-8A/U cable coupled the photomultiplier directly to an internally triggered wide-band width storage oscilloscope (Tektronix: 7834 mainframe, 7A19 vertical amplifier, 7B80 timebase) housed in the caravan. In the event of a suitable coincidence being detected between the photomultiplier output and the particle array, the pulse displayed on the oscilloscope screen was photographed for later analysis.

In the latter stages of the experiment the bandwidth of a pre-existing system, B, composed of a similar photomultiplier connected to a wide-bandwidth oscilloscope (Tektronix 7912), located in the central compound, by $\sim$200 metres of RG-8A/U cable, was upgraded by replacing the RG-8A/U with a similar length of cable

of much improved characteristics (Andrews LDF-50). These three systems were operated simultaneously for the period October 1981-April 1982. A fourth system, W, similar in concept to the first two described above, with the exception that the photomultiplier employed was of larger diameter (Philips 60DVP), was also constructed and a preliminary comparison made of its characteristics and those of one of the 5 inch systems. No data will be presented from either of these last two systems (B,W).

4.3.2 THE CHERENKOV DETECTORS

The night sky illumination observed at Buckland Park on clear, moonless nights has two distinct components. One due to astronomical objects and the other arising from the atmospheric scattering of the lights of the city of Adelaide, some forty kilometres to the south. The mechanical collimators were designed to eliminate as much as possible of this background without seriously interfering with the light collected from the majority of EAS detected at Buckland Park. As few showers detected by the array are inclined at greater than $\sim 40°$ to the zenith (figure 4.5) and most of the showers are observed within $\sim$150-275 metres of the core, the photomultipliers were collimated to provide a uniform response to light incident within 45° of the zenith and virtually no response to light incident at angles in excess of $\sim 48°$ (figure 4.9).

The UV extended S11(A) photocathode and UV transmitting window of the XP2040 photomultiplier enable

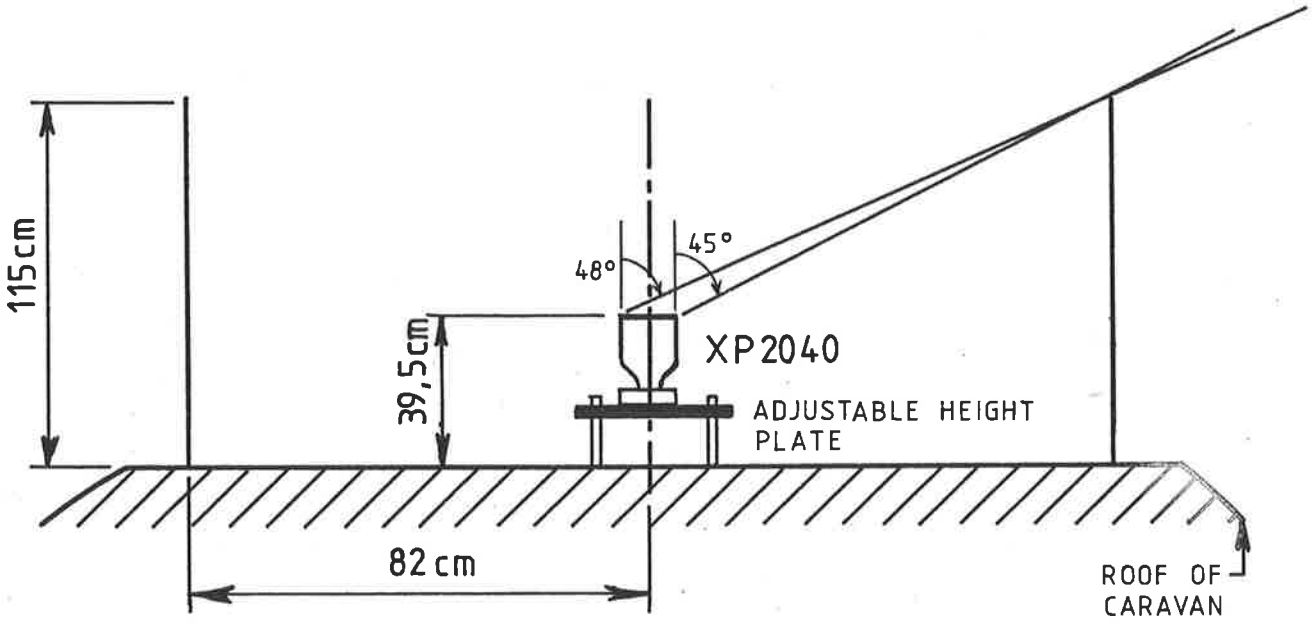

Figure 4.9(a): Mechanical collimation employed to reduce unwanted background illumination of the photomultiplier.

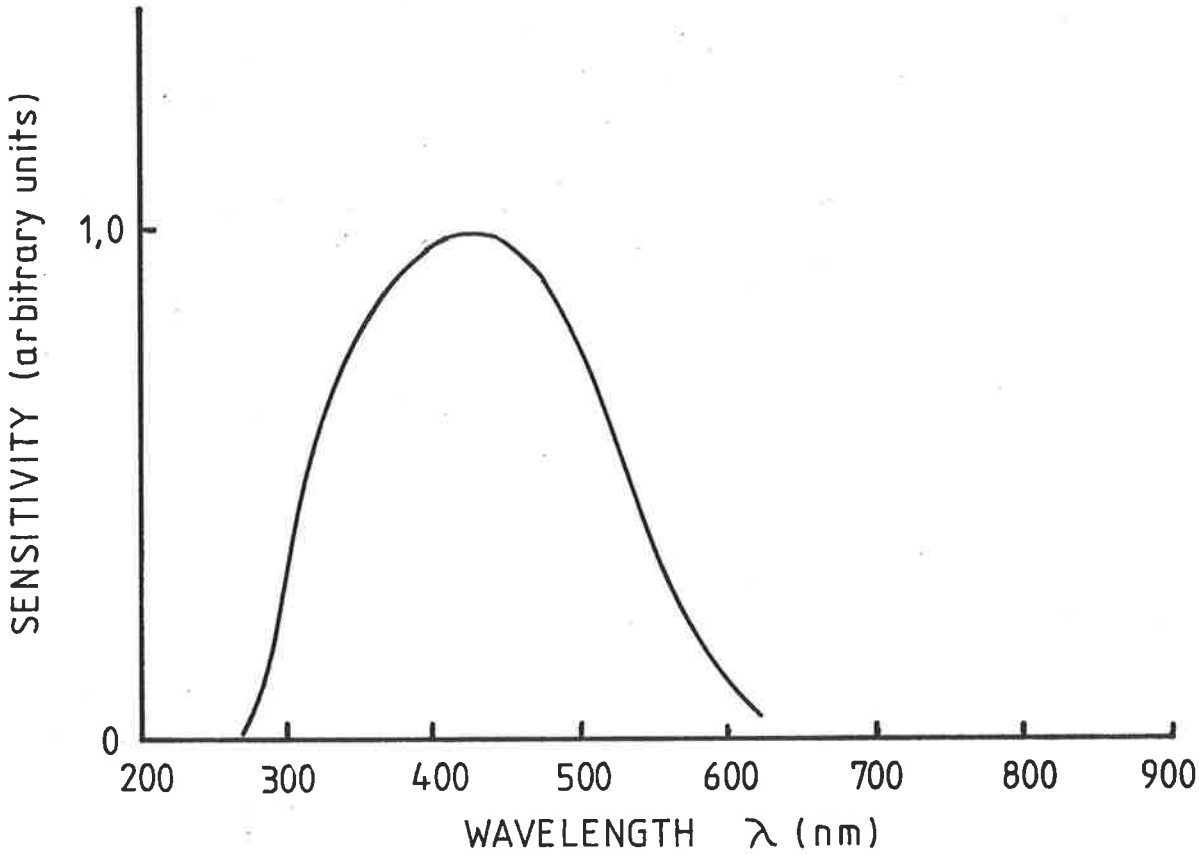

Figure 4.9(b): Spectral response of the XP2040 photomultiplier (incorporating plastic faceplate).

it to respond to wavelengths down to ∿200 nanometres. In practice this response was limited to wavelengths in excess of 350 nanometres (50% transmission), with a peak response at ∿420 nanometres, by operating the photomultiplier with the manufacturer supplied plastic faceplate in place. Thus measurements were not biased unnecessarily towards the UV portion of the spectrum (chapter 3, section 3.4.1). The base of each photomultiplier was constructed to ensure that the single photoelectron pulse shape observed on the 7834 oscilloscope was as smooth and of as short a duration as possible. Slight 'ringing' in the tail of this response was reduced, at the expense of a slightly increased FWHM, by the insertion of a 'damping' resistor (50Ω) between the last dynode and the divider chain. Further improvement was obtained by capactively coupling the last two dynodes to the braid of the 50Ω signal cable connected directly to the anode. Under the existing operating conditions the EHT applied to the photomultiplier (and hence the duration of its impulse response) was limited by the manufacturer's requirement that the continuous anode current (typically ∿100-150μA), not exceed 200μA. A typical single electron response, its power spectrum and the base diagram of the relevant photomultiplier appear in figure 4.10.

No controlled source of suitably brief pulses of light was available to measure the multi-photon (where transit time differences between photoelectrons emitted

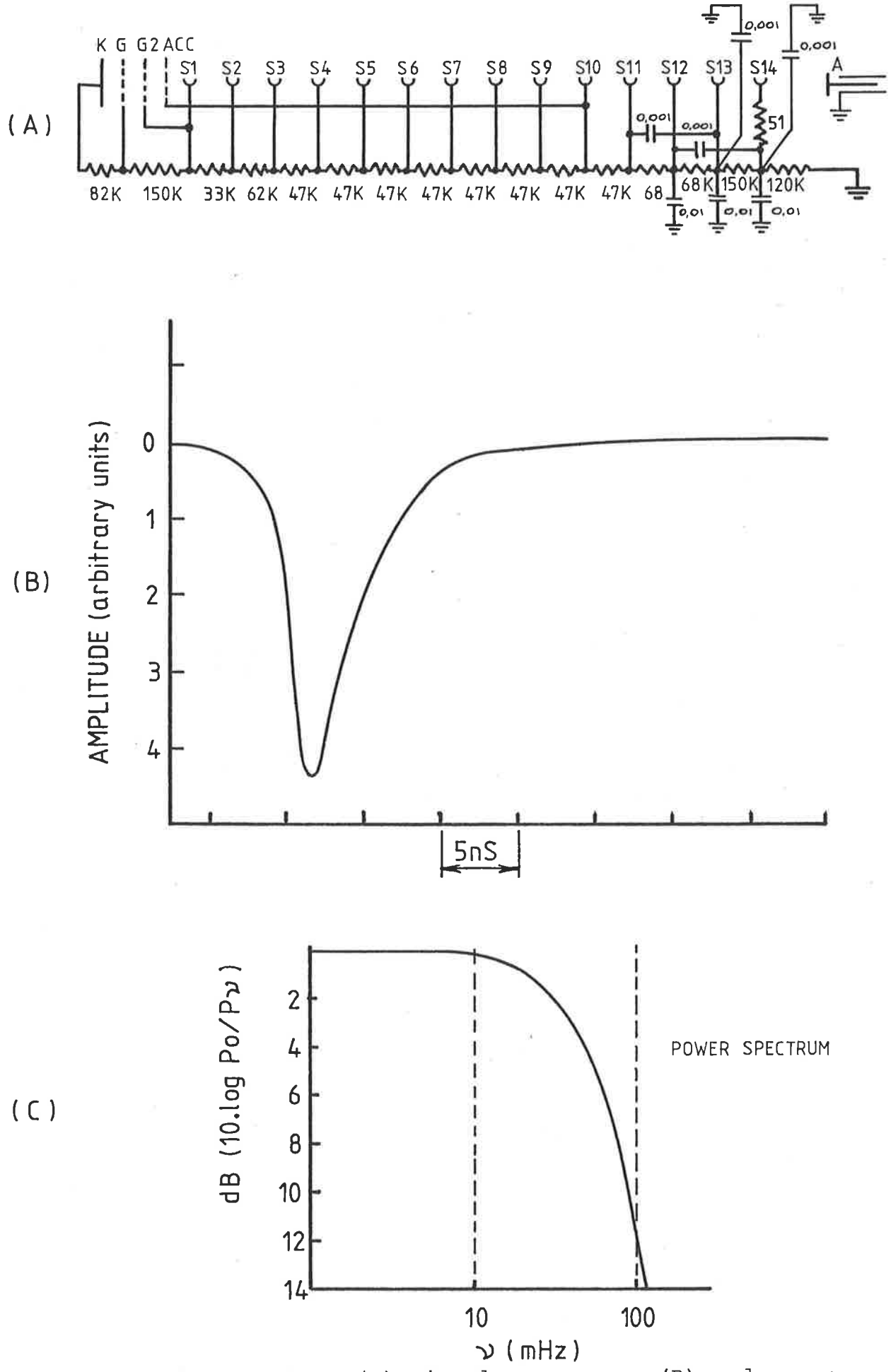

Figure 4.10: The base (A), impulse response (B) and power spectrum (C) of the impulse response of one of the photomultipliers employed in the experiment.

from different points on the photocathode will broaden the impulse response) impulse response of the system routinely. Instead it was deduced for each system from an examination of the largest amplitude (hence multi-photon), shortest duration pulses routinely detected by that system from the night sky background. It was assumed that the majority of such pulses originated in the numerous low energy EAS which reach maximum development high in the atmosphere with the consequent production of intrinsically narrow (<1ns) pulses. Thus the narrowest pulses routinely detected from the night sky background should be representative of the multi-photon impulse response. It was a relatively straightforward task to photograph a sequence of large amplitude background pulses by eliminating the requirement for a coincidence between the main array and each Cherenkov system and thus regularly monitor the impulse response. Photographs of either the single of multi-photoelectron impulse responses for all operative systems were taken at the commencement of most Cherenkov 'runs'. Neither of these pulse shapes were observed to alter significantly during the course of the experiment.

The overall shape of the multi-photoelectron response was observed to be only slightly broader ($\sim$0.5-1.0ns) than that of the single photoelectron response. The values of the multi-photoelectron impulse FWHM deduced from this method and employed in subsequent

analysis were 5.0 and 5.7ns for the Y and R systems respectively.

The 7834 oscilloscopes employed in each system were operated in the 'reduced scan' mode to maximise the writing speed and the timebase trigger AC-coupled to eliminate variations of the triggering rate arising from 'slow' variations ($\nu \lesssim 30$KHz) of the night sky background.

In any experiment it is highly desirable to place as low a discrimination level as possible on any recording apparatus, thus reducing the possibility of detecting a biased sample of data. The erasing of each trace stored on the oscilloscope screen and the preparation of the storage screen for the next trigger introduced and irreducible delay of $\sim$2 seconds between successive Cherenkov triggers. Clearly in such a system the oscilloscope trigger level cannot be reduced to an arbitrarily low value without seriously decreasing the time available to actually detect Cherenkov pulses (e.g. triggering the oscilloscope at a rate of $\sim$ten times/minute results in a $\sim$30% reduction of available viewing time).

Consequently a pragmatic approach of maximising the number of Cherenkov associated air showers detected by each system was adopted. After a series of trial experiments, a mean Cherenkov trigger rate of $\sim 8.5 \pm 1$ triggers/minute was decided upon and adopted for both systems for the duration of the experiment. Routine

monitoring of this rate was achieved by recording the number of Cherenkov triggers observed at each site over a ∿1-2 hour period, throughout the night. Any necessary adjustments were made manually at similar intervals.

Each successful Cherenkov trigger opened a 6μs gate (derived from the triggering of the oscilloscope timebase) in the associated electronics (figure 4.11) to allow the reception of any coincident particle array trigger. If an array trigger was received within the gate, the oscilloscope display was photographed and the camera automatically advanced. The storage screen enabled the camera shutter to be normally closed and opened only in the event of a particle/Cherenkov coincidence. As the rate of particle array triggers is ∿10/hour, their duration ∿800ns and the corresponding values for Cherenkov triggers are ∿510/hour and 6μs; then an upper limit to the rate of accidental (random) coincidences is given by:

$$\sim (10/3600)(510/3600)((6+0.8).10^{-6}) \text{ randoms/sec}$$

$$\sim 2.10^{-9} \text{ random/sec}$$

$$\sim 1 \text{ random/ten years}$$

4.3.3 CALIBRATION AND ROUTINE OPERATION

After initial verification of the manufacturer quoted chracteristics of each system, the sweep speed and frequency response of each oscilloscope was subjected to occasional checks in the field. Such tests were normally performed on all (up to four) oscilloscopes simultaneously. Master calibrations of the sweep rate

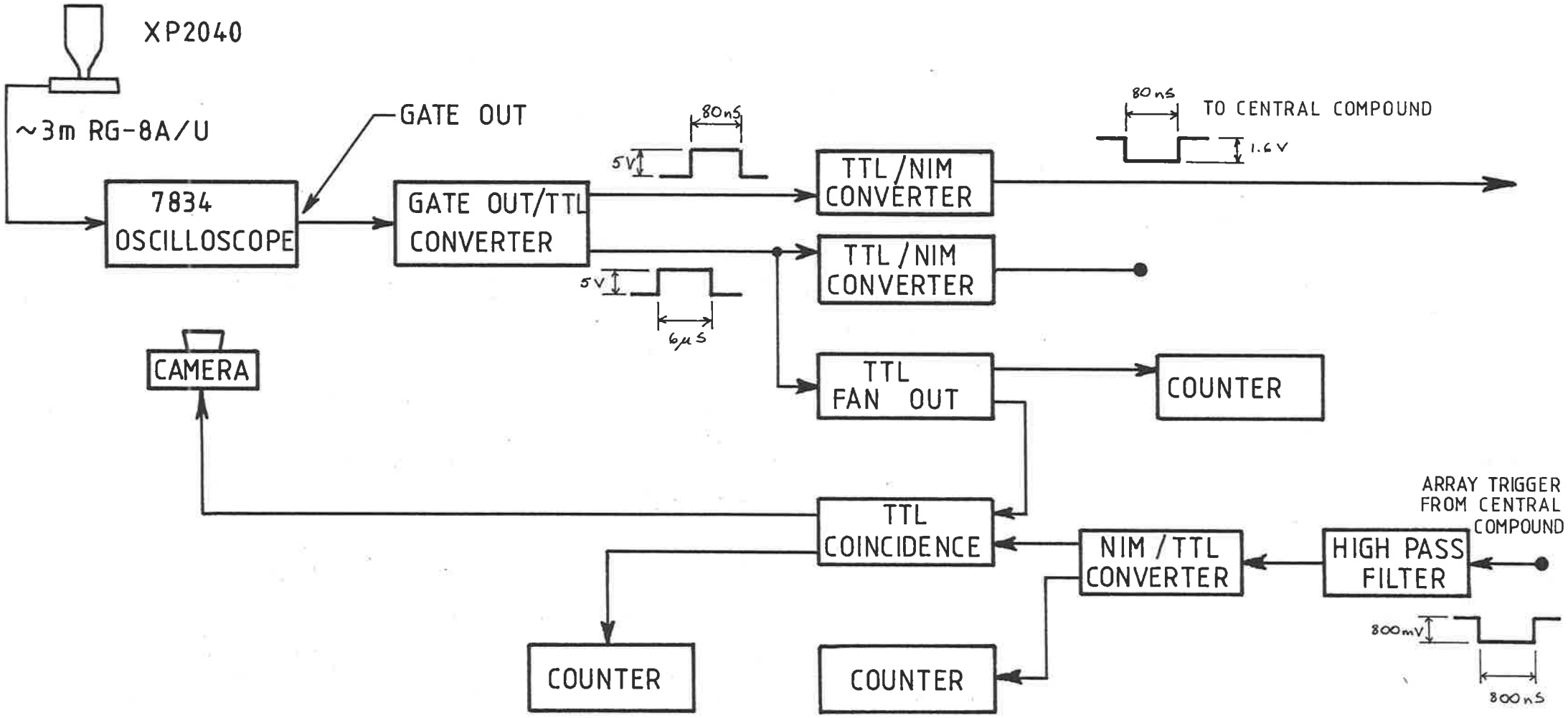

Figure 4.11: Block diagram of the electronics employed at each site to record Cherenkov pulses associated with EAS detected by the Buckland Park particle array.

were conducted with the aid of either a Wavetek (model 1002) or Hewlett Packard (model 8640B) signal generator by noting the frequency of the sinusoid required to produce exactly ten oscillations within ten divisions of the calibrated graticule (nominally 200MHz). It was noted that plug-ins (both horizontal and vertical) could not be exchanged between mainframes without re-calibration. As occasional replacement of mainframe of plug-in was necessary, usually at a time inconvenient for re-calibration, these occasions were noted and appropriate adjustments made retrospectively. We also note the routine observations of the single electron response section (4.3.2) provided a convenient monitor of the reliability of the sweep speed.

The frequency response of each oscilloscope was measured occasionally with the aid of a Hewlett Packard (model 8640B) signal generator. Throughout the life of the experiment only one significant deviation of the response was observed. Unfortunately, this fault was not isolated until the completion of a month's observing. Comparisons of photographs of a standard pulse shape before, during and after the fault was located indicated a detectable broadening of the pulses of $\lesssim$0.5ns in 10ns, which was considered irrelevant in terms of other typical errors.

The Cherenkov observations were performed on clear, moonless nights, usually during the six month

period October to March, weather permitting (figure 4.1), between the hours of astronomical twilight. Although moonless periods of sufficient duration are available on approximately fourteen nights of each lunar month, weather conditions limited observing to ∿4-5 mights in each new moon period, with a mean observing time of approximately four hours per night.

An automatic camera system to monitor the sky clarity, by recording half-hour exposures of the night sky within ∿20° of the zenith (broken star trails indicating the presence of cloud), was constructed and operated more or less routinely throughout the period of the experiment. The limited zenith angle response and poor ability to detect thin uniform cloud cover necessitated augmenting this data with visual observations at ∿1-2 hourly intervals.

Each night's observation commenced with the recording of either single or multi-electron impulse responses at each site (unless there had been a number of consecutive nights' observations). After initial setting of the Cherenkov trigger rate and measurement of the continuous anode current, the performance of each site was checked every 1-2 hours.

CHAPTER FIVE

DATA ANALYSIS

5.1 INTRODUCTION

We commence the chapter with a brief description of the computer simulations employed to interpret our observations. Expressions enabling the observed FWHM of the Cherenkov pulse (incorporating instrumental response) to be uniquely related to the height of maximum are then derived from these data. Selection effects inherent in the particle array/Cherenkov system employed to collect the experimental data are then discussed in some detail. The chapter concludes with an analysis of the observations, in the light of these effects.

5.2 COMPUTER SIMULATIONS

The simulations employed in the analysis have been described in detail elsewhere (Hillas 1982b,c, Patterson and Hillas 1983a,b). Only the relevant features are outlined below.

In contrast to the more usual method of simulating EAS (e.g. Protheroe 1977, McComb and Turver 1982b), Hillas (1982c) makes no attempt to simulate the complete air shower. Rather, the longitudinal development of the electromagnetic cascade is recognised as the determining feature of the Cherenkov emission. A separate simulation is employed to calculate the expected electron longitudinal

development for EAS initiated by protons of various energies (10^6,10^7,10^8 Gev) and various depths of maximum. The resulting electron development curves are then stored in a separate data-bank for future use. We note, in accord with our discussion in previous chapters, that the relationship between the depth of maximum and FWHM of the Cherenkov pulse is not expected to be sensitive to details of the mass or nuclear interactions of the primary particle (Hillas 1982c, McComb and Turver 1982b, Kalmykov et al 1977).

Hillas (1982c) views each development curve generated by the above technique as the sum of several electromagnetic cascades, each initiated by a 10 Gev photon, injected at regular intervals along the axis of the shower. The Cherenkov flux and its arrival time distribution for each longitudinal development curve is then calculated at 25 metre intervals in the core distance range of 125-300 metres by summing the contributions from individual 10 Gev 'sub-showers'. Again, the data for individual sub-showers have been previously calculated and are not simulated for each shower. The same set of development curves is employed to analyse the behaviour of inclined EAS by similar techniques.

Realistic models of atmospheric transmission incorporating Rayleigh scattering, aerosol scattering and ozone absorption are employed in the calculation to predict as accurately as possible the arrival-time

distribution and intensity of the Cherenkov light as it would appear to a system of infinite electronic bandwidth with a spectral response similar to that discussed in chapter four (extended S11(A) with plastic faceplate).

The simulation data available to the author comprised details of the expected arrival-time distribution of the Cherenkov radiation from 61 individual electron development curves (21 @ 10^6 Gev, 21 @ 10^7 Gev and 19 @ 10^8 Gev). Each curve was employed at four different zenith angles (0°, 15°, 30°, 40°) to yield a set of pulse shapes for each of 244 primary energy/zenith angle combinations at 25 metre intervals, in the plane of the showerfront, for core distances in the range 125-300 metres.

Every pulse shape in the data-bank was convolved by the author with both of two instrumental response functions. The functions were similar in shape to the pulse illustrated in figure 4.10 with the exception that the FWHM of the pulses were 5.0 and 5.7 nanoseconds, corresponding to the multi-photon impulse responses of the Y and R systems respectively. A separate data-bank detailing the characteristics of the shower (primary energy, zenith angle, depth and height of maximum) and the basic features of the pulse (core distance, area, peak flux, true width, convolved width) was constructed for each impulse response. Figure 5.1 illustrates the true and convolved pulse shapes predicted by this model

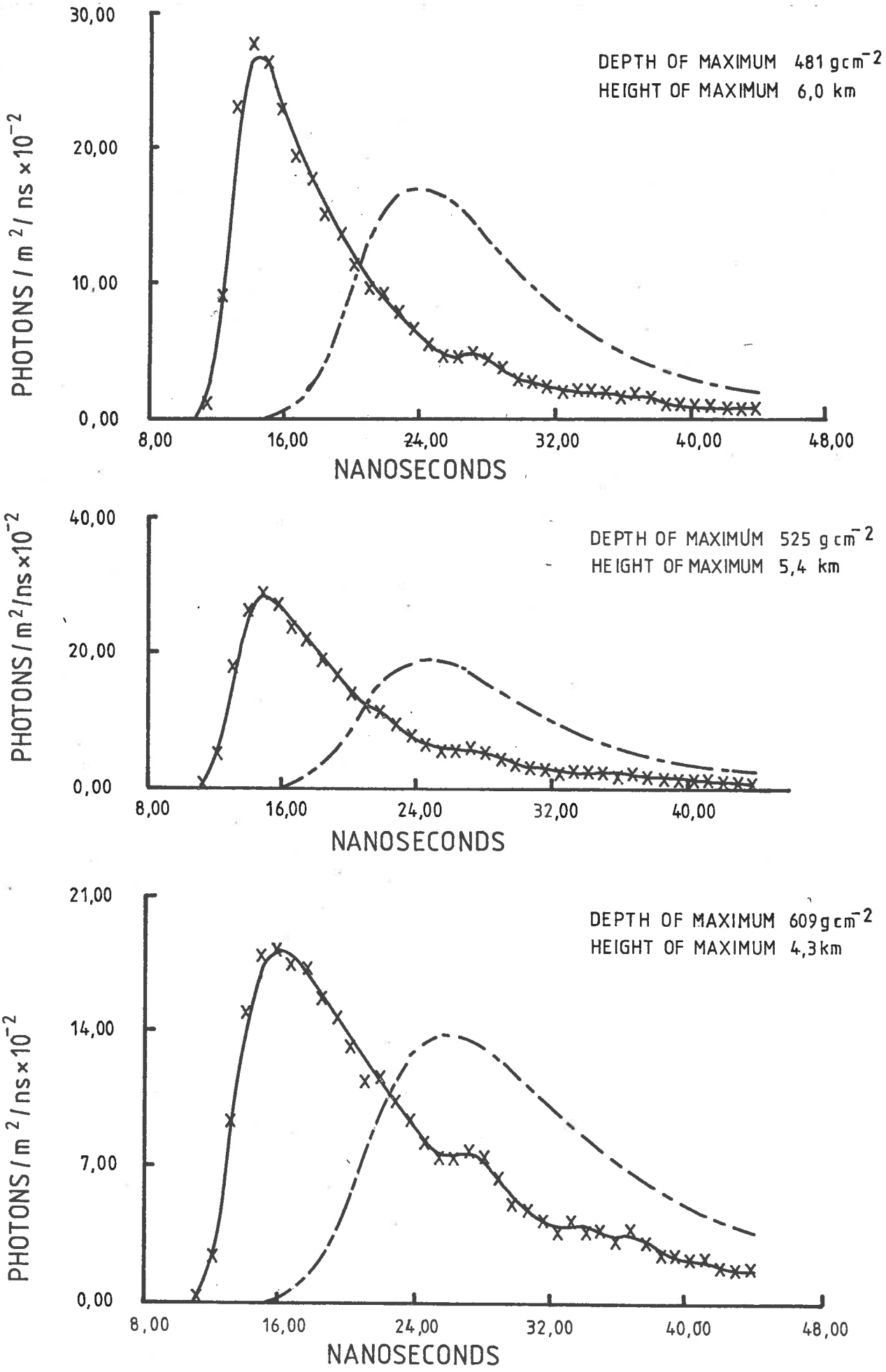

Figure 5.1: The true (solid line) and convolved (dashed line) pulse shapes predicted by the simulations employed in the data analysis. All showers were initiated by vertical 10^6 Gev protons and observed at 200 metres from the core.

at a core distance of two hundred metres for several vertical showers, each of 10^6 Gev primary energy.

Figure 5.2 illustrates the relationship between the width of the true pulse and height of maximum for the available sample of data of 10^6 Gev showers at several core distances. It is noted, in accord with the discussion of Hillas (1982c) and McComb and Turver (1982b), that inclined showers observed within $\sim$200 metres of their core demonstrate less sensitivity to development than do other, more nearly vertical, showers. McComb and Turver (1982b) suggest that the FWHM may be development sensitive in vertical showers at core distances down to $\sim$100 metres, whereas the FWHM of EAS inclined at sixty degrees to the zenith ceases to be development sensitive at $\sim$200 metres. This is not in disagreement with the data of Hillas (1982c). Consequently a conservative function, derived from the data of figure 5.2 and graphed in figure 5.3 was employed to ensure that inclined EAS were always observed sufficiently far from their axis that the above effect was negligible.

5.2.1 DEDUCTION OF HEIGHT OF MAXIMUM FROM THE OBSERVED FWHM

It was noted in chapter three that previous analyses have made it apparent that a relatively straightforward relationship exists between the logarithm of the width of the true Cherenkov pulse and the height of shower

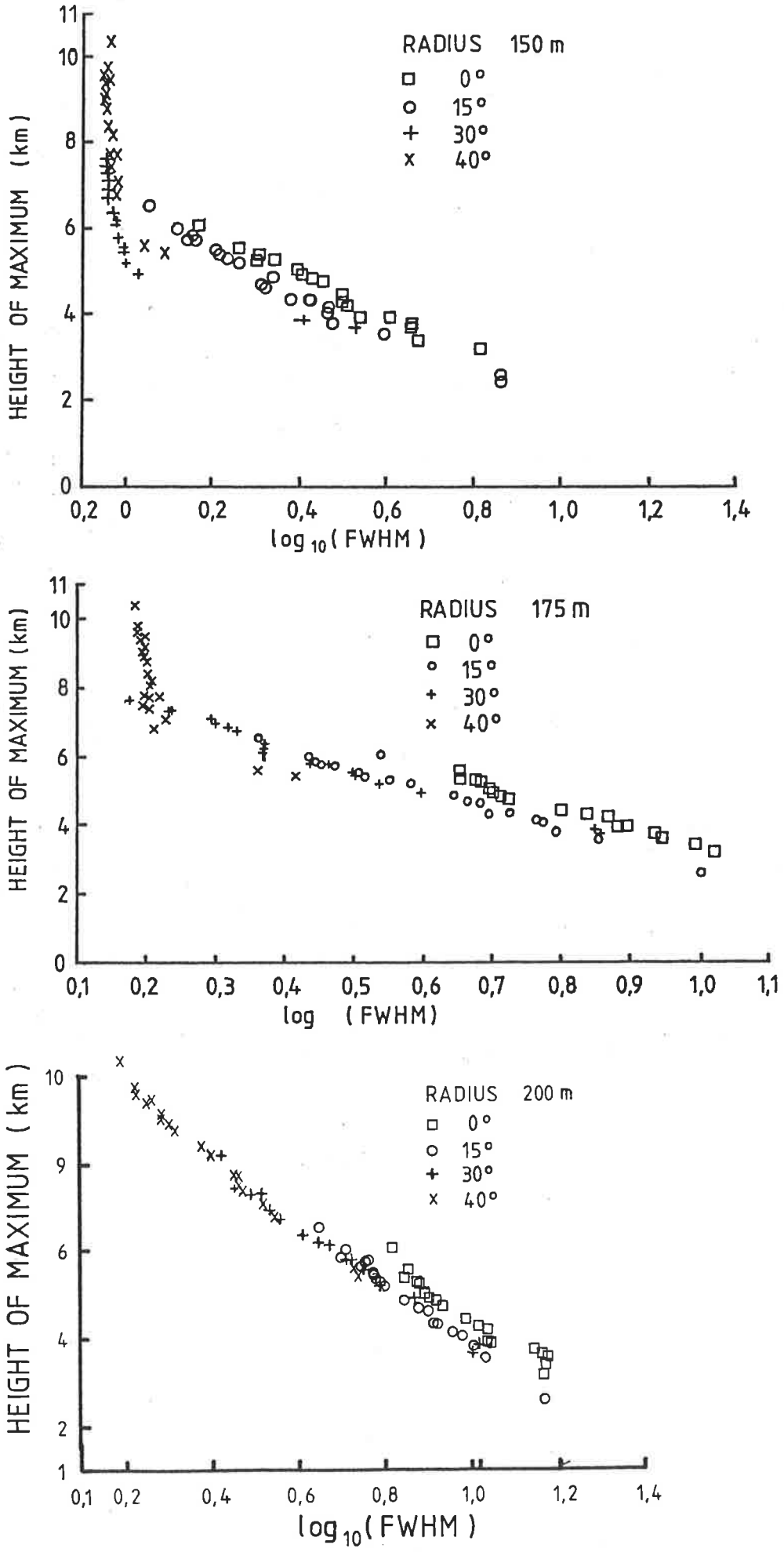

Figure 5.2: The dependence of the full width at half maximum on the height of maximum for core distances ≤200 metres. FWHM measured in ns.

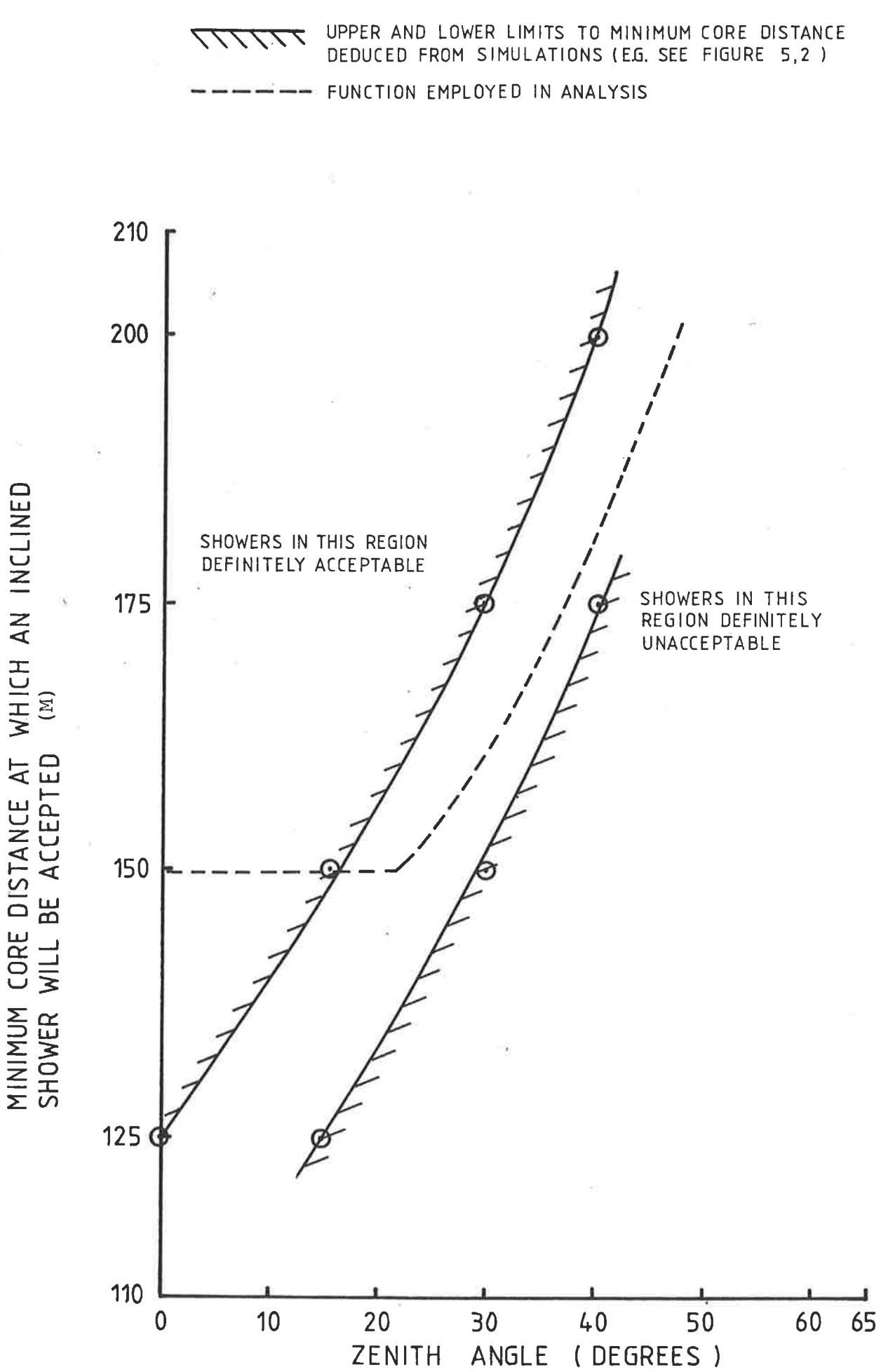

Figure 5.3: Function employed to deduce minimum core distance at which an inclined shower was accepted for analysis. Th two extremes were deduced from examination of the predicted FWHM of pulses recorded at 125,150,175,200metre from the core of EAS incident at 0°,15°,30° and 40°. (We note the general agreement with the comments of McComb and Turver 1982b)

maximum (e.g. figure 5.2). Figure 5.4 graphs, on the same scale the relationship between both the observed FWHM and the true FWHM and the height of maximum. Similar relationships were observed at other core distances. In view of this, it was thought reasonable to attempt to express the convolved widths in a functional form similar to that of Patterson and Hillas (1983a) (originally based on the expression of Kalmykov et al 1979) viz:

$$H_R = a + (b(\log(t_R)) + c(\log(t_R))^2 \quad ..(5.1)$$

t_R = FWHM of pulse recorded at R metres (ns)

H_R = height of maximum development (km)

The available data were found to be well-represented by such expressions over the range of relevant core-distances. In particular we have for the Y and R systems (impulsive FWHM 5.0 and 5.7ns respectively);

$$H_{200} = 52.52-70.98(\log(t_{200})) + 25.24(\log(t_{200}))^2 \quad ..(5.2)$$

$$H_{200} = 59.54-79.87(\log(t_{200})) + 27.98(\log(t_{200}))^2 \quad ..(5.3)$$

t_{200} = observed FWHM at 200 metres (ns)

H_{200} = height of maximum (km)

For both expressions the standard deviation of the residuals was $\sim$300 metres ($\sim$15g cm^{-2}) and the square of the multiple-correlation coefficient (R^2) 97%.

Figure 5.5 illustrates the radial dependence of the convolved FWHM (impulse response FWHM 5.0ns) for a number of vertical 10^6 Gev showers. A similar dependence was observed in data incorporating a 5.7ns impulse

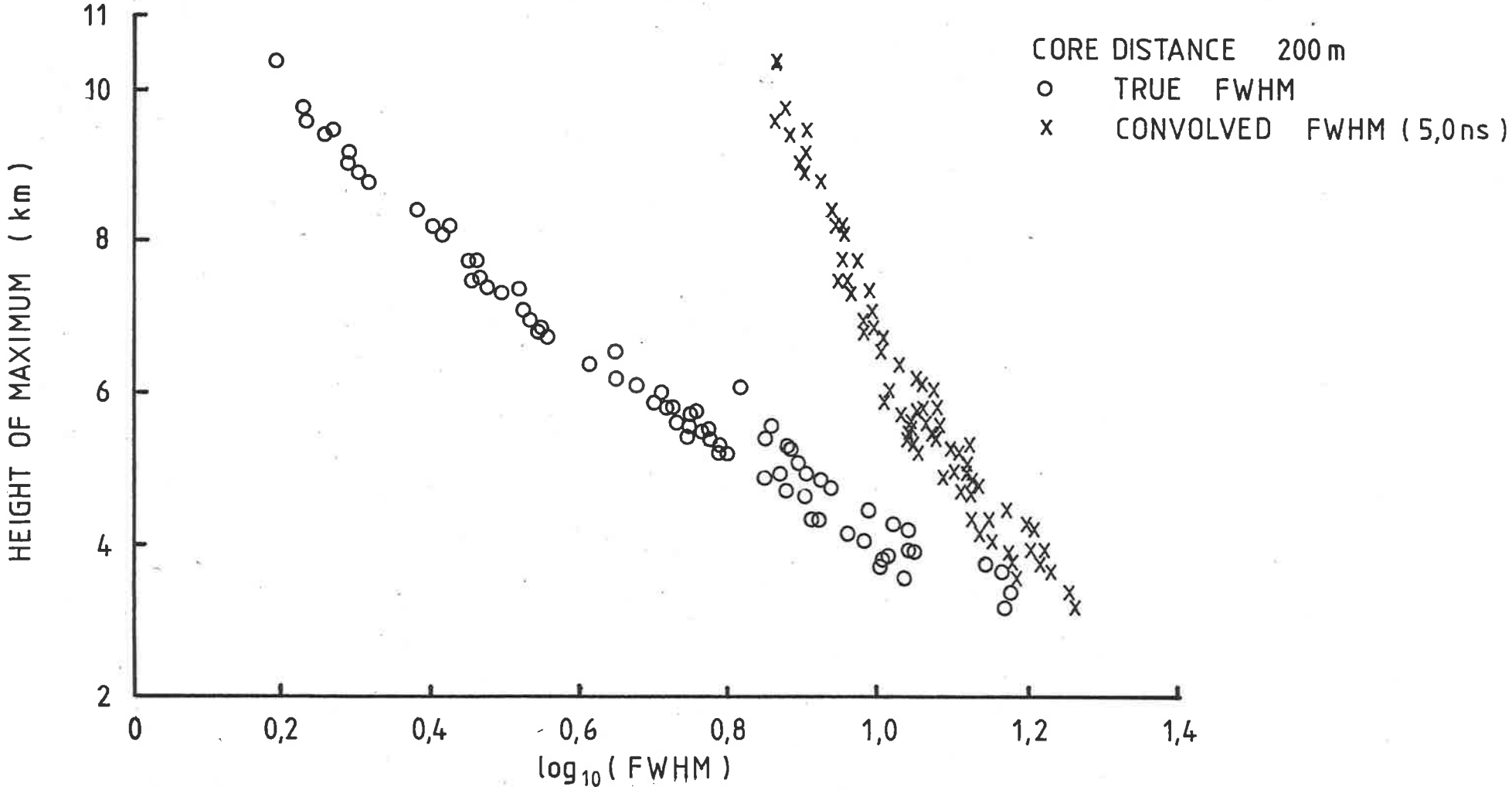

Figure 5.4: Plot of the true and convolved FWHM (nanoseconds) observed at 200 metres for a large sample of 10^6 Gev proton showers, incident at zenith angles of 0°, 15°, 30° and 40°.

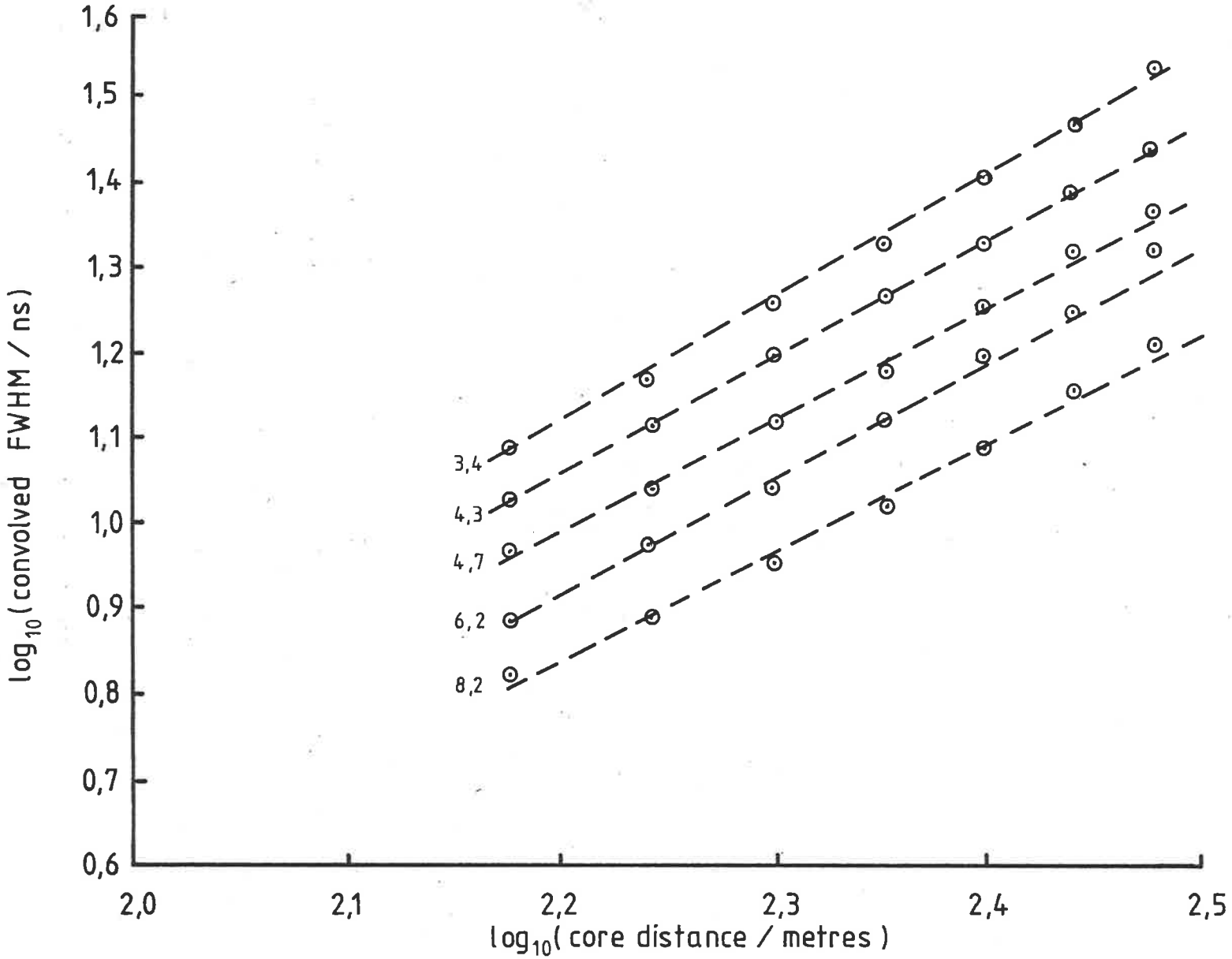

Figure 5.5: Radial dependence of the convolved (5.0ns) FWHM for several 10^6 Gev proton initiated showers at various zenith angles. The numerals attached to each curve indicate the height of maximum (km) of the shower.

response. The salient features are: the convolved FWHM, unlike the true FWHM (e.g. Patterson and Hillas 1983a) can be accurately represented by a power law whose index decreases slowly with the height of maximum. This relationship would appear to be somewhat fortuitous and is obviously dependent on the assumed shape and duration of the impulse response of the Cherenkov system. Nevertheless, for us, it provides an accurate and reliable means of interpolating between core-distances. The variation of the power law index for all showers in the data-bank was found to be well-fitted by expressions of the form

$$n = 1.57-0.030H \quad \text{(5.0ns impulsive FWHM)} \qquad ..(5.4)$$

$$n = 1.50-0.025H \quad \text{(5.7ns impulsive FWHM)} \qquad ..(5.5)$$

n = index of power law fitted between 150-300 metre

H = height of maximum (km)

For both fits the standard deviation of the residuals was $\lesssim 0.02$ and the square of the multiple correlation coefficient (R^2) $\sim 97\%$.

Equations 5.2-5.5 may be combined to yield a quadratic equation in H (height of maximum), the solution of which always yields two real roots, one of which appears to be infeasible ($\gtrsim$100's km). In routine analysis both roots were always examined for feasibility ($0.0<H<13.0$). On no occasion were two 'feasible' roots located.

5.3 ANALYSIS

The Cherenkov data available for analysis were divided into two main groups depending on which detector (R or Y) recorded the pulse. The data for system R were further divided into two smaller groups depending on whether a pulse was recorded with the detector at the (0,150) location or at the (0,200) location (see figure 4.2). The reasons underlying this partitioning will be discussed shortly.

Approximately 733 showers detected by the array during the course of the experiment triggered the R Cherenkov system. Of these, 112 were unsuited for further analysis as the peak of the pulse lay well outside the calibrated area of the oscilloscope display. The number of useful pulses associated with EAS of relatively well-determined core locations and sizes ($\psi_r^2 < 5.0$ and the core at least 5 metres inside the physical boundary of the array) was 543. The rejection of pulses recorded at core distances below 150 metres and the limited acceptance of showers in the core distance range of 150-200 metres (section 5.2) reduced this number still further to 299. Of these, 166 were recorded at the (0,150) site and 183 at the (0,200) site. Similar criteria applied to the data detected by system Y at the (164,-117) location reduced the number of possible Cherenkov pulses (for that system) from $\sim$320 to $\sim$170.

A subset of approximately forty showers in which a useful pulse was recorded on each of the R and Y systems while they were located at (0,200) and (164,-117) respectively was selected to compare the measured radial dependence of the FWHM and that predicted by the computer simulations. We note that at a 'typical' height of maximum of ∿5-6km, both systems are epxted to have observed FWHM which vary approximately as $R^{1.4}$ (equations 5.4 and 5.5) and the exponent is not strongly dependent on altitude. A reliable shower analysis is essential in determining the radial dependence experimentally. With only two measurements per shower, an error of a few metres in ∿200 metres can alter the derived value of the exponent by large amounts. Consequently, additional restrictions were placed on the value of ψ_r^2 for events employed in this analysis. The resulting data set and imposed restrictions are summarized below:

lower limit to ratio of core distances:	1.3	1.2	1.18	1.1
ψ_r^2 upper limit:	2	2	2	3
number of events accepted:	6	9	14	25
mean value of power law index:	1.42 ±.20	1.14 ±0.22	1.06 ±0.17	1.26 ±0.20

The columns in the above table progress from left to right in order of decreasing confidence of individual showers. We note that the most reliable data sample, although small, has a mean value close to the value of 1.4 predicted by the simulations. The less critically selected data sets have

mean values not inconsistent with that predicted by the simulations.

Thus the 3 sets of data described previously (system R at (0,150), system R at (0,200), system Y at (164, -117)) were analysed with the aid of equations 5.2-5.5 to determine the variation of the mean depth of maximum with vertical sea-level size. An exponential atmosphere, pressure scale height 8.0km, provides an adequate representation of the Adelaide atmosphere in the range 400-800g cm^{-2} (S. Young priv.comm.) and consequently was employed in this analysis.

5.4 INTERPRETATION

5.4.1 EFFECTS OF LIMITED DYNAMIC RANGE

Present indications (e.g. Kamata 1981) would seem to imply that the EAS detected by the Buckland Park particle array (vertical sea-level sizes $\sim 10^5$-10^7 particles) reach maximum development somewhere in the region $\sim$425-700g cm^{-2}. Ideally then, an experiment designed to measure the mean depth of maximum and its variations over this size range would be equally sensitive to all showers with a depth of maximum in the range $\sim$425-700g cm^{-2}, regardless of the vertical sea-level size of the shower. However, in any physically realizable system there is a minimum and a maximum pulse amplitude which may be recorded. In the case of oscilloscope based recording systems, this dynamic range of $\sim$10X is determined by the triggering level of the oscilloscope at one extreme and the physical dimensions of the oscilloscope screen at the other. Consequently, we might expect such systems to preferentially select early-developing showers at small sea-level sizes (low energy). Here the narrow FWHM, characteristic of

early-developing showers, confines the total Cherenkov flux to a pulse of amplitude sufficient to trigger the oscilloscope. Late-developing showers with their intrinsically broader FWHM (and consequently lower amplitude) fail to trigger the oscilloscope. At large vertical sea-level sizes (high energy) we expect the opposite bias, preferential detection of late-developing showers. Early-developing showers being lost from the data sample as their peak Cherenkov flux exceeds the limited dimensions of the oscilloscope screen, whilst the peak amplitude of late-developing showers (broader FWHM) is sufficient to trigger the system yet not exceed the dynamic range.

Thus, if the depth of maximum were truly uniformly distributed between the limits of 425 and 700g cm^{-2} (i.e. its mean value does <u>not</u> alter with vertical sea-level size), then a system of limited dynamic range (i.e. any physical recording system) would be expected to record data indicating a steady increase of the depth of maximum with vertical sea-level size (see figure 5.6). An attempt to quantify these effects and analyse the recorded data in view of them follows.

5.4.2 THE 'RESPONSE' FUNCTION

The computer simulations discussed previously were employed to develop a relationship between the peak amplitude of the observed pulse at some arbitrary core-distance in the range 150-300 metres and the depth of maximum, zenith angle and number of electrons at maximum

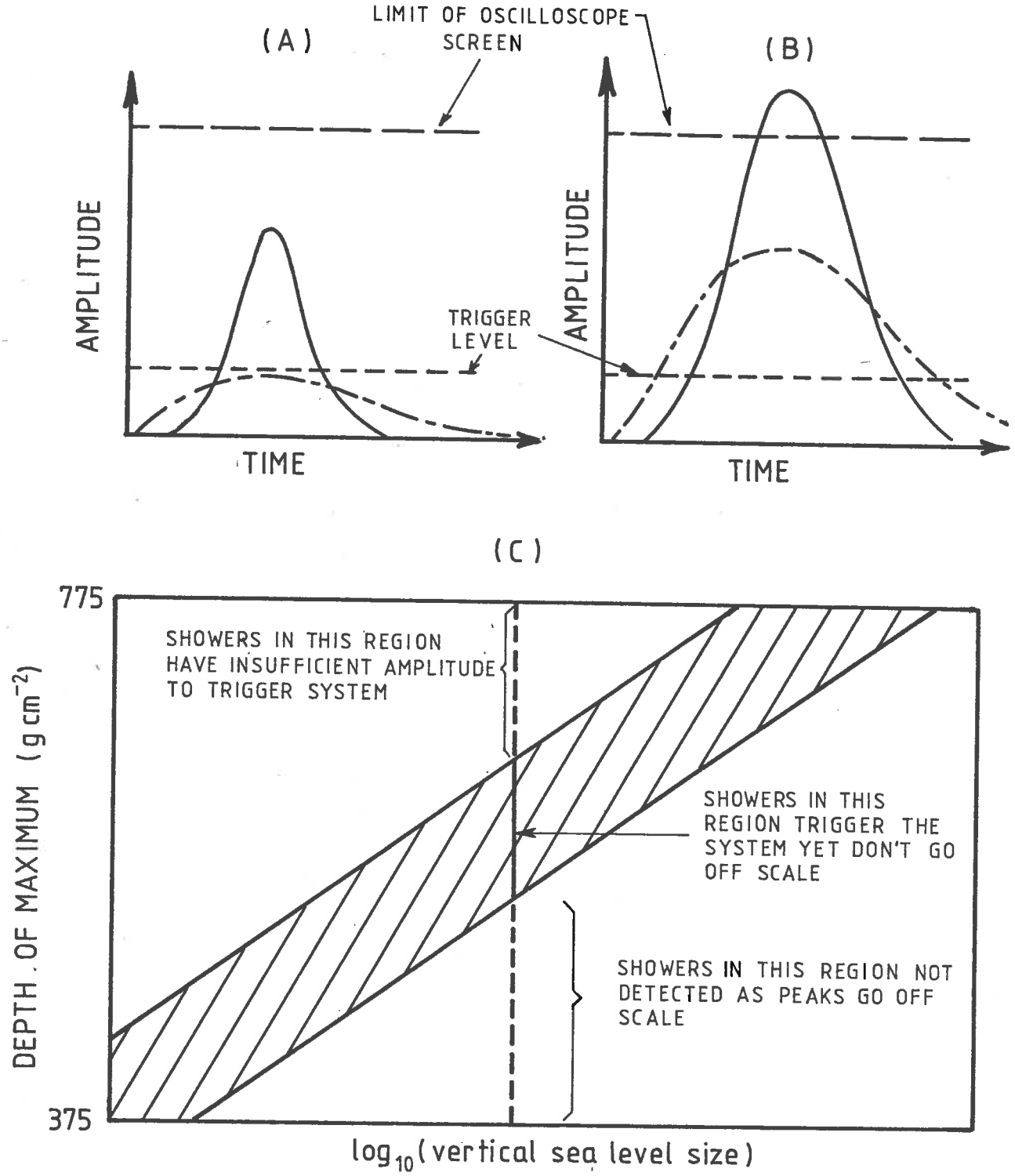

Figure 5.6: A series of sketches illustrating selection effects introduced by the limited dynamic range of the recording system.

(A) - At small sizes early developing (narrow pulse) showers are preferentially detected.

(B) - At large sizes late developing (broad pulse) showers are preferentially detected.

(C) - In progressing from small to large sizes we expect to detect showers reaching maximum in a limited range of atmospheric depths only. The maximum detectable depth is determined by the triggering level of the oscilloscope and the minimum by the extent of the screen. In this simple model all showers in the shaded area have 100% detection probability, whilst all those outside have 0% detection probability. Such a two-dimensional plot of detection probability has been termed a 'response' function in later discussion.

(primary energy). An excellent fit capable of predicting the peak flux for all 244 showers in the data sample at core distances in the range 150-300m to an accuracy of better than 10% was given by an expression of the form:

$$\ln(F) = k + a[\ln(R)]+b[\ln(H)]+c[\ln(N)] \quad ..(5.6)$$

F = peak flux of convolved pulse (photons/m^2/ns)

R = distance of detector from shower axis (metres) (in the plane of the showerfront)

H = height of maximum (km)

N = number of electrons at maximum

This functional form was well-fitted by the observed peak amplitudes deduced for both the 5.0 and 5.7ns impulsive FWHM systems:

	5.0ns	5.7ns
a:	(.234±.008)	(.208±.008)
b:	(-3.43±.01)	(-3.42±.01)
c:	(.998±.001)	(.998±.001)
k:	(11.75±.07)	(11.62±.07)

In both cases the square of the multiple correlation coefficient (R^2) was 99.7%. It is noted that showers differing from each other only by a factor of ten in primary energy (number of particles at maximum) are expected to produce pulses with aplitudes at the two extremes of the oscilloscope's dynamic range.

Conversion between the peak flux (photons) predicted by equation 5.6 and the actual measured amplitude (oscilloscope divisions) was achieved by performing a linear

regression between the prediction of equation 5.6 and the measured pulse amplitude for a sample of showers in which the height of maximum could be reliably determined from the measured FWHM. The number of particles at maximum was then deduced from the sea-level size and zenith angle of the EAS assuming an attenuation length of 185g cm^{-2}. Am empirical correction to allow for the shape of the cascade curve near maximum (i.e. electromagnetic component does not decay immediately with an attenuation length of 185g cm^{-2} from the point of maximum) was deduced from the available data-bank of proton cascade curves discussed previously.

A sample of $\sim$3,500 showers, assumed representative of the entire population of EAS detected by the Buckland Park particle array and analysed by the author in accord with the discussion in chapter four, was then employed to determine the range of atmospheric depths, as a function of vertical sea-level size, over which each detector could be expected to record a pulse reliably. Such 'response' functions are expected to depend on the physical location of the appropriate detector, as most well-analysed showers fall within a few tens of metres of the centre of the array.

A computer program selected showers from the sample of 3,500 which satisfied the usual restrictions placed on EAS employed in a determination of the depth of maximum (ψ_r^2<5.0, core at least 5 metres inside the array

and core falling at least 150 metres from the detector (or further in the case of inclined showers). The shower depth of maximum was then sampled from a random distribution uniformly distributed between 375 and 775g cm^{-2} and the expected peak flux, in oscilloscope divisions, calculated using equation (5.6). Again, the number of particles at maximum was inferred from the sea-level size, zenith angle and depth of maximum assuming an attenuation length of 185g cm^{-2} and allowance made for the exact shape of the cascade curve. Thus it was possible to calculate whether or not a shower of the given vertical sea-level size and depth of maximum, detected by the array, would have been recorded by an oscilloscope at a certain physical location.

The lower limit of acceptable amplitudes (trigger level) was selected after an analysis of the actual spectrum of pulse amplitudes recorded by each detector at each location. In all cases the spectra were consistent with a triggering level of 1.0 division. The upper limit was determined by the limited calibrated areas of the oscilloscope screens when operated in the 'reduced-scan' mode. This is nominally 8 divisions, although examination of the performance of each oscilloscope indicated that no significant error was introduced by accepting pulses of up to 10.0 divisions amplitude. The results of this analysis were binned in quarter decade intervals of vertical sea-level size and 25g cm^{-2} intervals of depth

of maximum to produce a two-dimensional plot of triggering probability as a function of depth of maximum and vertical sea-level size (the response function). To ensure that sufficient showers were recorded in each bin, the actual sample of 3,500 showers was cycled through four times, each shower being assigned a different depth of maximum each time.

Some examples of response functions deduced from this analysis appear in figure 5.7 which illustrates the effect of imposing a lower threshold on the detected amplitude, but no upper limit and vice-versa. We note that the general features are in accord with our earlier a-priori discussion of the effects of limited dynamic range. Figures 5.8-5.10 illustrate the response functions for each of the sites (0,150), (0,200) and (164,-117) as deduced from the above analysis. Superimposed on each response plot are curves illustrating the expected variation of the mean depth of maximum with vertical sea-level size for two extreme models of EAS development incorporating contemporary nuclear physics models. These curves have been deduced from the published data of Chantler et al (1983) assuming that an EAS initiated by a primary particle of E Gev has (E/2) particles at maximum (accurate to $\lesssim$10%, e.g. Linsley and Hillas 1981) and thereafter decays exponentially with an attenuation length of 185g cm^{-2}, again allowance is made for the actual shape of the cascade curve near maximum. The salient feature of these plots is the relatively poor sensitivity of each system to typical

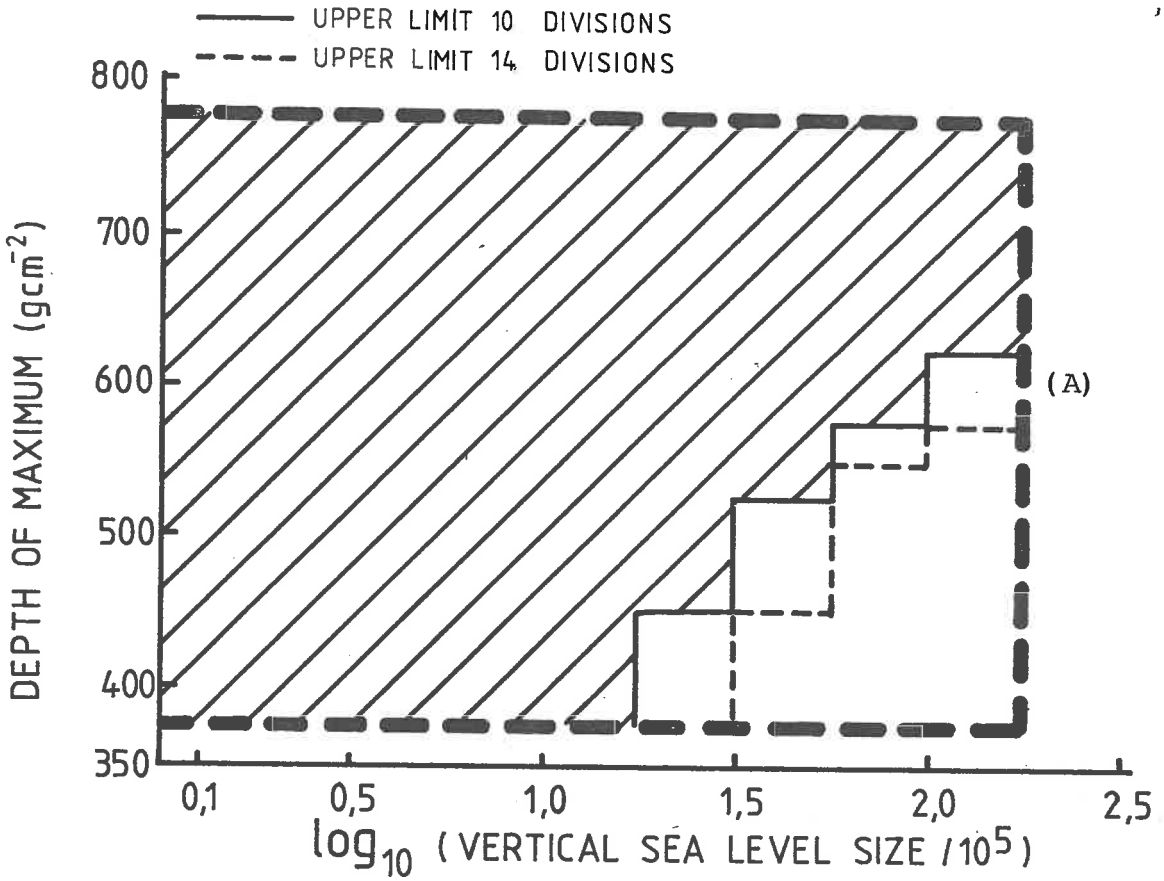

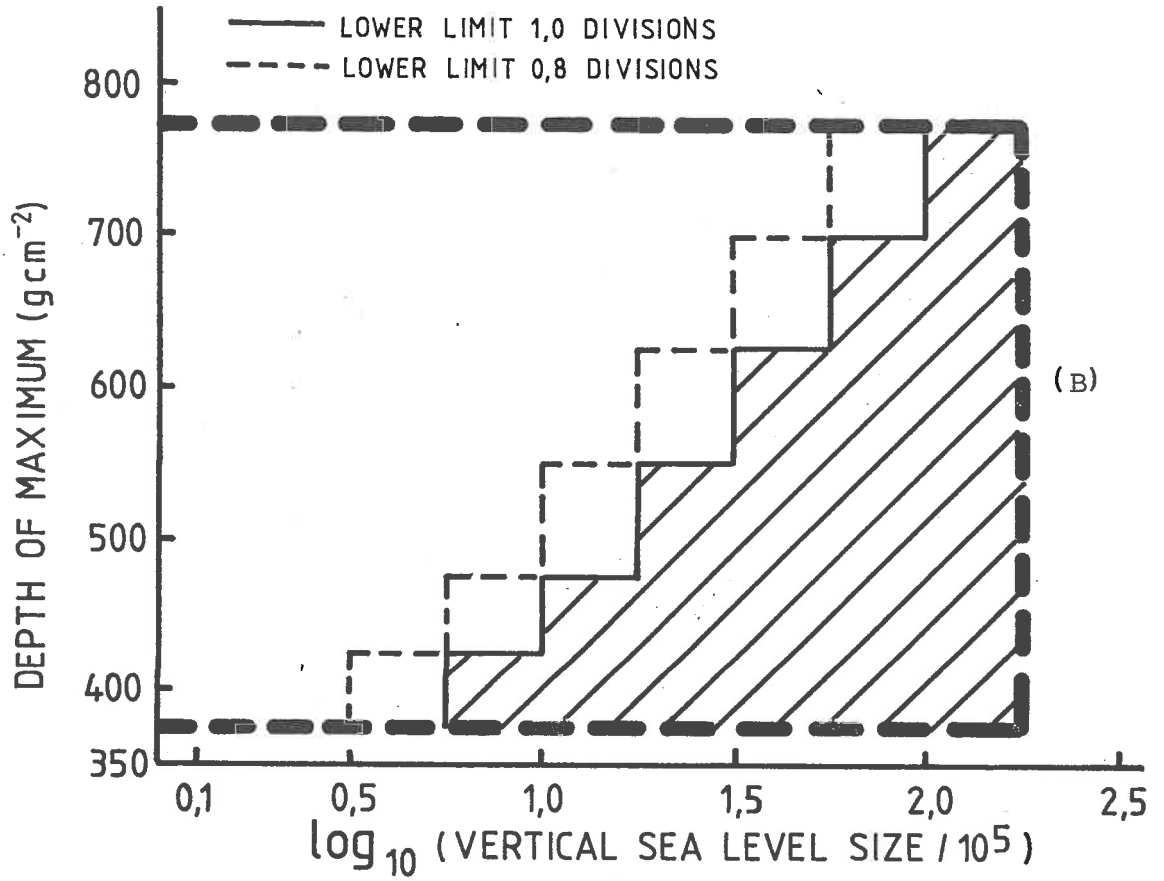

Figure 5.7: Some simple response functions. Shaded area indicates extent of ≥90% detection probability for system Y at (164,-117).
(A)- trigger level=0.0 divisions, upper limit=12 or 14 divisions
(B)- trigger level=0.8 or 1.0 division, no upper limit
'Staircase' effect results from finite size bins employed in analysis.

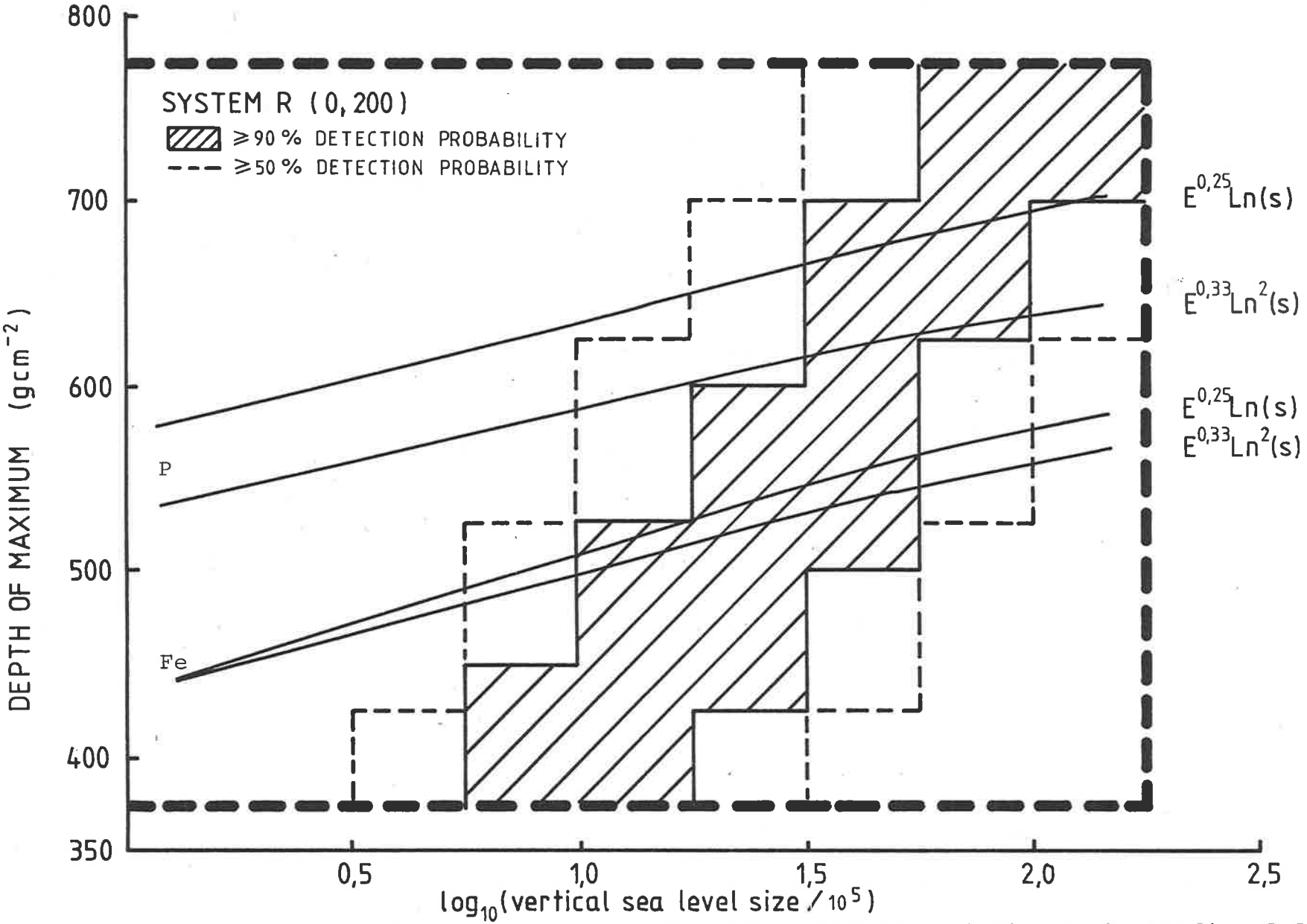

Figure 5.8: Response function of system R at (0,200). Solid lines indicate the predicted dependence of depth of maximum on vertical sea-level size for the models discussed in the text.

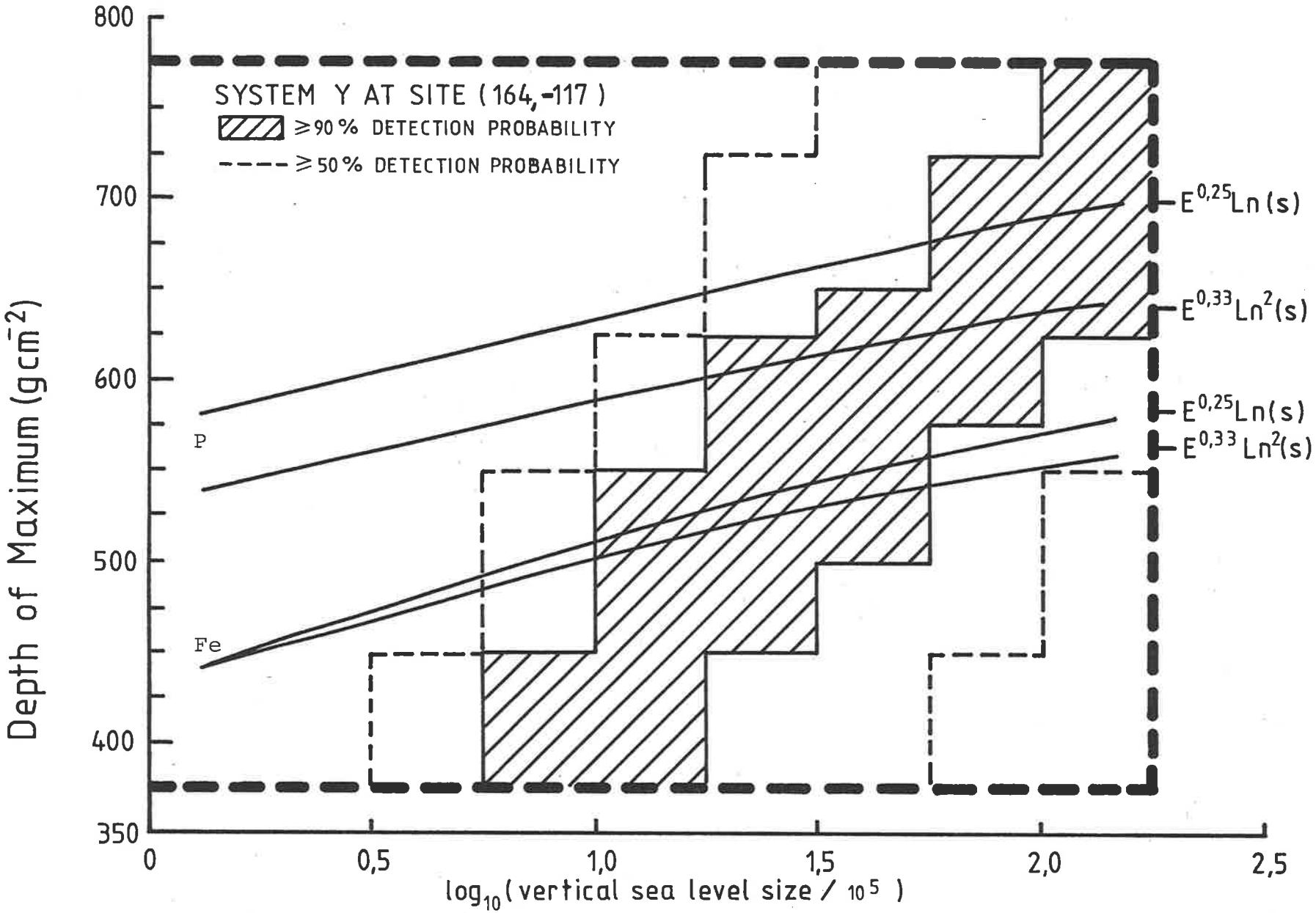

Figure 5.9: Response function for system Y at (164,-117). Solid lines are the predicted dependence of of depth on maximum on vertical sea-level size for the models discussed in the text.

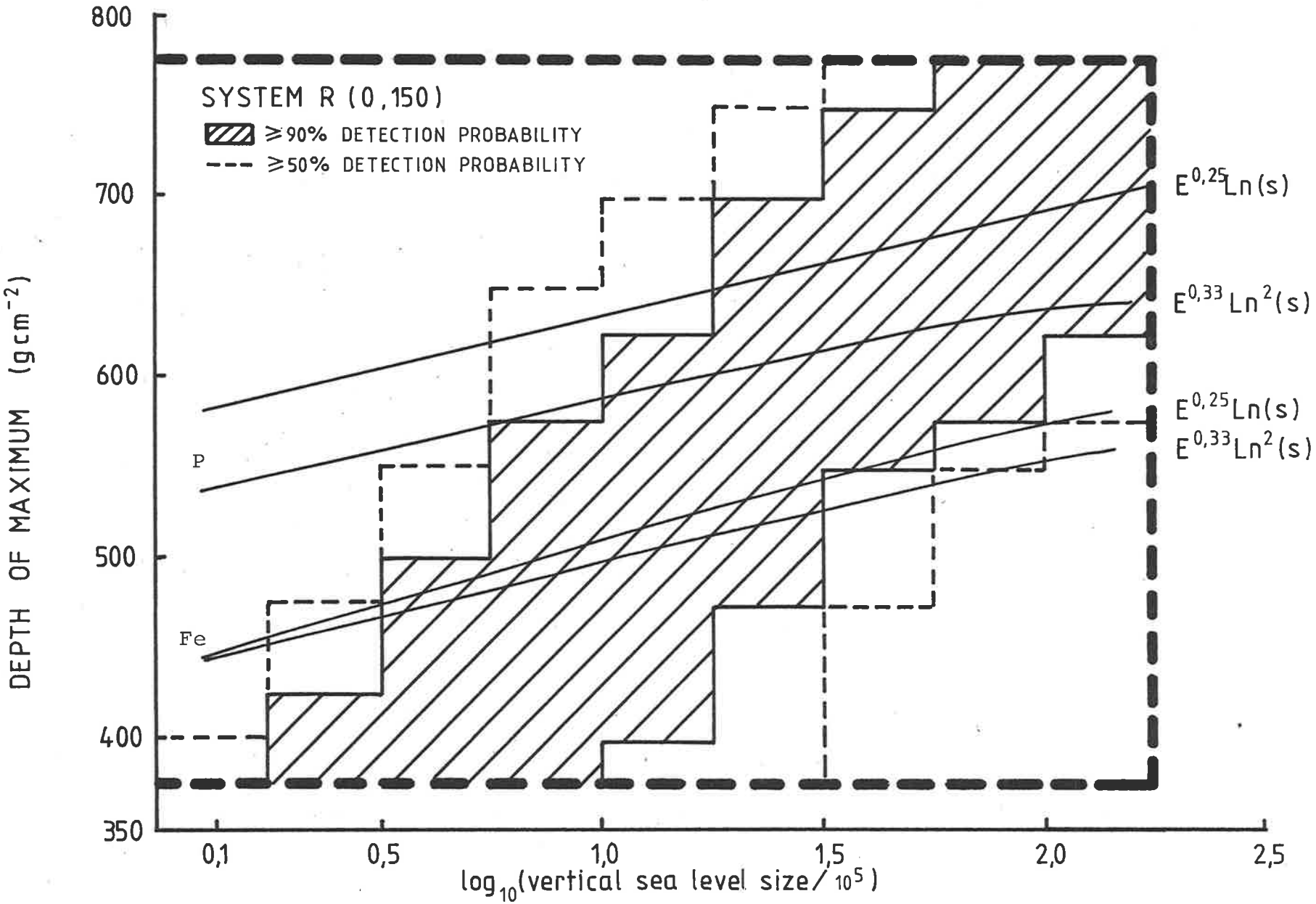

Figure 5.10: Response function of system R at (0,150). Solid lines indicate the predicted dependence of depth of maximum on vertical sea-level size for the models discussed in the text.

proton showers. It would seem that at sizes $\lesssim 2.10^6$ particles only extremely early developing proton showers will be detected, with a consequent distortion of the mean depth of maximum. We now discuss the effect of these detection biases on the observed depth of maximum.

5.4.3 EXPECTED VARIATION OF THE MEAN DEPTH OF MAXIMUM

The expected variation of the mean depth of maximum with vertical size for each possible combination of detector, composition (100% protons or 100% iron nuclei) and nuclear physics model (see Chantler et al 1983), was calculated assuming realistic models for the fluctuations in depth of maximum development.

For proton initiated EAS the published data of Chantler et al (1983) indicating the width of the distribution (standard deviation) expected for each of the two extreme nuclear physics models considered (central multiplicity rising as $E^{0.25}$, cross-sections as ln(s); central multiplicity rising as $E^{0.33}$, cross-sections as $\ln^2(s)$) served as a basis. As no published data detailing the expected shape of this distribution, at relevant energies, was available, it was assumed, in line with our discussion in chapter two, that the distribution could be adequately represented as the convolution of two distinct components. One, an exponential distribution (width characterized by the proton mean-free path) reflecting the variation in depth of initiation and the other, a gaussian, reflecting differences in development between showers initiated at similar depths.

The data of Chantler et al (1983) provided the relevant mean free path of the proton and hence the standard deviation of the exponential distribution. Convolution of this distribution with a gaussian of the appropriate width then provided a distribution whose standard deviation was consistent with that published by Chantler et al (1983). It was not thought realistic to attempt to introduce energy dependent fluctuations, rather the expected fluctuations of a 10^7 Gev shower were adopted for all primary energies in the range considered ($\sim 10^6$-10^8 Gev) the values employed (essentially after Chantler et al 1983) were:

model	proton mfp	overall width
ln(s)	62g cm^{-2}	90g cm^{-2}
$ln^2(s)$	54g cm^{-2}	70g cm^{-2}

Data on the expected distribution of the depth of maximum for iron nuclei are even more scarce than for proton initiated EAS. In light of the discussion of Watson (1982) an energy independent gaussian distribution with a standard deviation of 35g cm^{-2} was assumed as a reasonable upper limit at $\sim 10^7$ Gev. The choice of somewhat narrower, or perhaps even broader, distributions is not expected to affect to conclusions significantly due to the relative efficiency of the detecting systems at depths appropriate to iron nuclei (figures 5.8-5.10).

It should be noted that there is, unfortunately, a significant degree of arbitrariness in the above choices

due to the limited amount of information available (see e.g. Watson 1982). The final choices were, however, considered relatively realstic interpretations of the available data.

With these fluctuation models it was possible to produce two-dimensional plots - similar to the response plots - detailing the probability of a given primary particle/nuclear physics combination producing a shower of a given vertical sea-level size and depth of maximum. These are the depth of maximum distributions observed by an ideal system (i.e. its response function has 100% detection efficiency at all relevant depths and sizes). It was expected, and confirmed, that the mean depth of maximum, in each size bin, should correspond to the mean depth expected from the appropriate composition/nuclear physics model (these are the solid curves in figures 5.8-5.10). Multiplication of this 'ideal' distribution by the appropriate response function then yielded the expected variation of the depth of maximum with vertical size for each detector.

Figures 5.11-5.13 display these expected variations for each of the four composition/nuclear physics combinations discussed. Also plotted are the actual measured variations of the mean depth of maximum with vertical size. We note again that these measured values are not the 'true' values of depth of maximum at a given size. They are the product of the detector response function and the 'true' distribution of depth of maximum at that size. For the

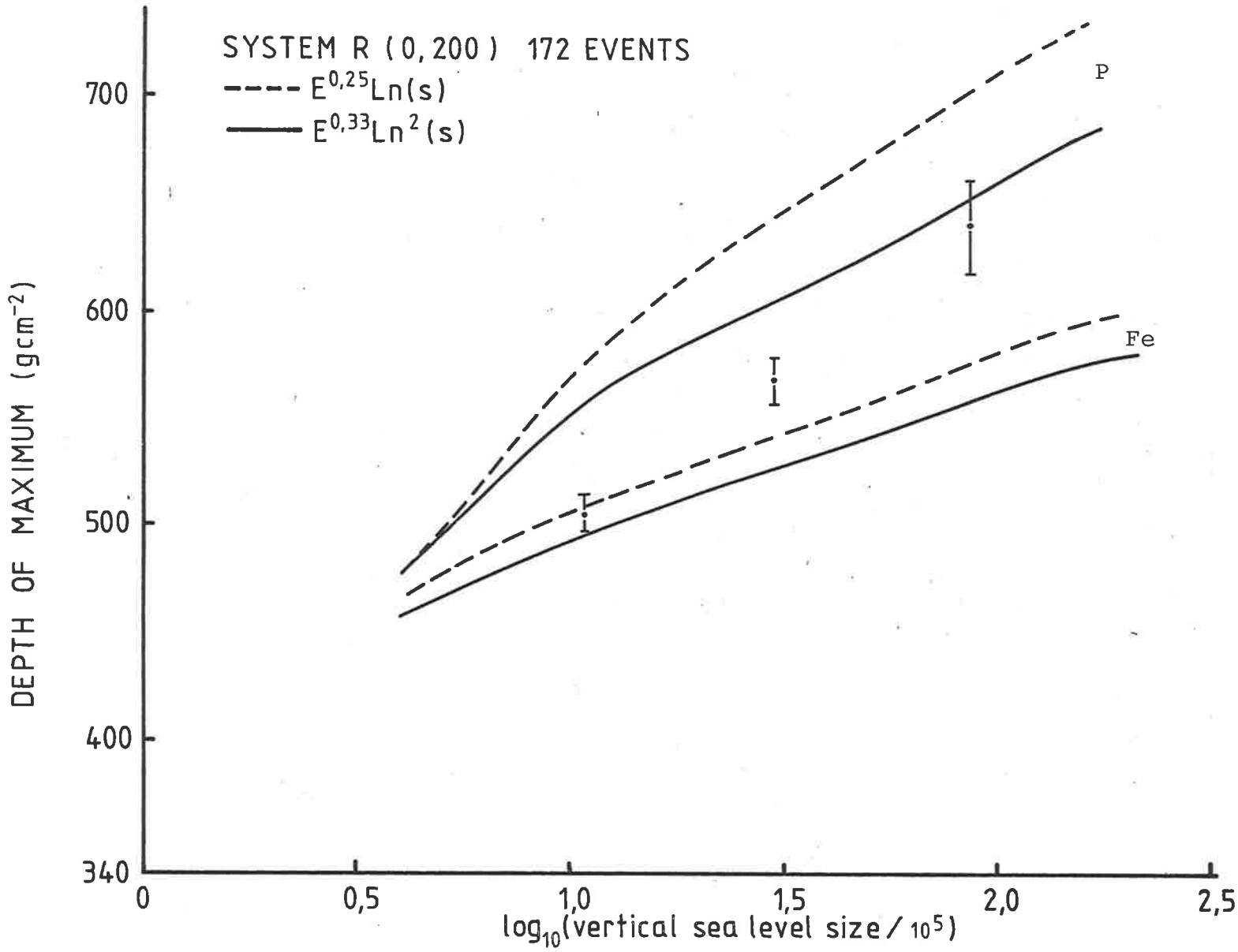

Figure 5.11: Comparison of the measured mean depth of maximum with that predicted for system R at (0,200) for each model discussed in the text. Data points are tabulated in table 5.1.

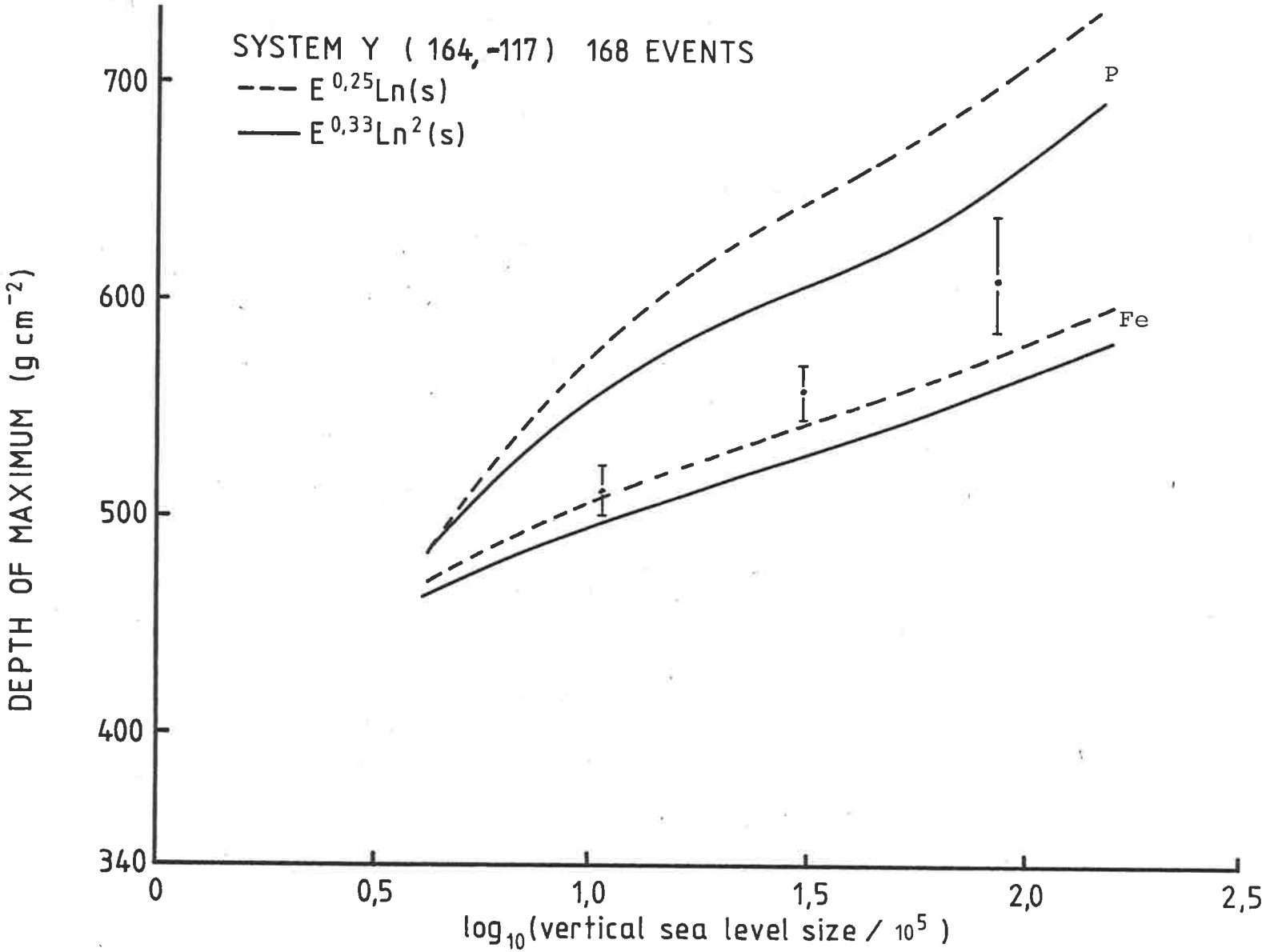

Figure 5.12: Comparison of the measured mean depth of maximum with that predicted for system Y at (164,-117), for each model discussed in the text. Data points are tabulated in table 5.1.

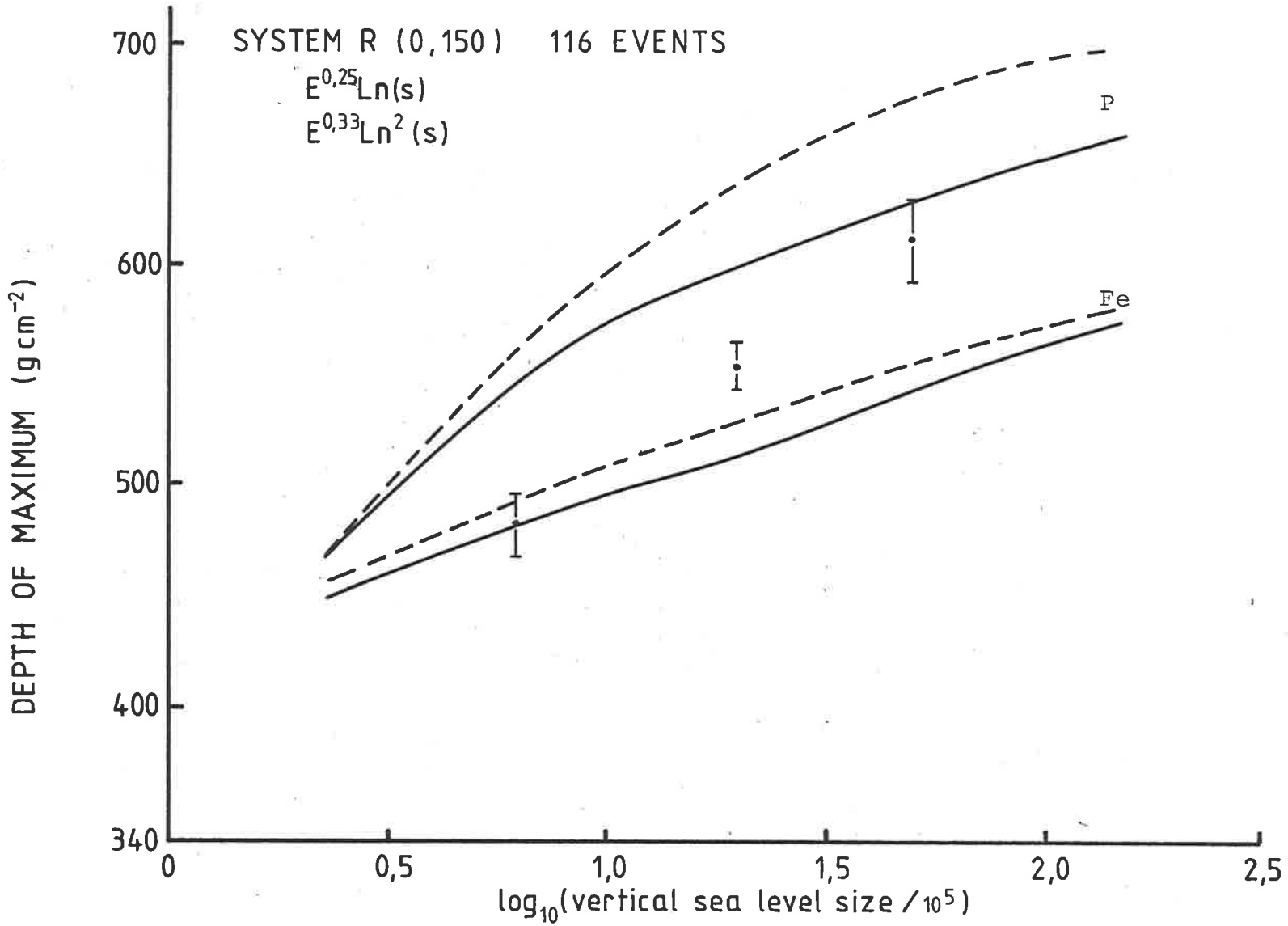

Figure 5.13: Comparison of the measured mean depth of maximum with that predicted for system R at (0,150), for each model discussed in the text. Data points are tabulated in table 5.1.

Table 5.1 Experimental data

Note: all vertical sizes have been divided by 10^5.

System R at (0,200):

$\log_{10}$(vertical size) limits:	.75-1.25	1.25-1.75	>1.75
number of events:	89	64	14
mean[$\log_{10}$(vertical size)]:	1.04±.01	1.48±.01	1.94±.03
mean depth (g cm^{-2}):	506±9	586±11	640±22

System Y at (164,-117):

$\log_{10}$(vertical size) limits:	.75-1.25	1.25-1.75	>1.75
number of events:	78	62	21
mean[$\log_{10}$(vertical size)]:	1.03±.01	1.49±.01	1.94±.05
mean depth (g cm^{-2})	513±11	557±11	612±25

System R at (0,150):

$\log_{10}$(vertical size) limits:	.5-1.0	1.0-1.50	>1.50
number of events	43	63	9
mean[$\log_{10}$(vertical size)]:	.77±.01	1.25±.01	1.73±.03
mean depth (g cm^{-2})	482±14	556±10	612±19

two sites (0,200) and (164,-117) no data for showers of vertical sizes $\lesssim 6.10^5$ particles have been included due to the extremely low overall detection probability below this size. This resulted in the exclusion of five and seven events respectively. For the (0,150) site where the response plot indicates increased sensitivity to smaller showers (as the detector, on average, is closer to the shower core) data have been included at all sizes in excess of $\sim 3.10^5$, only one shower of smaller size was reliably detected below this limit.

CHAPTER SIX

DISCUSSION AND CONCLUSIONS

6.1 INTRODUCTION

Our discussion in preceding chapters has been focused on successively smaller regions of the field of cosmic ray research. First we summarized the available observations of the fundamental properties of primary cosmic rays (their energy spectrum, mass composition and isotropy), discussed currently accepted theories of cosmic ray origin and acceleration arising from these observations and noted deficiencies in the available data. An examination of the properties and features of extensive air showers initiated in the terrestrial atmosphere by energetic ($\gtrsim 10^5$ Gev) primary cosmic rays followed with particular attention being paid to the electromagnetic component of the air shower and the Cherenkov radiation emitted by its ultra-relativistic electrons. The usefulness of this radiation as an indicator of the depth of maximum development of the electromagnetic cascade and hence of the properties of the initiating particle were also discussed at length. Finally an experiment, designed to examine one particular feature of the pulse of Cherenkov radiation (its full width at half maximum) with a view to determining the mean depth of maximum in the vertical

sea-level size range of $\sim 10^5$-2.10^7 particles, was described and the resulting data analysed in the light of limitations inherent to the apparatus. We now reverse this process of specialization and ask what conclusions, for cosmic rays as a whole, may be drawn from this one experiment.

6.2 DISCUSSION

The most noticeable feature of the data displayed in figures 5.11-5.13 is that three essentially independent experiments conducted by the author indicate that the mean depth of maximum of EAS with vertical sea-level sizes in the range $\sim 7.10^5$-2.10^7 particles increases more rapidly than would be expected if the primary composition were unaltered over this region and the high energy nuclear interactions, relevant to the formation of the EAS, similar in character to those observed at lower energies ($\sim 10^2$ Gev). The effect is most noticeable in two of the three experiments, and whilst the effect may not appear as pronounced in the third experiment (system Y at (164, -117)) the data are not inconsistent with the trend indicated by the other two experiments.

The conservative and therefore, arguably, the preferred interpretation of this experimental result would be to assume that the mean mass of the primary cosmic ray beam decreases significantly over this energy region ($\sim 10^7$-10^8 Gev). This appraisal of the data would be in accord not only with the results of similar

experiments (e.g. Chantler et al 1983) but also with a large body of data obtained by a variety of different techniques.

We noted in chapter one a growing consensus that many independent experiments (e.g. Goodman et al 1982, Yodh et al 1982, Elbert 1982) are consistent with the twin assumptions of an enrichment of heavy nuclei ($\sim$40% Fe) in the primary beam at energies $\sim 10^5$-10^6 Gev and no dramatic alteration in the character of nuclear interactions as we progress from $\sim 10^2$ Gev to $\sim 10^5$ Gev. Similarly, the most recent EAS data at primary energies $\sim 10^8$-10^9 Gev (ignoring Cherenkov results for the moment) (e.g. Walker and Watson (1981, 1982), McComb and Turver 1982c) and possibly the anisotropy data of Astley et al (1981) are consistent with a relatively light mean mass in this region. Hence one would expect, as this experiment seems to indicate, that the mean primary mass decreases in the region $\sim 10^7$-10^9 Gev. This is not a new proposal and has in fact been mooted for some time (e.g. Thornton and Clay 1979, Linsley and Watson 1981, Chantler et al 1983).

A necessary adjoint of this interpretation would be the assumption of a continuing increase in the percentage of iron in the primary beam over the decade 10^6-10^7 Gev from its value of $\sim$40% at $\sim 10^6$ Gev (e.g. Goodman et al 1982) to probably $\sim$100% at 10^7 Gev (10^6 particles). Assumption of a smaller fraction of iron

at this energy would require the mean depth of maximum to lie somewhere between the two extremes indicated by the proton and iron curves rather than almost on top of the iron curve as indicated by this experiment and that of Chantler et al (1983).

A different interpretation of the experiment is provided by noting that not all experimental observations at $\sim 10^5$-10^6 Gev are explicable in terms of the above model, especially those observations relating to studies of the hadronic core of EAS, where details of high energy nuclear interactions are likely to be important (e.g. Tonwar 1982, Hillas 1979b). Indeed the only direct, albeit preliminary, observation of the flux of iron nuclei in the region $\sim 10^5$-10^6 Gev (Sood 1983) indicates a flux of iron nuclei considerably lower than that predicted by several indirect experiments (e.g. Goodman et al 1982). These results may indicate that our understanding of the relevant nuclear interactions at these energies is not yet complete. Further evidence in favour of this point of view is provided by the observation of various anomalous nuclear interaction processes, possibly with a threshold energy of $\sim 10^5$-10^6 Gev, e.g. Centauro events, Tien Shan 'long flying' component. A useful discussion of these and other EAS anomalies, aimed at providing a consistent explanation for them (and the rapid development of EAS) in terms of

the appearance of quark matter in the primary beam at $\sim 10^5$ Gev is provided by Cleymans et al (1982).

Thus far we have limited our discussion to the observed variation of the mean depth of maximum with primary energy. Further evidence in favour of either of the two broad categories of models discussed above may be obtained by studying the fluctuations in the depth of maximum at a fixed sea-level size or primary energy. Due to the highly selective nature of the data obtained in the author's experiment, it was not thought practical to attempt a detailed analysis of the between-shower fluctuations of the depth of maximum. We note, however, that a comparison of the percentage of predicted triggers of each system for each nuclear physics/primary mass combination employed in the analysis (Table 6.1) would seem to indicate that the actual depth of maximum at $\sim 10^6$ particles, where the beam would appear dominated by iron, fluctuates more significantly (less triggers are produced) than would be predicted by the conservative interpretation of this experiment. Such an analysis provides no more than an indication of what may be occurring and is highly dependent on a correct analysis of the response function of each data set and the nuclear physics models employed to deduce the percentage of expected triggers.

In conclusion, we note that a conservative analysis of our experiment would necessitate a continuing

system	mean vertical size	observed percentage of triggers	Predicted Percentage of Triggers A	B	C	D
R (0,150)	$10^{5.8}$ particles	21%	27%	42%	69%	70%
R (0,200)	10^{6} particles	12%	7%	33%	56%	59%
Y (164,-117)	10^{6} particles	15%	13%	35%	57%	60%

A - $P/E^{0.25}\ln(s)$

B - $P/E^{0.33}\ln^2(s)$

C - $Fe/E^{0.25}\ln(s)$

D - $Fe/E^{0.33}\ln^2(s)$

Table 6.1: The recording of all EAS detected by the array during Cherenkov runs enables a comparison between the number of possible Cherenkov associated showers (core ≥150 metres, ψ_r^2<5.0, core inside array) and the actual number of Cherenkov associated showers as a function of vertical size. The 'observed percentage of triggers' deduced from this is then compared with that predicted by each composition/nuclear physics model. Within the limitations discussed in the text it would seem that depth of maximum fluctuates more than would be expected by a conservative interpretation of the data. Only the data from the lowest size bin, where this effect should be most pronounced is displayed. Suitable allowance has been made for the dead-time of each system.

increase in the percentage of iron in the primary beam over the decade 10^6-10^7 Gev, to reach approximately 100% at $\sim 10^7$ Gev. Thereafter, the mean mass of the primary beam decreases to become consistent with a beam of almost pure protons at $\sim 10^8$ Gev. It may be unwise, however, to exclude the possibility that some new nuclear phenomenon is responsible for the observed rapid development at 10^7 Gev, rather than an increasing proportion of massive primary nuclei.

REFERENCES

Note the abbreviation: Proc.Xth ICRC, stands for Proceedings of the Xth International Cosmic Ray Conference.

ABDULLAH, M.M. et al, 1981, Proc.17th ICRC, Paris, 6, Pg.151.

ABULOVA, V.G. et al, 1981, Proc.17th ICRC, Paris, 2, Pg.114.

ACHARYA, B.S. et al, 1981, Proc.17th ICRC, Paris, 11, Pg.385.

ALBROW, M.G. et al, 1974, Nucl.Phys., B73, Pg.40.

ALIEV, N. et al, 1981, Proc.17th ICRC, Paris, 11, Pg. 262.

ALLAN, H.R., 1971, Prog in Elem.Particle and Cosmic Ray Physics, 10, Pg.170.

ALLAN, H.R. et al, 1975, Proc.14th ICRC, 8, Pg.3071.

ALPGARD, R.E. et al, 1981, Phys.Lett., 107B, 315.

AMALDI. U.R. et al, 1977, Phys.Lett., B66, Pg.390.

AMENDOLIA, S.R. et al, 1974, Phys.Lett., 48B, Pg. 359.

ANDAM, A.A. et al, 1981a, Proc.17th ICRC, Paris, 11, Pg.281.

ANDAM, A.A. et al, 1981b, Proc.17th ICRC, Paris, 6, Pg.125.

ANDAM, A.A. et al, 1982, Phys.Rev., D26, N1, Pg.23.

ASAKIMORI, K. et al, 1981, Proc.17th ICRC, Paris, 11, Pg.301.

ASTLEY, S.M. et al, 1981, Proc.17th ICRC, Paris, 2, Pg.156.

BALASUBRAHMANYAN, V.K., and ORMES, J.F., 1973, Ap.J., 186, Pg.193.

BARCLAY, F.R., and JELLEY, J.V., 1955, Il Nuovo Cimento, 2, Pg.27.

BARRETT, M.L. et al, 1977, Proc.15th ICRC, Plovdiv, 8, Pg.172.

de BEER, J.F., Proc.Phys.Scc., 89, Pg.567.

BELL, A.R., 1978a, M.N.R.A.S., 182, Pg.147.

BELL, A.R., 1978b, M.N.R.A.S., 182, Pg.443.

BELL, M.C. et al, 1974, J.Phys.A., 7, Pg.420.

BENECKE, J. et al, 1969, Phys.Rev., 188, Pg.2159.

BEREZHKO, I.A. et al, 1979, Soviet J.Nucl.Phys., 30, N2, Pg.215.

BINNS, W.R. et al, 1982, Ap.J.Lett, 261, L117

BLACKETT, P.M.S., 1948, Rep.Gaissiat Comm.of the Royal Society on:
'Emission spectra of the night sky and aurora', Pg.34.

BLAKE, P.R. et al, 1982, J.Phys.G., 8, Pg.1605.

BLANDFORD, R.D., and OSTRIKER, J.P., 1978, Ap.J.Lett., 221, Pg.229.

BLANDFORD, R.D., and OSTRIKER, J.P., 1980, Ap.J. , 237 Pg.793.

BOLEY, F.I., 1964, Rev.Mod.Phys., 36, Pg.792.

BOSIA, G. et al, 1972a, Il Nuovo Cimento, 9B, N2, Pg.177.

BOSIA, G. et al, 1972b, Il Nuovo Cimento, 9B, N2, Pg.201.

BOSIA, G. et al, 1977, J.Phys.A., 10, N3, Pg.441.

BOSIA, G. et al, 1980, Il Nuovo Cimento, 3C, N3, Pg.215.

BOWER, A.J. et al, 1981, Proc.17th ICRC, Paris, 9, Pg.166.

BOWER, A.J. et al, 1983, J.Phys.G., 9, L53

BRAY, A.D. et al, 1981, Proc.17th ICRC, Paris, 11, Pg.239.

BRUHWEILER, F.C. et al, 1980, Ap.J., 238, L27

BURNETT, T.H. et al, 1982, Workshop of Very High Energy Cosmic Ray Interactions, University of Pennsylvania, Philadelphia, April 1982
(ed: M.L. Cherry, K. Lande, R.I. Steinberg) Pg.221.

CAPDEVIELLE, J.N., and GAWIN, J., 1982, J.Phys.G., 8, Pg.1317.

CARRUTHERS, P., and MINH DUONG-VAN, 1972, Phys.Lett., 41B, Pg.597.

CASSÉ, M., and GORET, P., 1978, Ap.J., 221, Pg.703.

CASSÉ, M., and PAUL, J.A., 1980, Ap.J., 237, Pg.236.

CASSÉ, M., 1981, Proc.17th ICRC, Paris, 13, Pg.11.

CASSÉ, M., and PAUL, J.A., 1982, Ap.J., 258, Pg.860.

CASSIDY, G.L. et al, 1982, Workshop on Very High Energy Cosmic Ray Interactions, University of Pennsylvania, Philadelphia, April 1982 (ed: M.L. Cherry, K. Lande, R.I. Steinberg) Pg.72.

CASTAGNOLI, C. et al, 1967, Phys.Rev., 160, N5, Pg.1186.

CESARSKY, C., and LAGAGE, P.O., 1981, Proc.17th ICRC, Paris, 9, Pg.250.

CHARMAN, W.N., 1965, Proc. 9th ICRC, London, 2, Pg.1066.

CHANTLER, M.P. et al, 1979, Proc.16th ICRC, Kyoto, 9, Pg.42.

CHANTLER, M.P. et al, 1982, J.Phys.G., 8, L 51

CHANTLER, M.P. et al, 1983, J.Phys.G., 9, L27

CHERENKOV, P.A., 1958, Nobel Lectures in Physics 1942-1962, (Elsevier Publishing Company), Pg.421.

CHUDAKOV, A.E., and NESTEROVA, N.M., 1958, Il Nuovo Cimento, Ser.10, 8, Pg.606.

CLAY, R.W. et al, 1981, Il Nuovo Cimento, 4C, N6, Pg.668.

CLAY, R.W., 1982, Proc.International Workshop on Very High Energy Gamma-Ray Astronomy, Ootacumund, India, Sept.1982 (ed: P.V. Ramana Murthy and T.C. Weekes, published: P.V. Ramana Murthy), Pg.257.

CLEYMANS, J. et al, 1982, Workshop on Very High Energy Cosmic Ray Interactions, University of Pennsylvania, Philadelphia, April 1982 (ed: M.L. Cherry, K. Lande, R.I. Steinberg) Pg.136.

COLGATE, S.A., and JOHNSON, H.M., PRL, 5, Pg.235.

COLGATE, S.A., and WHITE, R.H., 1966, Ap.J., 143, Pg.626.

COLGATE, S.A., 1981a, Proc.17th ICRC, Paris, 2, Pg.303.

COLGATE, S.A., 1981b, Proc.17th ICRC, Paris, 2, Pg.352.

COWSIK, R., and WILSON, L.W., 1973, Proc.13th ICRC, Denver, 1, Pg.500.

COWSIK, R., and WILSON, L.W., 1975, Proc.14th ICRC, Münich, 2, Pg.659.

COX, D.P., and SMITH, B.W., 1974, Ap.J.Lett.,L189,

COX, R.T., 1944, Phys.Rev., 66, Pg.106.

COY, R.N. et al, 1982, Workshop on Very High Energy Cosmic Ray Interactions, University of Pennsylvania, Philadelphia, April 1982 (ed: M.L. Cherry, K. Lande, R.I. Steinberg) Pg.120.

CROUCH, P.C., 1977, 'Shower analysis at Adelaide' (unpublished).

CROUCH, P.C., 1979, Ph.D.Thesis, University of Adelaide.

DIXON, H.E. et al, 1974, Proc.Roy.Soc., A339, Pg.157.

DWYER, R.D., and MEYER P., 1981, Proc.17th ICRC, Paris, 9, Pg.222.

EARNSHAW, J.C. et al, 1973, J.Phys.A., 6, Pg.1244.

EFIMOV, N.N., and SOKUROV, V.F., 1979, Proc.16th ICRC, Kyoto, 8, Pg.152.

EFIMOV, N.N. et al, 1981, August, Bull.Sci.Inf.Acad.Sci.USSR, Yakutsk.

EICHLER, D., 1979. Ap.J., 228, Pg.419.

EICHLER, D., 1980, Ap.J., 237, Pg.809.

ELBERT, J.W. et al, 1975, Phys.Rev., C12, N3, Pg.660.

ELBERT, J.W. et al, 1976, J.Phys.G., 2, Pg.971.

ELBERT, J.W., 1978, Proc.Dumand Summer Workshop, La Jolla, (ed: A. Roberts), 2, Pg.101.

ELBERT, J.W. et al, 1981, Proc.17th ICRC, Paris, 7, Pg.42.

ELBERT, J.W., 1982, Workshop on Very High Energy Cosmic Ray Interactions, University of Pennsylvania, Philadelphia, April 1982 (ed: M.L. Cherry, K. Lande, R.I. Steinberg) Pg. 312.

ELLSWORTH, R.W., 1977. Astr.Sp.Sci., 52, Pg.415.

ELLSWORTH, R.W. et al, 1982, Phys.Rev.D., 26, N1, Pg.336.

ELTERMAN, L., 1968, Air Force Cambridge Research Labs., Ref: AFCRL-68-0153.

FEINBERG, E.L., 1972, Physics Reports, 5C, N5, Pg.240.

FERMI, E., 1949, Phys.Rev., 75, Pg.1169.

FEYNMAN, R.P., 1969, Phys.Rev.Lett., 23, Pg.1415.

FOMIN, Yu.A., and KHRISTIANSEN, G.B., 1971, Soviet Jnl.Nucl. Physics., 14, Pg. 360.

FOWLER, P.H. et al, 1967, Proc.Roy.Soc.(London), A, 301, Pg.39.

FOWLER, P.H. et al, 1977, Proc.15th ICRC, Plovdiv, 11, Pg.15.

FOWLER, P.H. et al, 1981, Nature, 291, Pg.45.

FRANK. I.M., and TAMM. Ig., 1937, Dokl.Akad.Nauk., 14, Pg.109.

GADALOV, A.N. et al, 1972, Izv.Akad.Nauk.SSSR., Ser.Fiz, 36, Pg.8.

GAISSER, T.K. et al, 1978. Rev.Mod.Phys., 50, N4, Pg.859.

GAISSER, T.K. et al, 1979, Proc.16th ICRC, Kyoto, 9, Pg.275.

GAISSER, T.K., and YODH, G.B., 1980, Ann.Rev.Nucl.Part.Sci., 30, Pg.475.

GAISSER, T.K., 1981, Proc.17th ICRC, Paris, 6, Pg.223.

GAISSER, T.K. et al, 1982, Phys.Rev.D, 25, N9, Pg.2341.

GAISSER, T.K., 1982, Cmts.on Nucl.Part.Phys., 11, N1, Pg.25

GALBRAITH, W., and JELLEY, J.V., 1953, Nature, 171, Pg.349.

GALBRAITH, W., and JELLEY, J.V., 1955, J.Atmos.and Terrestrial Phys. 6, Pg.250.

GALKIN, V.I. et al, 1979, Proc.16th ICRC, Kyoto, 9, Pg.79.

GARCIA-MUNOZ, M. et al, 1977, Proc.15th ICRC, Plovdiv, 1, Pg.307.

GARCIA-MUNOZ, M. et al, 1981, Proc.17th ICRC, Paris, 9, Pg.195.

GARDNER, F.F. et al, 1969, Aust.J.Phys., 22, Pg.813.

GERHARDY, P.R. et al, 1981, Proc.17th ICRC, Paris 11, Pg.305.

GERHARDY, P.R., 1983, Ph.D.Thesis, University of Adelaide.

GIBSON, A.I. et al, 1981, Proc.17th ICRC, Paris, 6, Pg.16.

GILER, M. et al, 1980, J.Phys.G., 6, Pg.1561.

GINSBURG, V.L., 1940, Zh.fiz.SSSR, 2, Pg.441.

GOODMAN, J.A. et al, 1979, Phys.Rev.Lett., 42, Pg.13.

GOODMAN, J.A. et al, 1982, Phys.Rev.D, 26, N5, Pg.1043.

GREISEN, K.G., 1956, Prog.Cosmic Ray Phys., 3, Pg.1.

GREISEN, K.G., 1960, Ann.Rev.Nuc.Sci., 10, Pg.80.

GREISEN, K.G. 1966, Phys.Rev.Lett., 16, Pg.748.

GRIGOR'EV, V.M. et al, 1978, Soviet Jnl.Nucl.Physics, 27, N2, Pg.225.

GRIGOR'EV, V.M. et al, 1979, JETP Lett., 30, N11, Pg.708.

GRIGOROV, N.L. et al, 1971, Proc.12th ICRC, Hobart, 5, Pg.1746.

GRINDLAY, J.E., 1971, Il Nuovo Cimento, 2B, N1, Pg.119.

GUETTLER, K. et al, 1976, Phys.Lett., 64B, Pg.117.

GUZHAVIN, V.V. et al, 1975, Proc.14th ICRC, Münich, 8, Pg.2039.

HAMMOND, R.J. et al, 1978, Il Nuovo Cimento, 1C, N4, Pg.315.

HARA, T. et al, 1981, Proc.17th ICRC, Paris, 11, Pg.277.

HEILES, C., 1979, Ap.J., 229, Pg.533.

HEILES, C., 1976, Ann.Rev.Astron.Astrophys., 14, Pg.1.

HILLAS, A.M., and LAPIKENS, J., 1977, Proc.15th ICRC, Plovdiv, 8, Pg.460.

HILLAS, A.M., 1978, A.I.P.Conf.Proc.No.49, 'Cosmic Rays and Particle Physics', Bartel (ed: T.K. Gaisser) Pg. 373.

HILLAS, A.M., 1979a, Proc.16th ICRC, Kyoto, 8, Pg.7.

HILLAS, A.M., 1979b, Proc.16th ICRC, Kyoto, 9, Pg.13.

HILLAS, A.M., 1981a, Proc.17th ICRC, Paris, 2, Pg.125.

HILLAS, A.M., 1981b, Proc.17th ICRC, Paris, 13, Pg.69.

HILLAS, A.M., 1981c, Proc.Paris Workshop Cascade Stimulations, July 1981, Paris (ed: A.M. Hillas and J. Linsley, published: Texas Centre for the Advancement of Science and Technology) Pg.13.

HILLAS, A.M., 1982a, Proc.NATO Advanced Study Institute on Composition and Origin of Cosmic Rays, Erice 1982, (to be published).

HILLAS, A.M., 1982b, J.Phys.G., 8, N10, Pg.1461.

HILLAS, A.M., 1982c, J.Phys.G., 8, N10, Pg.1475.

INOUE, N., 1981a, Proc.17th ICRC, Paris, 11, Pg.270.

INOUE, N., 1981b, Proc.17th ICRC, Paris, 11, Pg.274.

ISRAEL, M.H., 1981, Proc.17th ICRC, Paris, 12, Pg.53.

IVANENKO, I.P. et al, 1976, F.I.A.N., preprint No.98.

IVANENKO. I.P. et al, 1977, Proc.15th ICRC, Plovdiv, 8, Pg.297.

IVANENKO. I.P. et al, 1979, Proc.16th ICRC, Kyoto, 9, Pg.88.

JAMES, F., and ROOS M., 1975, Computer Phys.Comm., 10, Pg.343.

JELLEY, J.V., and GALBRAITH, W., 1953, Phil.Mag., 44, Pg.619.

JELLEY, J.V., and GALBRAITH, W., 1955, J.Atmos.and Terrestrial Phys., 6, Pg.304.

JELLEY, J.V., 1967, Prog.Elem.Part.and C.R.Phys., 9, Pg.41.

JELLEY, J.V., 1982, Proc.International Workshop on Very High Energy Gamma-Ray Astronomy. Ootacamund, India, Sept.1982 (ed: P.V. Ramana Murthy, T.C. Weekes, published: P.V. Ramana Murthy) Pg.3.

JENKINS, E.B., 1978, Ap.J., 157, Pg.135.

JENKINS, F.A., and WHITE, H.E., 1950, 'Fundamentals of Optics', 3rd edition, New York (McGraw-Hill) Pg.478.

JULIUSSON, E., 1974, Ap.J., 191, Pg.331.

KAFATOS, H. et al, 1981, Proc.17th ICRC, Paris, 2, Pg.222.

KALMUS, P., 1982, Workshop on Very High Energy Cosmic Ray Interactions, University of Pennsylvania, Philadelphia, April 1982 (ed: M.L. Cherry, K. Lande, R.I. Steinberg) Pg.1.

KALMYKOV, N.N. et al, 1977, Proc.15th ICRC, Plovdiv, 8, Pg.244.

KALMYKOV, N.N. et al, 1979, Proc.16th ICRC, Kyoto, 8, Pg.73.

KALMYKOV, N.N. et al, 1981, Proc.17th ICRC, Paris, 6, Pg.114.

KAMATA, K., 1981, Proc.17th ICRC, Paris, 13, Pg.305.

KINOSHITA, K., and NODA, H., 1971, Prog.Theor.Phys., 46, Pg.1639.

KINOSHITA, K., and NODA, H., 1973a, Prog.Theor.Phys., 49, Pg.896.

KINOSHITA, K., and NODA, H., 1973b, Prog.Theor.Phys., 50, Pg.915.

KIRÁLY, P., and KÓTA, J., 1979, Rivista del Nuovo Cimento, 2, N7, Pg.1.

KIROV, I.N. et al, 1981, Proc.17th ICRC, Paris, 2, Pg.109.

KOCH-MIRAMOND, L., 1981, Proc.17th ICRC, Paris, 12, Pg.31.

LA POINTE, M. et al, 1968, Can.J.Phys., 46, Pg.568.

LATTES, C.M.G. et al, 1973, Proc.13th ICRC, Denver, 3, Pg.227; 4, Pg.2671.

LATTES, C.M.G. et al, 1980, Physics Reports, 65, Pg.3.

LIEBING, D.F. et al, 1981, Proc.17th ICRC, Paris, 6, 90

LIEBING, D.F. et al, 1983, Proc.18th ICRC, Bangalore, EA4-10.

LINSLEY, J., and WATSON, A.A., 1977. Proc.15th ICRC, Plovdiv, 2, Pg.188.

LINSLEY, J., 1977, Proc.15th ICRC, Plovdiv, 12, Pg.89.

LINSLEY, J., and WATSON, A.A., 1981, Phys.Rev.Lett., 46, N7, Pg.459.

LINSLEY, J., 1981, Proc.17th ICRC, Paris 11, Pg.246.

LINSLEY, J., and HILLAS A.M., 1981, Proc.Paris Workshop on Cascade Simulations, Paris, July 1981 (ed: J. Linsley and A.M. Hillas, Published: Texas Center for the Advancement of Science and Technology) Pg.27.

LLOYD-EVANS, J., and WATSON, A.A., 1982, Review paper presented at 8th European Cosmic Ray Symposium, Sept, 1982, Rome. (Unpublished)

LOWE, G.H. et al, 1975, Phys.Rev., C12, Pg.651.

MAKAROV, V.V. et al, 1981, Proc.17th ICRC, Paris, 11, Pg.289.

MAKHMUDOV, B.M. et al, 1979, Proc.16th ICRIC, Kyoto, 9, Pg.61.

MALOS, J. et al, 1962, J.Phys.Soc.(Japan), 17, Pg.114, Suppl.A-III.

MASON, G.W. et al, 1975, Proc.14th ICRC, Münich, 8, Pg.2943.

McCOMB, T.J.L., and TURVER, K.E., 1982a, J.Phys.G., 8, Pg.871.

McCOMB, T.J.L., and TURVER, K.E., 1982b, Il Nuovo Cimento, 5C, N2, Pg.131.

McCOMB, T.J.L., and TURVER, K.E., 1982c, J.Phys.G., 8, Pg.1119.

McCOMB, T.J.L., and TURVER, K.E., 1982d, J.Phys.Soc.Japan, 51, N10, Pg.3087.

McCRAY, R.A., and SNOW, T.P., 1979, Ann.Rev.Astron.Astrophys., 17, Pg.213.

McKEE, C.F., and OSTRIKER, J.P., 1977, Ap.J., 218, Pg. 148.

McKEE, C.F., 1981, Proc.17th ICRC, Paris, 12, Pg.69.

MEYER, J.P., 1979, Proc.16th ICRC, Kyoto, 1, Pg.374.

MEYER, J.P., 1981, Proc.17th ICRC, Paris, 2, Pg.265.

MEWALDT, R.A., 1981, Proc.17th ICRC, Paris, 13, Pg. 49.

MICHEL, F.C., and DESSLER, A.J., 1981, Proc.17th ICRC, Paris, 2, Pg.340.

MIYAKE, S. et al, 1981, Proc.17th ICRC, Paris, 11, Pg.293.

MORRIS, D., and BERGE, G.L., 1964, Ap.J., 139, Pg.1388.

MORRISON, D.R.O., 1973, Proc.Roy.Soc., A335, Pg.461.

MÜLLER, D., 1982, Workshop on Very High Energy Cosmic Ray Interactions, University of Pennsylvania, Philadelphia, April 1982 (ed: M.L. Cherry, K. Lande, R.I. Steinberg) Pg.448.

NESTEROVA, N.M., and CHUDAKOV, A.E., 1955, JETP, 28, Pg.384.

NISHIMURA, J., and KAMATA, K., 1951, Progr.Theor.Phys., 6, Pg.628.

NIKOLSKY, S.E. et al, 1981, Proc.17th ICRC, Paris, 2, Pg.129.

OLEJNICZAK, J. et al, 1977, Proc.15th ICRC, Plovdiv, 8, Pg.393.

ORFORD, K.J., and TURVER, K.E., 1976, Nature, 264, Pg.727.

ORMES, J.F., 1982, Workshop on Very High Energy Cosmic Ray Interactions, University of Pennsylvania, Philadelphia, April 1982 (ed: M.L. Cherry, K. Lande, R.I. Steinberg) Pg.466.

OULDRIDGE, M., and HILLAS, A.M., 1978, J.Phys.G., 4, Pg. L35.

PATTERSON, J.R., and HILLAS, A.M., 1983a, J.Phys.G., 9, Pg.323.

PATTERSON, J.R., and HILLAS, A.M., 1983b, (submitted to J.Phys.G.)

PERRON, C. et al, 1981, Proc.17th ICRC, Paris, 9, Pg.118.

PESSES, M.E. et al, 1982, Space Science Review, 32, Pg.185.

PETERS, B., 1961, Il Nuovo Cimento, 22, Pg.800.

PHILLIPS, S. et al, 1981, Astron.Astrophys., 98, Pg.286.

PRESCOTT, J.R. et al, Proc.18th ICRC, Bangalore, EA5-1.

PROTHEROE, R., 1977, Ph.D.Thesis, University of Durham.

PROTHEROE, R. et al, 1981, Ap.J., 247, Pg.362.

PROTHEROE, R., and ORMES, J.F., 1983, (to be published).

RAISBECK, G.M., 1979, Proc.16th ICRC, Kyoto, 14, Pg.146.

RICHARDS, J.A., and NORDHEIM, L.W., 1948, Phys.Rev., 74, N9, Pg.1106.

ROBERG, J., and NORDHEIM, L.W., 1949, Phys.Rev., 75, N3, Pg.444.

ROSSI, B., and GREISEN, K.G., 1941, Rev.Mod.Phys., 13, Pg.240.

RYAN, M. et al, 1972, Phys.Rev.Lett., 28, Pg.985, and erratum op cit., Pg.1497 (L972).

SAID, S.S. et al, 1982, J.Phys.G., 8, Pg.383.

SHIRK, E.K., and PRICE, P.B., 1978, Ap.J., 220, Pg.710.

SILBERG, R., and SHAPIRO, M.M., 1981, Proc.17th ICRC, Paris, 2, Pg.356.

SIMARD-NORMANDIN, M., and KRONBERG, P.P., 1979, Nature, 279, Pg.115.

SIMON, M. et al, 1980, Ap.J., 239, Pg.712.

SITTE, K., 1962, Il Nuovo Cimento, 25, Pg.86.

SNYDER, H.S., 1949, Phys.Rev., 76, Pg.1563.

SOOD, R.K., 1983, Nature, 301, Pg.44.

STANEV, T., and GAISSER T.K., L982, Workshop on Very High Energy Cosmic Ray Interactions, University of Pennsylvania, Philadelphia, April 1982 (ed: M.L. Cherry, K. Lande, R.I. Steinberg) Pg.125.

STREITMATTER, R.E. et al, 1983, (submitted to Astron.and Astrophys.)

TAMM, Ig., 1939, Zh.fiz, SSSR, 1, Pg.439.

TANAHASHI, G., 1982, Proc.International Workshop on Very High Gamma-Ray Astronomy, Ootacamund, India, Sept.1982 (ed: P.V. Ramana Murthy, T.C. Weekes, Published: P.V. Ramana Murthy) Pg.219.

TANAKA, Y., and BLEEKER, J.A.M., 1977, Space Sci.Rev., 20, Pg.815.

TAYLOR, F.E. et al, 1976, Phys.Rev.D, 14, N5, Pg.1217.

THOMÉ, K. et al, 1977, Nucl.Phys., B129, Pg.365.

THORNTON, G.J., and CLAY, R.W., 1979, Phys.Rev.Lett., 43, N21, Pg.1622.

THORNTON, G.J., 1983, Ph.D.Thesis, University of Adelaide.

TONWAR, S.C., 1981, Proc.17th ICRC, Paris, 13, Pg.325.

TONWAR, S.C., 1982, Workshop on Very High Energy Cosmic Ray Interactions, University of Pennsylvania, Philadelphia, April 1982 (ed: M.L. Cherry, K. Lande, R.I. Steinberg) Pg.160.

UCHAIKIN, V.V. et al, 1979, Proc.16th ICRC, Kyoto, 7,

VALLÉE, J.P., and KRONBERG, P.P., 1975, Astron.Astrophys., 43, Pg.233.

VALLÉE, J.P., 1982, Ap.J.Lett., 261,

VERNOV, S.N., and KHRISTIANSEN, G.B., 1967, Proc.10th ICRC, Calgary, (Pt.A), Pg.345.

VERNOV, S.N. et al, 1977, J.Phys.G., 3, Pg.1601.

VERSCHUUR, G.L., 1979, Fundamentals of Cosmic Physics, 5, Pg.113.

WALKER, R., and WATSON, A.A., 1981, J.Phys.G., 7, Pg.1297.

WALKER, R., and WATSON, A.A., 1982, J.Phys.G., 8, Pg.1131.

WATSON, A.A., 1981, Proc.16th Recontre De Moriond (to be published).

WATSON, A.A., 1982, Workshop on Very High Energy Cosmic Ray Interactions, University of Pennsylvania, Philadelphia, April 1982 (ed: M.L. Cherry, K. Lande, R.I. Steinberg) Pg.105.

WDOWCZYK, J., and WOLFENDALE, A.W., 1972, Nature, 236, Pg.29.

WEBBER, W.R., 1982, Ap.J., 255, Pg.329.

WESTFALL, G.D. et al, 1979, Phys.Rev.C, 19, Pg.1309.

WENTZEL, D.G., 1974, Ann.Rev.Astron.Astrophys., 12, Pg.71.

WHITE, J. et al, 1961, J.Atmos.Terr.Phys., 20, Pg.40.

WOLFENDALE, A.W., 1980, I.A.U.Symposium, No.94, 'Origin of Cosmic Rays'
(ed: G. Setti, G. Spada, A.W. Wolfendale,
Published: D. Reidel, Dordrecht-Holland)
Pg.309.

YAKOVLEV, V.I. et al, 1979, Proc.16th ICRC, Kyoto, 6, Pg.59.

YAMDAGNI, N., 1982, Workshop on Very High Energy Cosmic Ray Interactions, University of Pennsylvania, Philadelphia, April 1982
(ed: M.L. Cherry, K. Lande, R.I. Steinberg)
Pg.36.

YEN, E., 1974, Phys.Rev., 10, Pg.836.

YODH, G.B. et al, 1982, Workshop on Very High Energy Cosmic Ray Interactions, University of Pennsylvania, Philadelphia, April 1982
(ed: M.L. Cherry, K. Lande, R.I. Steinberg
Pg.200.

ZATSEPIN, G.T., and KUZMIN, V.A., 1966, JETP.(Lett.), 4, Pg.78.

ZATSEPIN, V.I., and CHUDAKOV, A.E., 1962, JETP, 15, Pg.1126.